# The Macroeconomic Cost of Climate Change: Local Damages, Spatial Adjustment, and Global Spillovers*

Diogo Baptista† OECD
Hélia Costa‡ OECD
Filiz Unsal§ OECD

October 20, 2026

**Abstract**

How do local climate damages translate into aggregate economic losses, and how does spatial adjustment shape their distribution? We combine granular economic and weather data with climate projections to quantify local damages from heat stress, changes in agro-climatic conditions, floods, and sea-level rise. We embed these damages in a global spatial general equilibrium model incorporating trade, migration, production networks, and capital accumulation to quantify their aggregate and regional effects. Relative to a baseline with climate conditions fixed at historical levels, global GDP per capita is 3% lower in 2050 and 6.4% lower in 2100 under our intermediate-emissions benchmark, compared with 5.9% and 18.5%, respectively, under a very high-emissions scenario. Losses vary widely across and within countries, with larger impacts in lower-latitude regions and heat stress accounting for most global damages. Under the intermediate-emissions benchmark, production networks amplify global losses in 2100 by around 72%, while trade and labour adjustment jointly reduce losses by around 11%. These adjustments also substantially redistribute losses across locations and reduce their relative cross-regional dispersion. The findings highlight the importance of distinguishing local exposure, economic propagation, and endogenous adjustment when assessing the macroeconomic costs of climate change.

**Keywords:** Climate change; spatial general equilibrium; climate damages; adaptation; trade and migration; production networks.

**JEL Codes:** Q54, F18, F12, R13.

*All authors are affiliated with the OECD Economics Department. We thank Enrico Botta, Eddy Casey, Jean Chateau, Francesco Filippucci, Catherine Gamper, Yvan Guillemette, Asa Johansson, Andy King, Luisa Lutz, Sherie Nicol, Mauro Pisu, Matthias Schief, Simon Touboul, and Sebastian Turban for helpful comments and discussions. We also thank seminar participants at the OECD, the IMF, and the University of Minho, as well as delegates of Working Party 1 of the OECD Economic Policy Committee, for helpful comments and suggestions. The views expressed in this paper are those of the authors and do not necessarily reflect those of the OECD or its member countries. All errors are our own.

†diogo.baptista@oecd.org.
‡helia.costa@oecd.org.
§filiz.unsal@oecd.org.

## 1. Introduction

Climate change is increasingly shaping global welfare and macroeconomic outcomes (IPCC, 2022; Bank of England, 2025; European Central Bank, 2021). Its economic impacts are expected to intensify, but estimates of future losses vary substantially across studies and remain uncertain. The key question is not only how large the losses will be, but also how they arise, how they spread across sectors and space, and how economies adjust. Local exposure alone does not determine economic losses: trade and production networks transmit shocks beyond their place of origin, while changes in sourcing, production and migration shape their ultimate effects. Quantifying these effects calls for analytical frameworks that integrate multiple climate hazards and trace their transmission through interconnected regions and sectors.

In this paper, we develop a micro-based, bottom-up approach to measure the economic cost of climate change around the world. Our approach is built around three steps (see Figure 1). We first map four climate hazards—heat stress, changes in agro-climatic conditions, floods, and sea-level rise—into location-specific shocks to productivity, capital depreciation, and land supply. This mapping combines econometric evidence from granular firm-level and weather data with climatological, hydrological, and agricultural models. We then combine these estimates with economic and climate projections to quantify future local damages through 2100. Finally, we aggregate these damages through a quantitative spatial model that we develop and calibrate to assess their macroeconomic and regional effects: the Climate and Adaptation Spatial General Equilibrium Model (CASGEM).

The model incorporates general equilibrium adjustments in goods, labour, capital, and real estate markets, and allows for heterogeneous impacts and endogenous adaptation through trade and labour reallocation. We calibrate the model to 927 regions and 11 sectors in OECD countries and three aggregate sectors elsewhere. We calibrate it using detailed information on production, employment, wages, trade flows, migration, and input–output relationships. Spatial frictions in goods and labour markets govern interactions across locations, while production networks connect sectors through purchases of intermediate inputs. The framework enables counterfactual analysis of two distinct questions: how economic linkages shape the propagation of local shocks, and how the ability to adjust trade and labour allocations changes their aggregate and regional consequences.

Our quantitative results show that climate change generates sizable macroeconomic losses that grow over time. Relative to a baseline in which climate conditions remain fixed at historical levels, global GDP per capita is 3% lower in 2050 and 6.4% lower in 2100 under our intermediate-emissions benchmark (SSP2-4.5). Under the very high-emissions scenario (SSP5-8.5), used as a higher-warming comparison, losses rise to 5.9% by mid-century and 18.5% by 2100, with substantial uncertainty surrounding these projections. These aggregate effects mask substantial heterogeneity: losses are larger in lower-latitude regions and vary greatly within countries, reflecting differences in exposure, economic structure, and connectivity to global markets. Heat stress emerges as the main source of economic losses worldwide, including in advanced economies, followed by losses due to changes in agro-climatic conditions. Flooding and sea-level rise play important roles in specific coastal and low-lying regions but contribute less to the global economic impact.

To understand the transmission channels through which local climate shocks translate into economy-wide impacts, we conduct counterfactual simulations that remove key economic linkages and recalibrate the model. We first remove cross-regional trade and migration linkages and then, in a separate exercise, input–output linkages. We find that spatial linkages and production networks substantially shape both the size and the distribution of climate damages. Trade and migration can cushion local losses or transmit adverse effects across regions and borders, reducing global losses while generating heterogeneous local effects. Supply chains act as a powerful amplification channel in most economies: global GDP per capita losses in 2100 under our intermediate-emissions benchmark are roughly 72% larger with input–output linkages than without them. Amplification is similar in relative terms under the very high-emissions scenario.

We next examine how the economy's ability to adjust influences the magnitude and distribution of impacts. Retaining the baseline calibration, we compare simulations in which trade and labour allocations respond to climate change with counterfactuals in which they remain fixed along their no-climate-change paths. At the global level, these adjustment margins act as a stabilising force, jointly lowering world GDP per capita losses in 2100 by roughly 11% under our intermediate-emissions benchmark and by around 8% under the very high-emissions scenario, relative to the corresponding counterfactual with both margins restricted. However, they can either mitigate or amplify local climate damages, depending on regions' exposure, economic structure and position in the global economy. Trade adjustment tends to reduce losses in many of the regions most exposed to climate damages, while redistributing part of the burden towards relatively less affected regions. Labour adjustment also reduces global losses, although its aggregate contribution is smaller than that of trade adjustment. Their importance therefore extends beyond the aggregate benefit: they substantially reshape the geographic distribution of losses.

Our analysis builds on quantitative spatial models of climate change, in which spatial frictions and the endogenous reallocation of economic activity shape both aggregate damages and their geographic incidence (Desmet and Rossi-Hansberg, 2015; Conte et al., 2021; Cruz and Rossi-Hansberg, 2024).[1] A central insight is that climate impacts depend not only on local exposure, but also on the scope for adjusting production, trade, and location as relative economic conditions change. Within this literature, Costinot et al. (2016) and Gouel and Laborde (2021) quantify adaptation through crop reallocation and international trade. Nath (2025) and Cruz (2024) examine adjustment across broader economic sectors, showing how income-dependent demand for food can limit reallocation towards less climate-sensitive activities. Related work studies migration and its distributional consequences in Africa (Conte, 2026) and globally (Burzyński et al., 2022), as well as the spatial adjustment of economic activity to coastal inundation (Desmet et al., 2021). Cruz et al. (2026) examine the spatial economic consequences of a climate tipping point associated with a collapse of the Atlantic Meridional Overturning Circulation.[2]

[1] For recent syntheses of this literature, see Desmet and Rossi-Hansberg (2024, 2026).

[2] A related strand of the literature uses spatial integrated assessment models to examine mitigation policy, including the geographic effects of carbon taxes (Conte et al., 2026), local social costs of carbon, and the effects of national emissions-reduction pledges (Cruz and Rossi-Hansberg, 2026).

Two contributions are particularly close to our analysis. Rudik et al. (2022) quantify temperature impacts in a global dynamic spatial economy with production networks, trade, and labour reallocation, identifying temperature effects on sectoral productivity from international trade flows. We complement this approach by distinguishing four climate hazards: heat stress, changes in agro-climatic conditions, flooding, and sea-level rise. Our damage inputs combine firm-level evidence on heat and flooding with other hazard-specific empirical evidence and physical projections. Beyond productivity effects, we capture flood-related capital destruction and sea-level-induced land loss, channels absent from their temperature-focused framework. Whereas their framework treats capital as non-accumulating, ours allows investment to respond to economic conditions, so that climate damages affect both existing capital and its subsequent accumulation. Bilal and Rossi-Hansberg (2023) study heat waves and severe storms in a dynamic model of US counties, emphasising anticipation, migration, and capital investment. They examine these responses in a setting with a single freely traded good, abstracting from intermediate-input linkages across sectors. We complement their analysis by incorporating costly goods trade and production networks in a global multi-sector economy that also allows migration within and across countries. This enables us to examine how damages originating in one country affect production and adjustment elsewhere through international sourcing, demand, and labour movements.

Our analysis also relates to the literature on production networks and the aggregate consequences of local shocks (Acemoglu et al., 2012; Caliendo et al., 2018). Empirical studies document the propagation of natural-disaster shocks through supplier–customer relationships (Barrot and Sauvagnat, 2016; Carvalho et al., 2021), while climate-specific studies quantify the transmission of agricultural heat shocks and the supply-chain amplification of projected heat losses (Zappalà, 2024; Sun et al., 2024). Firms also adapt by relocating production, changing supplier relationships, and diversifying sourcing across space (Pankratz and Schiller, 2024; Balboni et al., 2025; Castro-Vincenzi et al., 2025). These responses can reduce exposure while redistributing economic activity and losses. Dingel and Meng (2025) further show how the spatial correlation of climate-induced productivity shocks changes the distribution of gains from trade.[3] We bring these transmission and adjustment mechanisms together in a global assessment of multiple climate hazards. By separately examining the role of economic linkages and the scope for trade and labour adjustment, our counterfactuals show how production networks can amplify aggregate damages even as adjustment moderates global losses and redistributes them across locations.

Our approach also draws on bottom-up assessments that combine empirical evidence with climate projections to quantify geographically detailed economic damages (Hsiang et al., 2017; Carleton et al., 2026). Computable general equilibrium assessments trace multiple climate impacts through interconnected sectors and countries (Bosello et al., 2007; Kompas et al., 2018; Dellink et al., 2019). In particular, Dellink et al. (2019) link climate impacts to changes in productivity, capital, and land supply. We combine this treatment of distinct damage channels with subnational

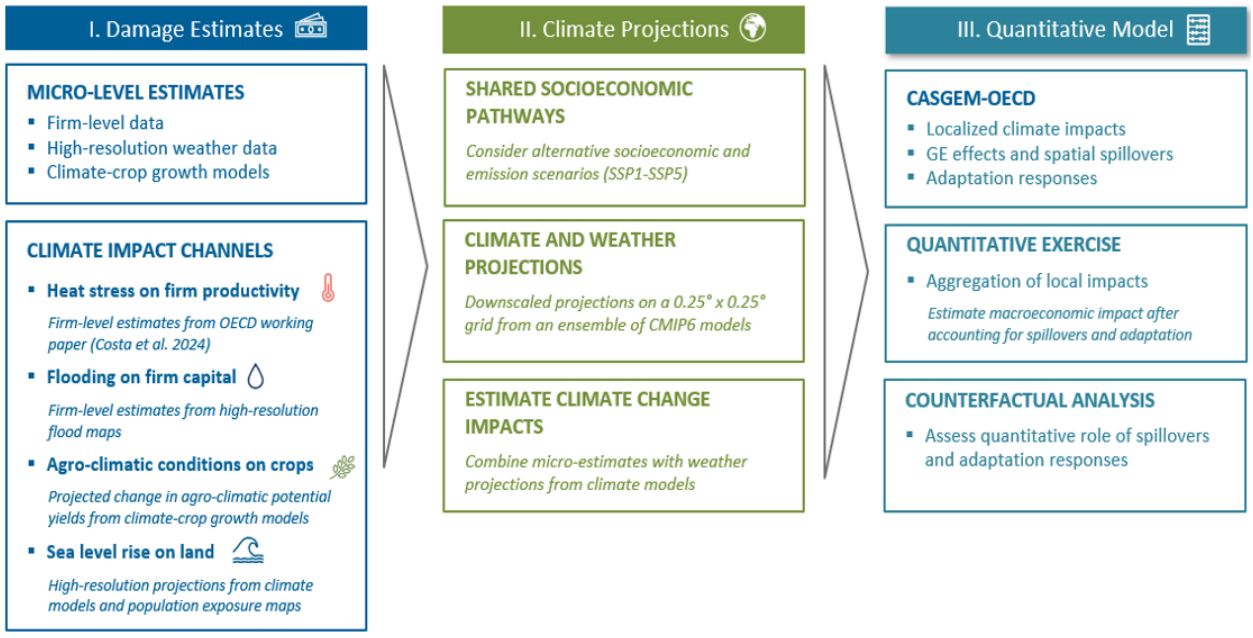
[3]Related work examines how trade and migration reshape the geographic distribution of uncertainty in climate damages (Bearpark et al., 2025).

economic detail and spatial frictions governing the movement of goods and workers. National losses therefore reflect not only country-level exposure, but also where damages occur within countries, the economic structure of affected regions, and the scope for reallocating activity across locations.[4]

Finally, macro-econometric studies use historical variation in economic outcomes and climate to estimate impacts and project future losses (Dell et al., 2012; Burke et al., 2015; Kahn et al., 2021; Bilal and Känzig, 2026). Subnational studies examine temperature effects on regional production (Kalkuhl and Wenz, 2020) and spatial spillovers from extreme weather events (Costa and Hooley, 2025). This evidence can capture equilibrium responses and spillovers present in the observed variation.[5] Our structural approach complements this evidence by making explicit how the transmission and adjustment mechanisms embedded in historical outcomes operate under projected climate conditions. It allows us to examine how future losses change when these mechanisms are restricted or economic linkages are altered, conditional on the damage inputs and calibrated economic structure.

The remainder of the paper is organised as follows. Section 2 describes the climate hazards considered and their estimation. Section 3 outlines how climate projections are translated into future damages. Section 4 presents the structure and calibration of our spatial quantitative model, CASGEM. Section 5 reports the results, and Section 6 concludes.

**Figure 1:** Quantifying the Cost of Climate Change: A Micro-based, Bottom-up Approach




*Notes:* This figure describes the three modules making up our micro-based, bottom-up approach.

[4]Other quantitative studies examine explicit investment in adaptation, including protective capital (Fried, 2022) and infrastructure investment under future coastal inundation (Balboni, 2025). These investments are distinct from the trade and labour adjustment margins studied here.

[5]For a recent discussion of the relationship between reduced-form and structural approaches, including the treatment of adaptation and spatial spillovers, see Lemoine et al. (2025).

## 2. Estimation of local climate damages

We focus on four impact channels that capture salient and well-documented first order effects of climate, whose choice is guided by existing literature and insights from our micro-level analysis described below. Heat stress affects productivity, with impacts that vary across sectors and climatic conditions. Flooding is another important climate hazard and, as shown below, operates mainly through the destruction and accelerated depreciation of firms' physical capital. Changes in temperature, solar radiation, and precipitation (agro-climatic conditions) affect agricultural productivity through biophysical impacts on crop growth conditions. Finally, sea-level rise represents a slow-onset event that reduces the effective supply of productive land in low-lying coastal areas. Together, these channels provide a parsimonious representation of the core economic impacts of climate.

While this approach aims to provide a consistent and empirically grounded assessment of first-order climate damages, several caveats are worth noting. First, estimates based on historical variation may not fully capture the economic consequences of rare extreme events, threshold effects or potential tipping points that could become more prevalent under future climate conditions, implying that damages could be nonlinear at higher levels of warming. Second, hazards may interact in ways that are not purely additive, such that the combined effects of multiple shocks may exceed the sum of their individual impacts. Where feasible, we mitigate this risk by jointly controlling for correlated climate variables in our empirical specifications.[6] Third, historical estimates implicitly embed past adaptation responses, while future adaptation capacities, costs and technological developments remain uncertain, possibly resulting in over- or underestimation of future damages. Fourth, our analysis does not incorporate several important climate hazards like storms (i.e. tropical cyclones, hurricanes and typhoons), wildfires, and landslides, all of which are expected to become increasingly frequent and/or severe in many parts of the world. Excluding these hazards means that our estimates may understate the full spectrum of climate-related risks, particularly for countries where these hazards are a dominant source of losses. Finally, this analysis focuses on market-based channels and abstracts from broader impacts such as food security, health impacts or irreversible ecosystem losses, all of which have impacts on welfare.

### 2.1. Flooding and the capital stock

Floods are a major climate-related risk to economic activity, primarily through their effects on firms' physical capital and balance sheets. To quantify these impacts, we rely on firm-level estimates from Baptista et al. (forthcoming), an original empirical analysis linking balance-sheet data from Moody's Orbis with geographically detailed information on major flood events from the Global Flood Database (Tellman et al., 2021), covering over 2.5 million firms across 17 European

[6] For example, the empirical analysis of flooding controls for concurrent heat stress to reduce the risk of confounding correlated climate shocks. Moreover, projections for future agro-climatic conditions are derived from climate-crop growth models that simultaneously account for the effect of changes in temperature, drought conditions (i.e. precipitation and evapotranspiration) and solar radiation.

and Asian advanced economies from 2000 to 2018. The analysis exploits high spatial resolution in flood exposure, allowing us to distinguish between firms directly affected by flooding and nearby firms exposed only through local spillovers.

The analysis relates firm value added and its determinants—including capital stock, productivity, and employment—to flood exposure. It compares firms directly affected by floods with otherwise similar firms located more than 100 km away, while accounting for spillovers to nearby but unflooded firms. The specification controls for firm characteristics, local weather conditions, and firm, sector-year, and country-year fixed effects.

The results indicate that floods primarily affect firms through capital destruction rather than sustained productivity or employment losses. On average, direct flood exposure reduces firms' capital stocks by 2.7% over the four years following the event. Estimated effects on multifactor productivity are modest and statistically insignificant, and labour appears to be unaffected. The decline in capital stock is accompanied by a decrease in value added consistent with conventional estimates of capital's share in production.

The analysis also documents economically meaningful spillovers to nearby firms and substantial heterogeneity in impacts. Longer-lasting flood events generate larger losses than shorter events, and smaller firms experience significantly greater capital losses than larger firms, consistent with more limited capacity to absorb and recover from large shocks. These estimates are used to calibrate flood-related capital destruction in the quantitative model. Further details are described in Baptista et al. (forthcoming) and Appendix B.

### 2.2. Heat stress and productivity

Heat stress is an increasingly important climate-related condition for economic activity, particularly through its impact on labour productivity. To quantify these effects, for all sectors apart from the agriculture sector, we rely on estimates from Costa et al. (2024), who link firm-level data from Orbis (covering over 2.7 million firms across 23 advanced economies from 2000 to 2021) with high-resolution ERA-5 reanalysis data. We follow their approach, which exploits granular daily temperature variation, measuring exposure to hot days in different temperature ranges, and allows impacts to vary by local climatic conditions.

The empirical strategy relates firm-level multi-factor productivity (MFP) to the annual number of hot days in each temperature bin while controlling for firm characteristics, other weather variables, firm and country-year fixed effects, and the interaction between heat exposure and long-run average local temperatures. This design captures both heterogeneous sectoral vulnerability and the role of baseline climate in mediating adaptation capacity.

The results show consistent losses in firm productivity on days exceeding 30°C, with impacts rising sharply at higher temperatures. Heat effects are largest in cooler regions where adaptation levels are lower. Impacts of days above 35°C are on average larger than those between 30°C and 35°C, and the difference increases for firms in colder climates. Days above 40°C have much larger impacts, with each additional day costing almost 0.2% of annual productivity, on average,

compared to 0.02% for days in the 30–35°C range and 0.05% for days in the 35°–40°C range. These elasticities are used to calibrate annual sector-level productivity shocks from heat stress across all sectors except for agriculture. The full results are available in Annex C.

### 2.3. Changes in agro-climatic conditions and agricultural productivity

Agricultural productivity is highly sensitive to climate, particularly temperature, precipitation, and soil moisture, and is therefore especially vulnerable to climate change. To quantify the effects of future climate on agricultural productivity, we follow Conte (2026) and draw on data from the FAO's Global Agro-Ecological Zones (GAEZ) Data Portal, which provides high-resolution estimates of agro-climatic potential yields. These yields represent the maximum attainable output under given climatic, soil and terrain conditions and are calculated under alternative assumptions regarding water management (rain-fed versus irrigated) and input intensity (low versus high input use). By focusing on potential rather than observed yields, this approach isolates the biophysical suitability of land for crop production, abstracting from differences in soil and crop management, and market conditions.

The GAEZ framework integrates outputs from a set of five climate–crop growth models to generate projections of agro-climatic conditions over different periods (2011–2040, 2041–2070 and 2071–2100).[7] These models simulate the impact of future climate conditions on key determinants of crop growth, in particular soil moisture, temperature and solar radiation. We compute model-specific percentage changes in agro-climatic potential yields using 2011–2040 as the reference period. We then take the ensemble median of these relative changes across models, yielding a central estimate of the effect of future climate on agricultural potential.

The analysis covers fifteen major crops spanning cereals (barley, maize, millet, rice, sorghum and wheat), roots and tubers (cassava, sweet potato, white potato and yams), legumes (cowpeas and groundnuts), and cash crops (palm oil, sugarcane and soybeans), as well as grasslands for capturing changes in livestock productivity. All data are available at a spatial resolution of approximately 10×10 km grid cells, allowing us to capture fine-scale heterogeneity in agricultural suitability across space. We then combine these spatial projections of relative yield change with gridded information on current crop areas and production to construct crop-weighted changes in effective crop productivity at the sub-national level. In parallel, information on the geographic distribution of livestock, drawn from the Gridded Livestock of the World (GLW 4) 2020 dataset, is used to measure the spatial distribution of livestock density around the world.

These spatially detailed, crop-specific changes in agro-climatic potential yields are subsequently translated into productivity shocks to the agricultural sector in each region. For each crop and climate model, we first aggregate projected yield levels to administrative regions using baseline harvested-area weights and calculate changes relative to the corresponding 2011–2040 yield level. We then take the median of these changes across the five climate models and combine crops and grassland using fixed weights based on crop production values and the livestock share of agricultural

[7] These are GFDL-ESM2M, HADGEM2-ES, IPSL-CM5A-LR, MIROC-ESM-CHEM and NORESM1-M

production.[8] These shocks serve as direct inputs in the model, capturing the local, first-order impact of future climate on agricultural productivity before any behavioural or general equilibrium adjustments take place.

### 2.4. Sea level rise and land loss

Sea-level rise represents a structural, rather than episodic, event: in some low-lying coastal areas, the continued rise in mean sea level may result in permanent inundation, leading to structural loss of land (Nicholls and Cazenave, 2010). To capture this dimension, we combine coastal flood projections from the World Resources Institute's (WRI) Aqueduct Floods framework, in combination with information on existing coastal protection standards (Tiggeloven et al., 2020). All grid cells where future projected coastal water levels exceed protection thresholds with 50% annual probability are classified as permanently submerged, reflecting locations that are expected to be chronically under water in the long run if protection standards remain unchanged.

We treat land as a key input in the real estate sector, which produces physical structures used by households for housing and by firms as production space. Sea level rise reduces the available supply of land in affected locations, thereby constraining the inputs available to the real estate sector. This reduction in land availability raises construction costs, which are passed through to households in the form of higher rents and to firms in the form of higher production costs. In contrast to fast-onset coastal flooding events, which directly destroy capital and structures and are captured through the flooding impact channel, sea-level rise is a slow-moving process. As a result, it does not directly lead to the destruction of existing capital stocks: real estate developers are assumed to be able to anticipate gradual inundation and relocate investment toward non-submerged areas.

Consequently, the economic costs of sea-level rise in our framework arise through changes in the production efficiency and cost structure of the real estate sector induced by land scarcity, rather than through direct physical losses. This channel is distinct from intermittent coastal flooding impacts and captures the long run structural effects of land loss on housing markets, production costs, and spatial economic activity.[9]

## 3. Climate projections and calibrating climate impacts

This module combines physical climate projections with our empirically estimated damage functions to construct forward-looking, region- and sector-specific economic shocks.[10] Climate models describe how temperature, precipitation, flood risk and sea levels evolve under alternative emissions

[8] This aggregation abstracts from endogenous adaptation through changes in crop mix in response to evolving relative yields. In other words, crop and livestock production weights are held fixed at their baseline levels, so that productivity shocks reflect changes in agro-climatic conditions absent any endogenous reallocation within agriculture.

[9] The role of land as an input into the real estate sector, and its interaction with housing supply, firm location, and production costs, is modelled explicitly within the quantitative spatial general equilibrium framework described in Section 4 and, in more detail, in Appendix E.

[10] Note we estimate empirical damage functions for heat stress and flooding impacts only. The physical impacts of changes in agro-climatic conditions and sea level rise are obtained directly from existing climate projections.

pathways, but these projections are not directly usable in an economic model. We therefore translate projected changes in climate conditions and their associated costs into calibrated shocks to the model. This calibration step ensures internal consistency across hazards and provides a transparent mapping from physical climate impacts to fundamental determinants of economic output in the general equilibrium model.

### 3.1. Climate projections

To project future climate impacts consistently across the four climate hazards—heat stress, flooding, changes in agro-climatic conditions, and sea-level rise—we combine historical impact estimates with geographically disaggregated climate projections based on Shared Socioeconomic Pathways (SSPs) and their associated radiative forcing pathways. We consider two scenarios: SSP2-4.5, an intermediate-emissions pathway, and SSP5-8.5, a very high-emissions pathway. SSP2-4.5 combines a middle-of-the-road socioeconomic trajectory, characterised by moderate population and economic growth and gradual technological progress, with radiative forcing of approximately 4.5 $\mathrm{W\,m^{-2}}$ by 2100. SSP5-8.5 reflects rapid fossil-fuel-driven economic growth, energy-intensive development, and limited climate mitigation, with radiative forcing of approximately 8.5 $\mathrm{W\,m^{-2}}$ by 2100. The IPCC's assessed best estimates of global mean warming for 2081–2100 relative to 1850–1900 are 2.7 °C under SSP2-4.5 and 4.4 °C under SSP5-8.5 (IPCC, 2021).

We use SSP2-4.5 as our central benchmark and retain SSP5-8.5 as a higher-warming comparison to examine economic losses and adjustment mechanisms under more severe climate change. Recent assessments regard the emissions levels underlying SSP5-8.5 as implausible in light of developments in energy technologies, climate policies, and emissions trends (van Vuuren et al., 2026). The reduced plausibility of this emissions pathway does not rule out warming comparable to that projected under SSP5-8.5, given uncertainty in carbon-cycle feedbacks and climate sensitivity (Hausfather, 2025).[11] These scenarios provide conditional assessments rather than forecasts, and we do not assign probabilities to them. In particular, SSP2-4.5 is not treated as a direct projection of currently implemented climate policies.

Using these scenarios, we obtain projections of future temperature patterns, flooding events, sea-level rise, and agro-climatic conditions. This provides a coherent basis for assessing how the frequency and intensity of different climate hazards are expected to evolve over time and for translating these changes into sector- and region-specific economic damages. It is worth noting, however, that the use of climate projections to construct future impact scenarios entails important sources of uncertainty. First, climate models differ in their spatial and temporal resolution, which can affect their ability to capture highly localised climate conditions and short-lived extreme events. Coarse spatial units may fail to capture localised extreme weather events or heterogeneous weather

[11] Carbon-cycle feedbacks, including carbon release from thawing permafrost and changes in natural carbon uptake, can increase atmospheric greenhouse-gas concentrations for a given anthropogenic emissions trajectory. Separately, uncertainty in climate sensitivity affects warming for a given radiative forcing level. These uncertainties do not establish that lower anthropogenic emissions would reproduce SSP5-8.5 forcing by 2100 (Sarofim et al., 2024). Our simulations use the scenario-specific climate projections and do not model these feedbacks separately.

patterns within broader regions. Second, climate projections are inherently uncertain due to a combination of emissions uncertainty, climate model uncertainty, and internal climate variability.[12]

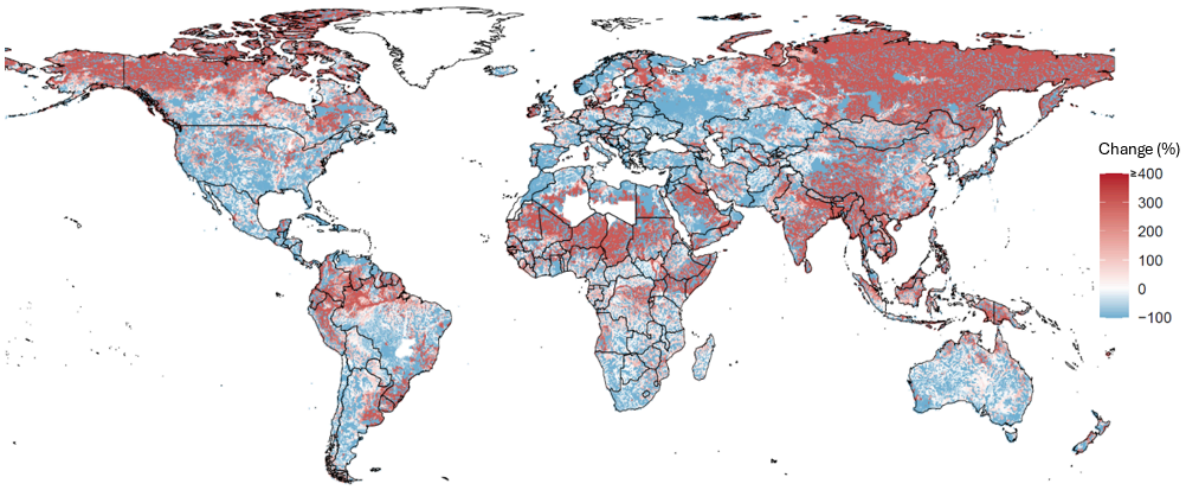
### 3.1.1 Flood projections

Projecting future flood risk requires linking changes in climatic conditions to existing protection standards and baseline probability of flooding. Observed flood exposure reflects not only natural hydrological processes but also the capacity of local flood protection infrastructure. We therefore combine spatially detailed information on current protection levels from the FLOPROS (Flood Protection Standards) database (Scussolini et al., 2016) with forward-looking hazard projections to assess how the effective probability of damaging floods evolves under climate change, holding protection infrastructure fixed at historical levels.

Future riverine and coastal flood hazards are derived from global climate-driven hydrological projections provided by the World Resources Institute. For each location, we evaluate whether projected flood depths exceed the historical protection threshold implied by local protection standards. An increase in exceedances implies a higher likelihood of overtopping or protection failure, and thus a rise in the frequency of damaging flood events. This framework isolates the effect of climatic shifts on flood risk, abstracting from endogenous adaptation or future upgrades in protection.

**Figure 2:** Effect of climate change on flood frequency in 2080 relative to 1980

Percent change in the annual frequency of riverine flooding under RCP8.5 (ensemble mean)




*Source:* Scussolini et al. (2016), World Resources Institute (Aqueduct), and authors' own calculations.
*Notes:* The map reports values at the resolution of a 0.25° × 0.25° grid cell (approximately 25 km at the equator). Values greater than 400% are winsorised at 400%. The projections assume flood protection standards remain the same as in the baseline period (i.e. 1980).

The resulting projections reveal substantial spatial heterogeneity in changes in flood frequency

[12]Following standard practice in the literature, our analysis relies on bias-corrected, geographically disaggregated climate data and on multi-model ensembles of climate models to characterise variation in projected climate outcomes within each scenario.

(Figure 2). Under RCP8.5, some regions experience pronounced increases in riverine flood occurrence by the end of the century, while others display more moderate changes or localised reductions. Importantly, the reported changes are relative to each location's baseline probability of flooding. Regions that are historically dry may register large proportional increases despite remaining low risk in absolute terms, whereas densely populated floodplains with high baseline risk may exhibit smaller percentage changes despite substantial exposure.

To assess economic relevance, we combine the geographic extent of flood-prone areas with spatial population data provided by the Gridded Population of the World, Version 4 (GPWv4) dataset. This allows us to compute, for each location, the share of the population residing in areas subject to flooding under baseline protection standards. We do this by first identifying the pixels in which the projected flood depth exceeds zero in a 1-in-100-year flood and then computing the share of total population in each GPW grid cell residing in flood-exposed land.

### 3.1.2 Heat projections

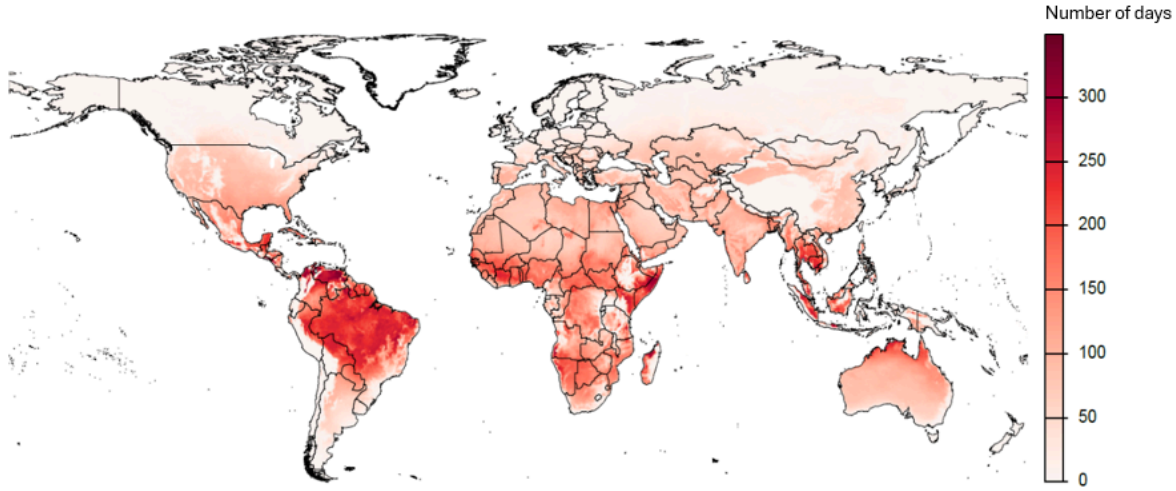
We use the World Bank's Climate Change Knowledge Portal (CCKP) to obtain projections of future annual hot days and average annual temperatures. The dataset compiles climate projections from 29 general circulation models, providing annual realisations of key climate variables on a $0.25° \times 0.25°$ grid (approximately 28 km $\times$ 28 km at the equator). From these projections, we extract the annual number of days exceeding 30°C, 35°C and 40°C, as well as average annual temperatures, under different emissions pathways.[13] We then combine these climate projections with our productivity impact estimates to construct a panel of annual, sector-level productivity losses from heat stress for each subnational region over the period 2025–2100. To isolate the effect of future climate conditions on heat stress - recognising that high temperatures would still occur regardless of which future climate scenario is considered - we compare projected hot days in each scenario to a no-climate-change baseline. Specifically, we measure heat-related productivity changes relative to average conditions over 1950–1979.

Figure 3 shows that projected increases in the number of hot days are highly uneven across the globe, with the largest changes concentrated in low-latitude regions. Panel A indicates that days above 35°C are expected to rise sharply across much of the tropics and subtropics, with even mid-latitude regions - including the southern United States and the Mediterranean - experiencing noticeable increases. Panel B reveals an even more concentrated pattern for days above 40°C: the largest increases occur in a broad belt stretching from North Africa through the Middle East into South Asia, where many areas see more than 100 additional days per year exceeding this extreme threshold. Outside this band, and in most OECD regions, increases in 40°C days remain modest. Overall, the maps underscore the strong latitudinal gradient in exposure to extreme heat, with the most dramatic intensification occurring in regions that are already among the hottest in the world.

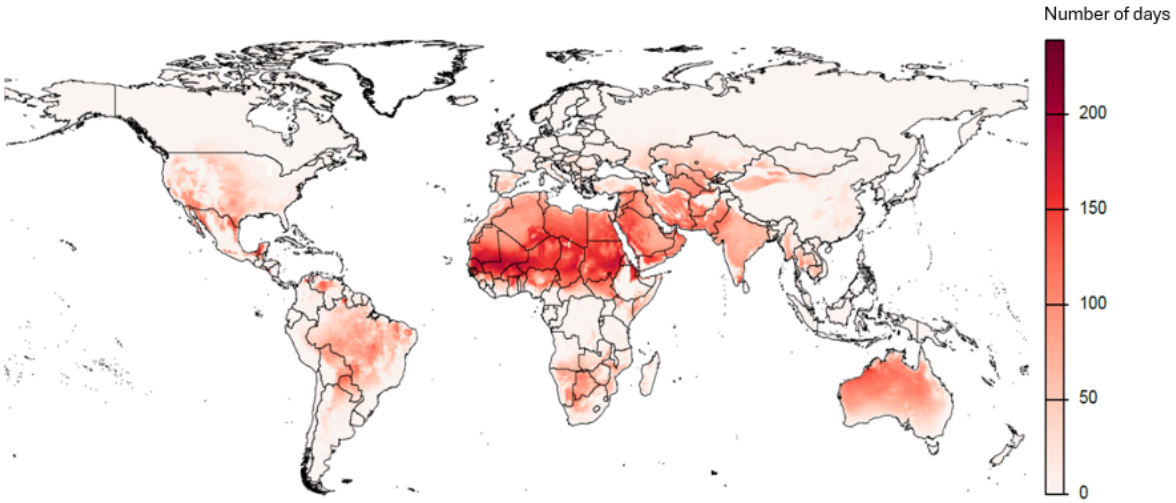
[13] We take the median value provided by the CCKP which corresponds to the median projection across all general circulation models included in the CCKP sample. We apply GIS spatial matching tools to match the administrative units in the CCKP data with the 927 regions used in the model calibration shown later.

**Figure 3:** Projected change in annual number of hot days (2081-2100 vs 1950-1979) under the very high-emissions scenario (SSP5-8.5)

**(a)** Change in annual number of days above 35°C




**(b)** Change in annual number of days above 40°C




*Source:* Climate Change Knowledge Portal (World Bank) and authors' own calculations.

### 3.1.3 Projections of agro-climatic conditions

Figure 4 shows the estimated change in average agro-climatic potential yields in 2071–2100 relative to 2011–2040 under RCP8.5 across all fifteen crops, weighted by their production value in each location. The figure excludes impacts on livestock, which we capture separately through changes in grassland yields. The map reveals a predominantly negative pattern, with substantial declines in several major mid-latitude agricultural zones, including parts of the United States, southern Europe, and Australia among OECD countries, as well as much of Sub-Saharan Africa, Central and South America, and South and Southeast Asia. By contrast, some high-latitude regions - most notably Canada and the northern United States, and northern Europe - show pockets of projected yield gains, reflecting potential benefits from longer growing seasons and improved thermal conditions. Nevertheless, these gains are relatively limited in spatial extent compared with the widespread declines observed elsewhere.

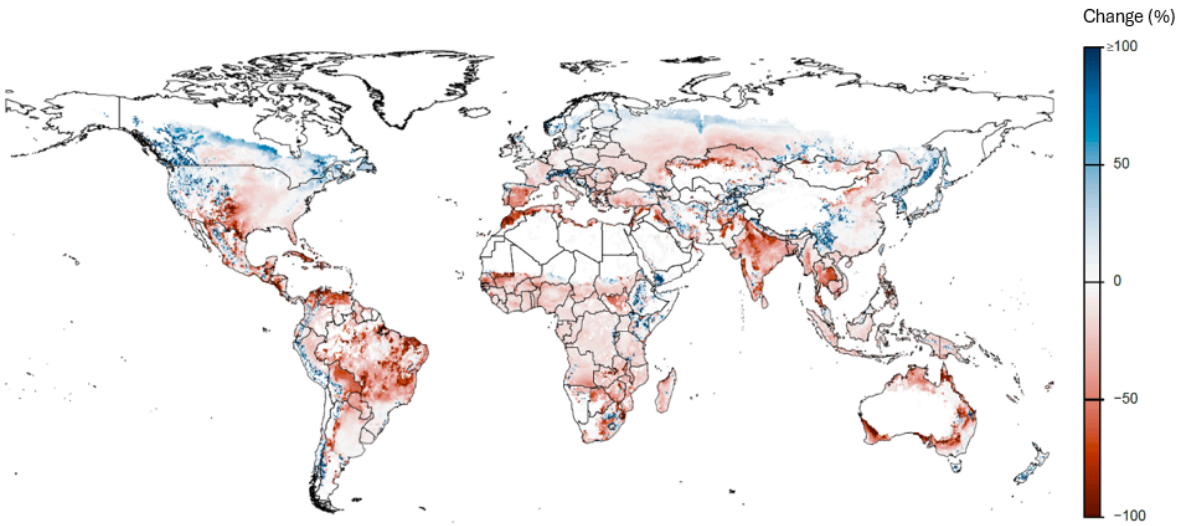
The map highlights a clear global asymmetry: agro-climatic potential yield decreases are concentrated in regions that are already warm and agriculturally vulnerable, while potential gains are restricted to a narrow set of cooler areas. Taken together, these projections suggest a systematic redistribution of agricultural potential away from many of today's major crop-producing regions in the Global South towards regions in the Global North, with important implications for global food production, trade patterns, and food security. Figure A.2 in Annex A shows the projected change in agro-climatic potential yields for the four crops that account for the largest share of global human and animal calorie consumption - maize, wheat, rice and soybeans. The figure reveals substantial spatial heterogeneity in the projected impacts of future climate on agro-climatic potential yields, with clear differences both across crops and across regions. These estimates underscore that future climate will likely alter the geographic distribution of comparative advantage in crop production.

### 3.1.4 Sea-level rise

In line with our treatment of flood exposure, we construct a measure of population potentially affected by sea level rise. To do so, we overlay high resolution (30 arc-seconds) historical coastal flood hazard maps for a 1-in-1000-year event from the WRI with gridded population data. This very high return-period threshold allows us to capture the full extent of low-lying coastal areas that, while rarely flooded under historical conditions, may be increasingly exposed as sea levels rise in the future. As before, we use population data from GPWv4 as a proxy for the underlying distribution of capital and economic activity. Then, to identify which of these areas will be permanently inundated, we rely on future coastal flood hazard maps from WRI to estimate the annual probability of coastal flooding in each grid cell, assuming coastal protection standards remain at their historical levels. Grid cells that at any moment in time have an estimated annual flooding probability exceeding 50% are assumed to become effectively uninhabitable.

We combine these two layers - the areas classified as permanently flooded and the population in flood-prone coastal zones - to estimate the share of land that effectively becomes uninhabitable.

**Figure 4:** Projected change in crop yields in 2071-2100 relative to 2011-2040 under the very high-emissions scenario (SSP5-8.5)




*Source:* FAO-GAEZ and authors' own calculations.
*Notes:* The map reports values at the resolution of a 0.25° × 0.25° grid cell (approximately 25 km at the equator). Values greater than 100% are winsorised at 100%. The central projection uses the median yield change across the five climate models for each crop before aggregation across crops.

This population-weighted measure serves as a proxy for the reduction in the effective supply of productive land due to sea level rise and provides a direct input into the model as a negative shock to local land availability.

Figure 5 illustrates the share of the population living in areas projected to be permanently submerged by 2100 under RCP8.5. Exposure in OECD countries is highly concentrated in a limited number of low-lying coastal regions, particularly in sections of the Gulf Coast of the United States and in Northern Europe. In contrast, most of the world's interior regions and higher-elevation coastlines show negligible exposure. Importantly, this map reflects areas expected to be permanently inundated, rather than subject to episodic flooding, and therefore highlights zones where continued human settlement would require substantial protective infrastructure or relocation. These estimates represent potential physical exposure and do not account for future adaptation measures, such as building or reinforcing coastal defences, that could mitigate realized impacts.

### 3.2. Calibration of climate impacts

The final step translates the local damage estimates and physical projections into changes in the economic fundamentals of the spatial general equilibrium model. The four hazards enter through three distinct channels: sectoral productivity $A_{nt}^{j}$, flood-related destruction of inherited capital $d_{nt}$, and usable land $T_{nt}$. The shocks are constructed for the 927 model regions using the hazard-specific reference conditions described above. They are imposed on these fundamentals rather than

**Figure 5:** Population affected by sea level rise in 2100 under the very high-emissions scenario (SSP5-8.5)

Percentage of population living in land that will be permanently submerged (ensemble median)




*Source:* World Resources Institute (Aqueduct), Gridded Population of the World (GPW v4.11), and authors' own calculations.
*Notes:* The map reports values at the resolution of a 0.25° × 0.25° grid cell (approximately 25 km at the equator). Values greater than 60% are winsorised at 60%.

directly on GDP, allowing the model to determine how local damages affect production, prices, capital accumulation, and the spatial allocation of workers.

For heat stress, projected hot-day exposure is combined with the estimated productivity responses, accounting for differences in temperature intensity and local climatic conditions, to construct non-agricultural productivity shocks. Agricultural productivity shocks instead draw on projected changes in crop yields, aggregated using baseline production-value weights. Flood projections are combined with local exposure and the calibrated severity of capital destruction to construct annual flood-damage inputs. The event-level destruction parameter is calibrated to reproduce the observed post-flood capital-stock response, rather than equating that response directly with the fraction of capital destroyed on impact. Finally, sea-level rise reduces effective usable land through the population-weighted measure of exposure to permanent inundation described above. This measure serves as a proxy for economically relevant land loss, rather than a direct measure of the geographical share of land submerged. Appendix E.3.9 provides further details on how the hazard-specific projections are translated into model inputs.

Appendix Figure E.1 maps the resulting climate-damage inputs in 2100 under the intermediate-emissions benchmark and the very high-emissions scenario. Heat-related productivity losses are concentrated in warmer regions, whereas agricultural impacts vary more widely in sign and magnitude across locations. Riverine flood damage to capital and sea-level-rise effects on usable land are more geographically concentrated, reflecting local exposure to these hazards. Common colour scales within each impact channel are used in order to facilitate comparison across scenarios. These

maps describe the direct shocks imposed on the model, whose aggregate and regional economic consequences are examined in the following sections.

## 4. The climate and adaptation spatial general equilibrium model (CASGEM)

Our model describes a dynamic spatial economy composed of multiple subnational locations across different countries, where households and firms interact through production, trade, and migration. The framework draws on contributions to economic geography (Krugman, 1991), Ricardian trade (Eaton and Kortum, 2002; Costinot et al., 2016), regional production networks (Caliendo et al., 2018), migration and spatial adjustment (Desmet and Rossi-Hansberg, 2015; Conte, 2026), and dynamic adjustment with capital accumulation (Kleinman et al., 2023).[14] These building blocks capture how local advantages, economic networks, and mobility costs jointly determine outcomes across regions. Trade and migration frictions influence the distribution of workers and production across space, as well as the degree of vulnerability to local and external shocks, while input–output linkages and capital accumulation shape the transmission and persistence of these shocks.

### 4.1. Model description

The model distinguishes workers, capital owners, and landowners. Workers choose where to live based on amenities, real wages, and migration frictions, and allocate their income between goods and housing. Capital owners and landowners are immobile: capital owners use rental income to consume and invest, while landowners spend their land rents on goods. On the production side, intermediate goods producers combine labour, capital, floor space, and material inputs to produce differentiated varieties. Final goods producers source these varieties from the lowest-cost suppliers, taking trade costs into account, and combine them into sectoral goods used for consumption, investment, and intermediate production. A competitive real estate sector combines land and capital to supply housing and commercial floor space.

We describe these building blocks and their interactions below, beginning with the economic environment and the timing of climate damages and adjustment. Appendix E provides the supporting derivations and the complete equilibrium system.

#### 4.1.1 Environment and timing

There are $N$ locations and $J$ production sectors, with $\sigma(n)$ denoting the country to which location $n$ belongs. Each location has amenities $B_n > 0$, sectoral productivities $A_{nt}^j$, and an exogenously given supply of usable land $T_{nt}$. Goods trade and migration are subject to bilateral frictions. Throughout, the first index of a bilateral share or friction denotes the destination and the second denotes the origin.

[14] See Redding and Rossi-Hansberg (2017) for a review of quantitative spatial economics and Desmet and Rossi-Hansberg (2024) for a review of its applications to climate change.

The climate-damage estimates enter through three sets of fundamentals: heat stress and changes in agro-climatic conditions affect $A_{nt}^{j}$, flooding destroys a fraction $d_{nt} \in [0, 1)$ of inherited capital, and sea-level rise reduces $T_{nt}$. Capital inherited at the beginning of period $t$ is denoted by $K_{nt}$. Flood destruction occurs before production, leaving $\widetilde{K}_{nt} = (1 - d_{nt})K_{nt}$ available for use during that period. Workers choose locations, and current wages, goods prices, and structures rents adjust jointly to clear markets. After production, ordinary depreciation and investment determine the capital stock inherited in the next period. Capital accumulation and changes in the population distribution therefore generate transition dynamics, even though workers' location choices depend on current utility rather than a continuation value.

### 4.1.2 Workers and labour mobility

Workers supply one unit of labour inelastically, earn the local wage $w_{nt}$, and spend their entire income on goods and housing. They allocate the share $\alpha \in (0, 1)$ of expenditure to goods and the remaining share to housing services, rented at price $Q_{nt}$. Goods consumption is a Cobb–Douglas aggregate across sectors, with expenditure shares $\alpha^{j} > 0$ summing to one and price index $P_{nt} = \prod_{j}(P_{nt}^{j})^{\alpha^{j}}$.

A worker $\omega$ initially located in $i$ chooses a destination $n$ to maximise current indirect utility:

$$V_{it}(\omega) = \max_{n \in \{1,\dots,N\}} \left\{ \frac{b_{ni,t}(\omega)}{\kappa_{ni}} \frac{B_n w_{nt}}{P_{nt}^{\alpha} Q_{nt}^{1-\alpha}} \right\}. \tag{1}$$

Here, $\kappa_{ni}$ is a multiplicative utility cost of moving from $i$ to $n$, with staying costs normalised to $\kappa_{ii} = 1$. The idiosyncratic location preferences $b_{ni,t}(\omega)$ are independently drawn across workers, destinations, and periods from a Fréchet distribution $F(b) = \exp(-b^{-\varepsilon})$, where $\varepsilon > 0$. These preferences imply that the share of workers from origin $i$ choosing destination $n$, including those who stay, is

$$\lambda_{nit} = \frac{\left[B_n w_{nt} / (\kappa_{ni} P_{nt}^{\alpha} Q_{nt}^{1-\alpha})\right]^{\varepsilon}}{\sum_{m=1}^{N} \left[B_m w_{mt} / (\kappa_{mi} P_{mt}^{\alpha} Q_{mt}^{1-\alpha})\right]^{\varepsilon}}. \tag{2}$$

Migration therefore responds to differences in amenities and real wages, while migration frictions limit reallocation. The parameter $\varepsilon$ governs the responsiveness of location choices to differences in destination attractiveness: a higher value implies a stronger response of migration odds to changes in relative amenities, wages, or living costs.

Let $L_{it}^{-}$ denote the population in origin $i$ immediately before migration in period $t$, incorporating the external population assumptions described in Appendix E. The population available for production in destination $n$ is

$$L_{nt} = \sum_{i=1}^{N} \lambda_{nit} L_{it}^{-}. \tag{3}$$

Migration redistributes this population across locations. Workers can move freely across sectors within a location, so all sectors face the same local wage in the unrestricted equilibrium.

### 4.1.3 Production and trade

Intermediate goods producers hire labour, capital, and floor space and purchase material inputs from all sectors, including their own. A producer of variety $\iota^j$ in location $n$ and sector $j$ has technology

$$q_{nt}^j(\iota^j) = A_{nt}^j z_n^j(\iota^j) \left[(L_{nt}^j(\iota^j))^\lambda (K_{nt}^j(\iota^j))^\eta (H_{nt}^j(\iota^j))^{1-\lambda-\eta}\right]^{\beta_n^j} \prod_{k=1}^{J} (M_{nt}^{jk}(\iota^j))^{\gamma_n^{jk}}. \tag{4}$$

The inputs $L$, $K$, and $H$ denote labour, capital services, and floor space, while $M^{jk}$ denotes purchases of goods from sector $k$. The parameter $\beta_n^j$ is the expenditure share on the labour–capital–floor-space bundle, within which $\lambda$, $\eta$, and $1-\lambda-\eta$ are the respective input shares. The parameters $\gamma_n^{jk}$ are expenditure shares on material inputs from sector $k$ and describe the input–output linkages across sectors. The parameters satisfy $\lambda > 0$, $\eta > 0$, $\lambda + \eta < 1$, and $\beta_n^j + \sum_k \gamma_n^{jk} = 1$.

Idiosyncratic productivity follows a Fréchet distribution $F_j(z) = \exp(-z^{-\theta^j})$, independently across locations and varieties. Cost minimisation implies the input-bundle cost

$$x_{nt}^j = \mu_n^j \left(w_{nt}^\lambda r_{nt}^\eta Q_{nt}^{1-\lambda-\eta}\right)^{\beta_n^j} \prod_{k=1}^{J} (P_{nt}^k)^{\gamma_n^{jk}}, \tag{5}$$

where $r_{nt}$ is the rental price of capital and $\mu_n^j$ is a constant determined by expenditure shares. Production networks transmit shocks through the prices of intermediate inputs, while wages, capital rentals, and structures rents transmit changes in local factor scarcity. Under perfect competition, a variety's factory-gate price equals its input-bundle cost divided by its productivity, $x_{nt}^j/[A_{nt}^j z_n^j(\iota^j)]$. Delivered prices additionally reflect bilateral trade costs.

Competitive final goods producers combine varieties with elasticity of substitution $\nu > 1$ and source each variety from the supplier offering the lowest delivered price. Shipping goods from origin $i$ to destination $n$ incurs iceberg cost $\tau_{ni}^j \geq 1$, with $\tau_{nn}^j = 1$. The expenditure share on goods from origin $i$ is

$$\pi_{nit}^j = \frac{(A_{it}^j)^{\theta^j}(x_{it}^j \tau_{ni}^j)^{-\theta^j}}{\sum_{m=1}^{N}(A_{mt}^j)^{\theta^j}(x_{mt}^j \tau_{nm}^j)^{-\theta^j}}, \tag{6}$$

and the corresponding sectoral price index is

$$P_{nt}^j = g^j \left[\sum_{i=1}^{N}(A_{it}^j)^{\theta^j}(x_{it}^j \tau_{ni}^j)^{-\theta^j}\right]^{-1/\theta^j}. \tag{7}$$

The parameter $\theta^j$ governs productivity dispersion and the responsiveness of sourcing shares to relative costs: a higher value implies less dispersion and greater sensitivity to cost differences across origins. The constant $g^j$ depends on $\nu$ and $\theta^j$, with $\theta^j > \nu - 1$ ensuring a finite price index. Appendix E gives its expression and describes the parameterisation of bilateral trade and migration costs in the calibration subsections. These equations connect local productivity and

production costs to sourcing patterns and goods prices throughout the economy. Sectoral goods are used for consumption, investment, and intermediate production.

#### 4.1.4 Structures and land

A competitive real estate sector combines capital services and land to supply structures, which workers use as housing and intermediate goods producers use as floor space:

$$H_{nt} = (K_{nt}^H)^{\mu} T_{nt}^{1-\mu}, \qquad 0 < \mu < 1. \tag{8}$$

Housing and commercial floor space draw on the same local supply of structures and therefore face a common rental price $Q_{nt}$. Capital employed in real estate, $K_{nt}^H$, is drawn from the surviving local stock and earns the same rental rate as capital used in intermediate goods production. Cost minimisation implies $r_{nt}K_{nt}^H = \mu Q_{nt}H_{nt}$. Immobile local landowners receive the remaining revenue as land rents, $\mathcal{R}_{nt}^T = (1-\mu)Q_{nt}H_{nt}$, and spend it on goods with sectoral shares $\alpha^j$. They do not save or supply labour. A reduction in usable land raises the cost of supplying structures, affecting both workers' housing costs and firms' production costs.

#### 4.1.5 Capital accumulation

Capital owners are immobile and rent the surviving stock $\widetilde{K}_{nt}$ to intermediate goods producers and the real estate sector. Rental income $r_{nt}\widetilde{K}_{nt}$ constitutes their sole income source. They choose consumption and investment to maximise discounted logarithmic utility, taking prices and flood-related destruction as given. Consumption and investment use the same local final good, priced at $P_{nt}$, and $C_{nt}^K$ denotes capital owners' goods consumption. Investment is reversible at this price within a location, but capital cannot be transferred across locations. Surviving capital depreciates at the ordinary rate $\bar{\delta} \in [0,1)$ after production, giving the budget constraint

$$P_{nt}C_{nt}^K + P_{nt}\left[K_{n,t+1} - (1-\bar{\delta})\widetilde{K}_{nt}\right] = r_{nt}\widetilde{K}_{nt}. \tag{9}$$

Available resources consist of real rental income plus the undepreciated value of surviving capital. Under logarithmic utility, capital owners consume a fraction $1-\beta$ of these resources and carry the remaining fraction $\beta$ into the next period as capital, where $\beta \in (0,1)$ is the discount factor.[15] Capital therefore evolves according to

$$K_{n,t+1} = \beta\left(\frac{r_{nt}}{P_{nt}} + 1 - \bar{\delta}\right)(1-d_{nt})K_{nt}. \tag{10}$$

Flooding reduces both capital available for current production and the resources from which future capital is accumulated. Its effects persist through the capital stock, while investment responds endogenously to local rental returns and goods prices. Appendix E states the intertemporal problem

[15] With rental income as the sole income source, a linear accumulation technology, and reversible investment, logarithmic utility implies a constant saving fraction, as in Kleinman et al. (2023, Lemma 1).

and the associated consumption rule.

#### 4.1.6 Equilibrium and transmission

Equilibrium requires goods and factor markets to clear in every location. Let $X_{nt}^j$ denote total expenditure on sector-$j$ goods in destination $n$. Producer revenue in location $n$ and sector $j$ equals sales across destinations, $R_{nt}^j = \sum_i \pi_{int}^j X_{it}^j$.

Final expenditure on goods includes workers' consumption, capital owners' consumption and investment, and landowners' consumption. Capital owners' consumption and investment together exhaust their rental income, so their combined contribution to final expenditure is $r_{nt}\widetilde{K}_{nt}$. Using the capital owners' budget constraint gives $E_{nt} = \alpha w_{nt} L_{nt} + r_{nt}\widetilde{K}_{nt} + \mathcal{R}_{nt}^T$. Goods market clearing requires

$$X_{nt}^j = \sum_{k=1}^{J} \gamma_n^{kj} R_{nt}^k + \alpha^j E_{nt}. \tag{11}$$

The first term is intermediate demand from local producers in all sectors, and the second is final demand. Labour, capital, and structures market clearing imply

$$w_{nt} L_{nt} = \sum_{j=1}^{J} \lambda \beta_n^j R_{nt}^j, \tag{12}$$

$$r_{nt}\widetilde{K}_{nt} = \sum_{j=1}^{J} \eta \beta_n^j R_{nt}^j + \mu Q_{nt} H_{nt}, \tag{13}$$

$$Q_{nt} H_{nt} = (1-\alpha) w_{nt} L_{nt} + \sum_{j=1}^{J} (1-\lambda-\eta) \beta_n^j R_{nt}^j. \tag{14}$$

Capital-market clearing includes both goods production and real estate, while structures accommodate both housing and firms' floor-space demand. Local ownership of capital and land, together with the absence of interregional financial transfers, implies trade balance at the location level. Bilateral and sectoral trade balances need not be zero.

An equilibrium is a sequence of prices and allocations satisfying workers' location and consumption choices, capital owners' saving decisions, firms' cost minimisation, and all market-clearing conditions, given initial capital and population, economic frictions, and the exogenous paths of climate-related fundamentals. Appendix E collects the complete system and provides the derivations of the conditions used above.

A local climate shock changes production costs and factor incomes, affecting trade shares and the prices of intermediate and final goods across connected locations. Changes in real wages induce labour reallocation, which in turn affects local factor scarcity and expenditure. Rental returns and goods prices also influence capital accumulation, carrying the effects into future periods. The distinction between these transmission mechanisms and the ability to adjust trade and labour allocations motivates the counterfactual exercises in Sections 5.2 and 5.3.

### 4.2. Model calibration

We calibrate the model to observed patterns of economic activity, trade, and migration across locations. This subsection describes the coverage and data, the parameters and fundamentals that discipline the model, and the construction of the initial economy and reference path. Appendix E provides the detailed calibration procedures.

#### 4.2.1 Coverage and data

The model is calibrated for 927 regions across 186 countries, covering 11 sectors of production in OECD member countries and three aggregate sectors—agriculture, manufacturing, and services—in all other countries. For OECD members, we use Territorial Level 2 (TL2) regions; for OECD accession countries and key partners, we use first-level administrative units from the GADM database; and for the remaining countries, we treat each country's territory as a single location. Figure A.3 maps the calibrated regions. Appendix E.3.1 provides the country groupings and sectoral classification.

The calibration combines information on regional economic activity, production linkages, trade, and labour mobility. OECD regional accounts provide gross value added, employment, and population for member countries, complemented by the Database of Sub-national Economic Output (DOSE v2) for accession countries and key partners and the World Bank's World Development Indicators for the remaining countries. OECD input–output tables discipline sectoral production and expenditure shares, while the International Trade and Production Database for Estimation (ITPD-E) provides bilateral trade flows. International migration is measured using the OECD International Migration Database and the global flow estimates of Abel and Cohen (2019), based on UN DESA migrant stocks; OECD regional mobility data discipline internal migration. Appendix E.3.2 describes the datasets, their coverage, and the construction of the calibration inputs.

#### 4.2.2 Parameters and calibration

We combine parameters taken from the literature, shares constructed from the data, and economic fundamentals recovered through model inversion. Table 1 summarises these components; Table E.2 in Appendix E provides the detailed parameter inventory. We set the trade elasticity to $\theta^j = 6$ across sectors (Eaton and Kortum, 2002) and the location-choice parameter to $\varepsilon = 4.5$ (Morten and Oliveira, 2024). These parameters govern the responsiveness of trade and migration to differences in relative costs and destination attractiveness. The elasticity of structures supply with respect to its rental price, holding the capital rental rate fixed, is set to $\zeta = 1.75$, drawing on Saiz (2010). Workers allocate 66% of expenditure to goods and the remaining 34% to housing services. Capital owners' discount factor is set to $\beta = 0.95$, and ordinary capital depreciation is set to 5% per year.

Model inversion uses observed economic activity and the model's equilibrium conditions to recover unobserved fundamentals, including local productivities, amenities, and spatial frictions.

**Table 1:** Overview of the model calibration

| Calibration block | Model objects | Source or empirical information |
|---|---|---|
| Trade response | $\theta^j = 6$ | Eaton and Kortum (2002) |
| Migration response | $\varepsilon = 4.5$ | Morten and Oliveira (2024) |
| Structures supply | $\zeta = 1.75$ | Saiz (2010) |
| Goods and housing expenditure | $\alpha = 0.66$ | Goods receive 66% of workers' expenditure; housing receives 34% |
| Saving and capital accumulation | $\beta = 0.95$ | Capital owners' discount factor |
| Capital depreciation | $\bar{\delta} = 0.05$ | Annual depreciation rate |
| Production and expenditure | $\beta_n^j$, $\gamma_n^{jk}$, $\alpha^j$ | OECD input–output tables |
| Trade frictions | $\tau_{ni}^j$ | Bilateral trade and domestic expenditure shares; geographical distance |
| Local productivities | $A_n^j$ | Wages, sectoral employment, and equilibrium expenditure and sourcing conditions |
| Migration frictions and amenities | $\kappa_{ni}$, $B_n$ | International flows, internal mobility, and the spatial distribution of population |
| Initial capital | $K_{n0}$ | Stationary capital conditional on the reference population distribution and historical climate |

*Notes:* The table summarises the main calibration blocks. Data sources and their coverage are described in Appendix E.3.2 and summarised in Table E.1; the detailed parameter inventory is reported in Table E.2. The elasticity $\zeta$ is defined holding land and the capital rental rate fixed.

We begin with trade. Following Head and Ries (2001), bilateral and domestic expenditure shares identify an index of bilateral trade costs relative to domestic costs. Together with the distance component, these estimates discipline the trade-cost matrix. Conditional on trade costs and the spatial distribution of sectoral expenditure and producer revenue, the gravity system of Anderson and van Wincoop (2003) recovers normalised price terms. We then use the production, expenditure, and sourcing conditions to recover local sectoral productivities consistent with observed wages and employment. These steps are linked by the equilibrium conditions, as detailed in Appendix E.

Migration costs and amenities are calibrated using international migration flows, within-country mobility, and the spatial distribution of population. Bilateral flows and geographical distance discipline cross-border and distance-related frictions. A nested moment-matching procedure then updates local mobility factors and amenities: conditional on amenities, mobility factors are adjusted to match observed movement rates; conditional on these factors, amenities are updated to match the population targets. The procedure is repeated until the targeted moments and parameter values converge. Figure A.4 in Appendix A shows that the model provides a good fit in describing the cross-country distribution of GDP per capita.

### 4.2.3 Initialisation and reference path

We initialise capital at a stationary stock conditional on the reference population distribution, calibrated fundamentals, and historical climate conditions. Starting from a guess for local capital stocks, we solve the within-period equilibrium and update capital using the accumulation equation until the stock in each location is unchanged. This initialisation does not require the full spatial economy to be in steady state: once the simulations begin, migration changes the distribution of population and capital responds to the resulting paths of rental returns and goods prices.

We define the calibrated model incorporating all the features described above as the baseline model. The baseline path is the implied equilibrium sequence over 2025–2100 when climate conditions remain fixed at their historical levels. This reference path can exhibit transition dynamics even in the absence of additional climate change. Climate-change simulations start from the same initial economy and introduce the projected changes in productivity, flood-related capital destruction, and usable land described in Section 3, holding the other scenario assumptions common to each comparison. Climate losses are measured relative to the corresponding baseline path. Appendix E.3.8 provides further details on initialisation and the scenario inputs.

## 5. Quantitative results

This section presents the macroeconomic implications of climate change generated by CASGEM. We begin by reporting the country-level impact of climate change on GDP per capita and other aggregate outcomes, capturing direct, local impacts, within-region propagation through supply chains, and cross-region and international spillovers through trade and mobility, as well as the ability of economies to adjust over time. This is computed by feeding projected damages from productivity losses, capital destruction, and loss of land, derived from the local, micro-level damages and climate projections, into the calibrated model. We solve for the economy's future equilibrium path in 2025-2100 and compare it to that of an economy in which losses from climate change are absent, i.e. the baseline path. This allows countries to interact through trade and migration and to adjust both patterns of specialization and population distribution as climate conditions evolve. This benchmark simulation provides us with a comprehensive estimate of climate damages.

We then use a sequence of counterfactual exercises to disentangle the mechanisms that shape these outcomes and to identify the channels through which economies adapt. These exercises address two questions. First, how much do economic linkages, both within and across regions, shape the transmission of climate shocks? Second, how important is the ability of economies to adjust trade and labour allocations in response to climate change?

The first set of counterfactuals examines how climate damages would unfold if key economic linkages were disabled. We begin by shutting down cross-region spatial linkages, preventing trade and migration flows across sub-national regions – including across those in the same country. This "local-only world" attributes all economic losses solely to local exposure and internal (i.e. within-region) adjustments. Comparing this to the full model highlights the role of cross-region spillovers

in amplifying or mitigating climate impacts. We then perform an additional experiment in which input–output linkages are removed. This allows us to isolate the importance of production networks and supply chains, i.e. firms' purchases of intermediate inputs from other firms, both domestic and foreign. Together, these two exercises show that both within- and cross-regional linkages shape the magnitude and distribution of climate damages.

The second set of counterfactuals examines the importance of adjustment through trade and labour reallocation. Economies remain interconnected, and we retain the baseline calibration, but restrict selected allocation shares to their no-climate-change paths. We first hold trade shares fixed while allowing labour allocations to adjust, then hold migration and sectoral labour shares fixed while allowing trade to adjust, and finally restrict both margins. Comparing each restricted scenario with the full model quantifies how adjustment through trade, labour reallocation, or their combination changes the magnitude and distribution of climate damages. These exercises provide complementary assessments of the mechanisms shaping climate damages. The first set changes the economy's linkages and requires recalibration, while the second retains the baseline calibration and restricts adjustment along selected margins. All simulations use the same climate projections, but the comparisons answer different questions about the role of economic integration and the scope for adjustment. The outcome reported throughout is real GDP per capita, which reflects changes in both production and population. It is distinct from workers' welfare, which depends on wages, goods and housing prices, amenities, location preferences, and migration costs. A location can attract workers while experiencing a decline in GDP per capita, since migration decisions depend on utility rather than average local production. Consequently, a larger local GDP per capita loss when adjustment is allowed does not, by itself, establish that workers are worse off.

### 5.1. The macroeconomic impact of climate change

Climate change generates substantial GDP per capita losses that intensify over time, with considerably larger impacts under the very high-emissions scenario. Relative to the no-climate-change baseline, global GDP per capita is 3% lower in 2050 and 6.4% lower in 2100 under the intermediate-emissions scenario (SSP2-4.5), compared with losses of 5.9% and 18.5%, respectively, under SSP5-8.5. Figure 6 compares the regional distribution and hazard composition of these impacts in 2100 under both scenarios. These estimates fall within the broad range reported in the climate-economics literature, although differences in warming trajectories, damage coverage, and modelling assumptions limit direct comparisons.[16]

The geographical distribution of losses is highly uneven under both scenarios. Under SSP2-4.5, GDP per capita losses by 2100 are approximately 7–10% in Northern Africa, Western Asia, Southern Asia, and Sub-Saharan Africa, compared with much smaller losses in Northern Europe.

[16]For high-warming projections towards the end of the century, Barrage and Nordhaus (2024) report global output losses of around 7%, while Burke et al. (2015) project losses of about 23%. Kahn et al. (2021) estimate losses of about 7% by 2100, and Kalkuhl and Wenz (2020) report losses of 7–14%. These estimates refer to different climate and economic scenarios and should therefore be interpreted as broad benchmarks rather than directly comparable predictions.

Under SSP5-8.5, losses reach approximately 25–30% in Northern Africa and Southern Asia and around 20% in Western Asia and Sub-Saharan Africa. Latin America and the Caribbean and Oceania also face substantial losses, of around 15% under the very high-emissions scenario. These regional comparisons show that the global average conceals considerably greater damages in several lower-latitude regions, while the gap between the two scenarios becomes especially consequential in locations that are already highly exposed.

Heat stress is the main source of economic losses across most world regions, including historically cooler areas such as Northern Europe and North America. Changes in agro-climatic conditions further increase losses in Northern Africa, Southern Asia, and Sub-Saharan Africa, while partly offsetting heat-related damages elsewhere. This offset is particularly visible in Central Asia under SSP2-4.5, but becomes much smaller relative to heat losses by 2100 under SSP5-8.5. The regional patterns therefore reflect both differences in exposure to individual hazards and whether their economic effects reinforce or offset one another. Flooding and sea-level rise generally make smaller contributions to the regional aggregates, although their effects remain important in exposed coastal and low-lying locations. Figures A.9 and A.10 in Annex A report the corresponding results for 2050 alongside the 2100 estimates, showing how the magnitude and composition of losses evolve over the century.

Country-level results illustrate the scale of these differences. Among the countries reported in Figures A.5 and A.6 in Annex A, Thailand and India face particularly large losses: GDP per capita is approximately 11% and 8% lower, respectively, by 2100 under SSP2-4.5, with losses increasing to around 30% and 27% under SSP5-8.5. Brazil, Indonesia, and South Africa also experience substantial losses under the very high-emissions scenario, alongside heavily affected OECD members such as Australia, Greece, and Mexico. For comparison, aggregate OECD losses reach 3.1% under SSP2-4.5 and 9% under SSP5-8.5 in 2100, below the corresponding global averages. The country charts cover the OECD+ group, with Figures A.7 and A.8 reporting the OECD subset.[17]

National averages also conceal substantial differences within countries, reflecting local exposure, economic structure, and interactions with other locations. Figures 7 and 8 show the spatial distribution of GDP per capita impacts in 2050 and 2100 under SSP2-4.5 and SSP5-8.5, respectively. The maps reveal variation within large economies such as Brazil, India, the United States, and Australia, alongside pronounced differences across neighbouring countries. Losses generally become more widespread and severe over time, particularly under SSP5-8.5, but local outcomes remain heterogeneous even where national averages indicate substantial damages. In some countries, the largest losses occur in regions that are already poorer, potentially widening regional income disparities.[18] This heterogeneity highlights the importance of subnational analysis wherever the calibration provides that detail, as country-level estimates can mask concentrations of economic vulnerability.

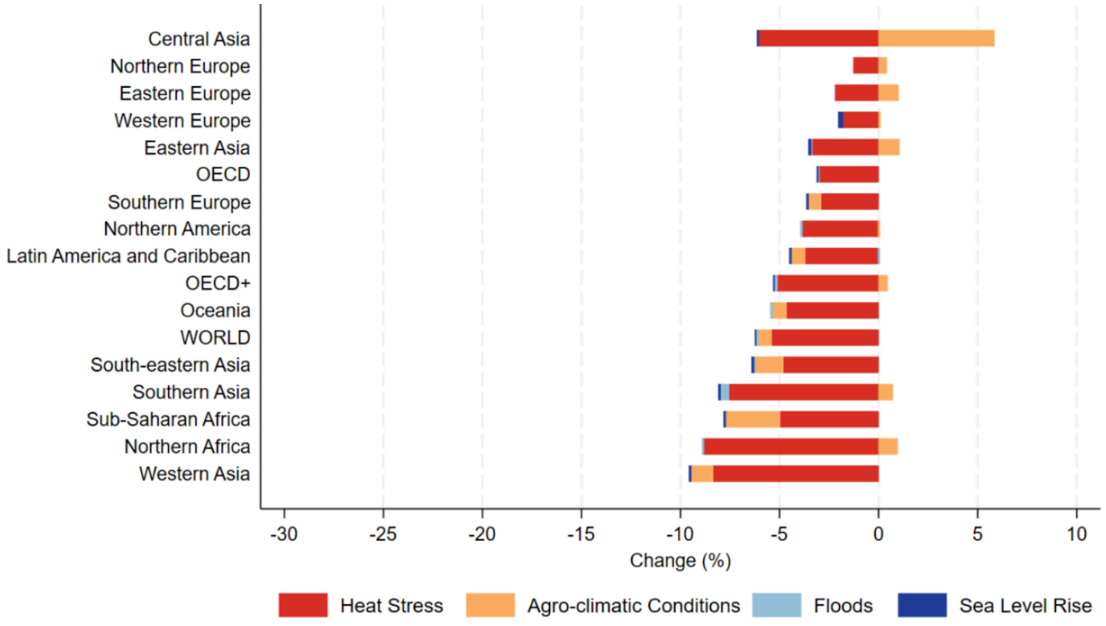
The projected magnitudes remain sensitive to uncertainty about future climate conditions. Fig-

[17] OECD+ includes OECD member countries, accession countries, and key partners.

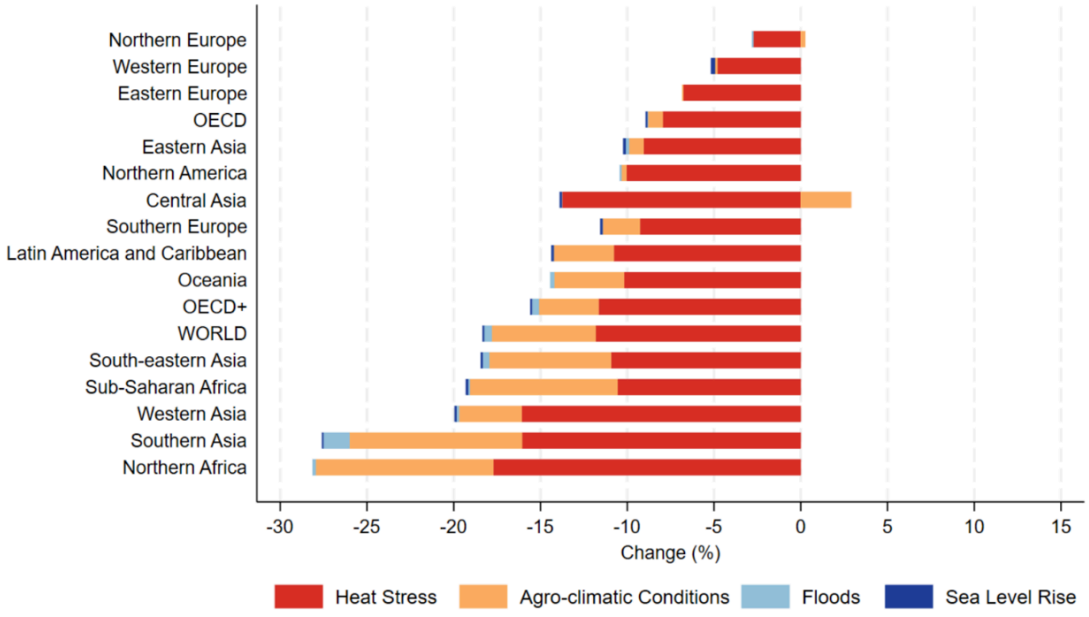
[18] For example, in Italy under SSP5-8.5, Sicily and Molise experience some of the largest losses by 2050, while South Tyrol and Trento experience gains.

**Figure 6:** Regional GDP per capita impacts by climate hazard in 2100

**(a)** Intermediate-emissions scenario (SSP2-4.5)



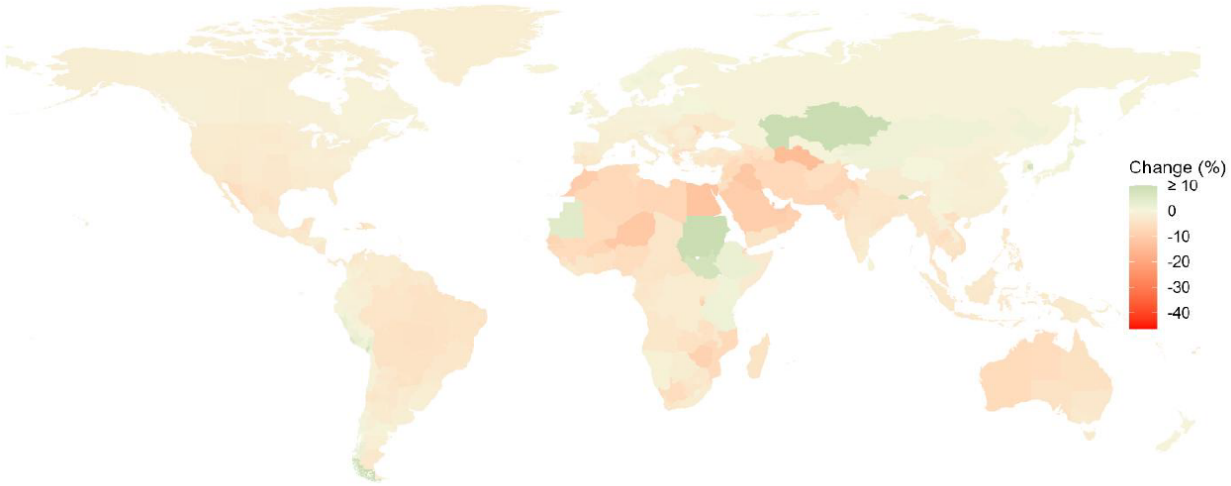

**(b)** Very high-emissions scenario (SSP5-8.5)



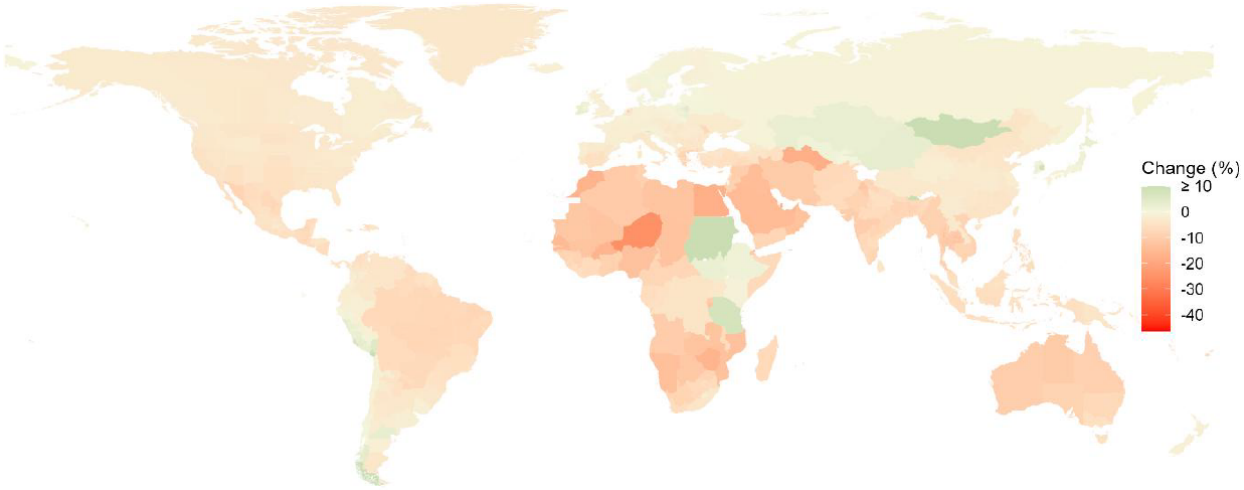

*Source:* Authors' calculations.
*Notes:* The panels show model-implied percentage changes in annual GDP per capita in 2100 relative to the no-climate-change baseline, by climate hazard. Regional impacts are computed as population-weighted averages of country-level impacts. OECD+ includes OECD member countries, accession countries, and key partners. Positive values indicate gains and negative values indicate losses. The complete results for 2050 and 2100 are reported in Figures A.9 and A.10 in Annex A.

**Figure 7:** Economic impact of climate change under the intermediate-emissions scenario (SSP2-4.5)

**(a)** Percentage change in GDP per capita in 2050



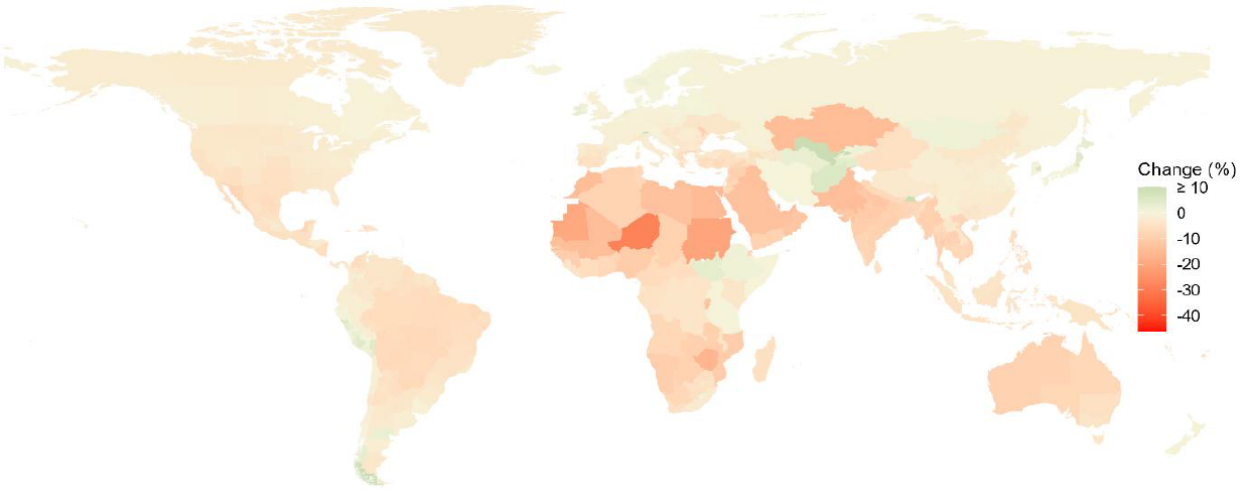

**(b)** Percentage change in GDP per capita in 2100



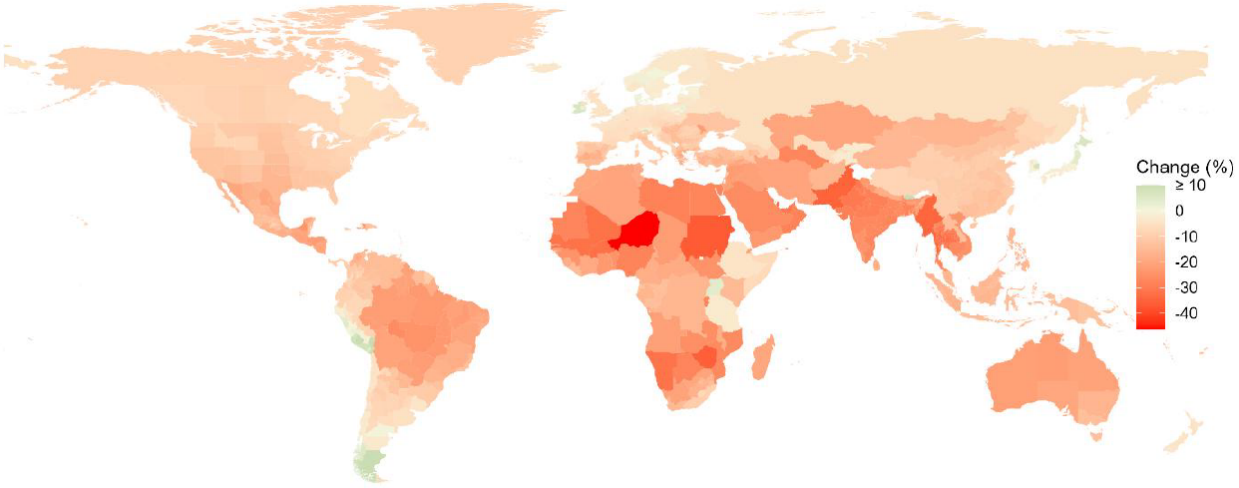

*Source:* Authors' calculations.
*Notes:* The maps show percentage changes in annual real GDP per capita relative to the no-climate-change baseline. Changes in real GDP are computed by aggregating sector-level changes using sectoral value-added weights. GDP per capita impacts additionally account for changes in population relative to the baseline. Positive values indicate gains and negative values indicate losses. For display, gains above 10% are capped at 10%.

**Figure 8:** Economic impact of climate change under the very high-emissions scenario (SSP5-8.5)

**(a)** Percentage change in GDP per capita in 2050




**(b)** Percentage change in GDP per capita in 2100




*Source:* Authors' calculations.
*Notes:* The maps show percentage changes in annual real GDP per capita relative to the no-climate-change baseline. Changes in real GDP are computed by aggregating sector-level changes using sectoral value-added weights. GDP per capita impacts additionally account for changes in population relative to the baseline. Positive values indicate gains and negative values indicate losses. For display, gains above 10% are capped at 10%.

ures A.11 and A.12 in Annex A report OECD country impacts under the central climate projections together with ranges constructed from alternative projections for the individual hazards. These ranges indicate substantial uncertainty about the size of losses, particularly towards the end of the century, and in some relatively less affected countries extend across zero. They capture variation in the underlying climate projections, while uncertainty about the estimated damage relationships and the economic model provides additional reasons to interpret the point estimates cautiously.

The model also predicts endogenous changes in the spatial distribution of population as households respond to differences in climate-induced economic conditions. Under SSP5-8.5, Northern Africa, Western Asia, Southern Asia, and Sub-Saharan Africa experience population declines relative to the no-climate-change baseline, while Northern Europe, Central Asia, North America, and Oceania generally gain population, with these contrasts becoming more pronounced towards the end of the century. Adjustment also takes place within countries as households relocate towards relatively less affected areas. These population changes, documented for both scenarios in Annex F, arise from households' location choices in response to changes in productivity, capital depreciation, and land supply. They form part of the equilibrium response underlying the GDP per capita results, motivating the counterfactual exercises below that separately assess the role of economic linkages and the ability to adjust.

### 5.2. The role of economic linkages in transmitting climate shocks

Having quantified the macroeconomic cost of climate change, we now examine how economic linkages shape these outcomes. We simulate the same climate shocks in counterfactual economies in which selected linkages are removed, recalibrating the model in each case. Comparing these simulations with the full model allows us to assess how economic integration changes the magnitude and distribution of climate damages. We focus on cross-regional spatial linkages and input–output linkages. The results reported here and in Section 5.3 focus on 2100 under our intermediate-emissions benchmark. Table 2 compares the global results under both scenarios, and Appendix A reports the corresponding figures for the very high-emissions scenario.

Cross-regional spatial linkages connect locations through trade and labour mobility, allowing shocks to spill over beyond their location of origin. If a shock lowers TFP in one location, its trade partners experience changes in import costs and demand, so that even countries not directly affected by heat stress can be impacted. Trade linkages have an ambiguous effect on GDP losses. Access to alternative sources of goods and inputs reduces dependence on any single location, but trade also transmits adverse shocks from suppliers and customers elsewhere.

Migration provides another spatial linkage through which climate impacts spread. As conditions worsen in one region, workers may move to locations with more favourable economic conditions, either within or across borders. This redistribution of labour changes productive capacity, wages, and expenditure in both origin and destination regions. It can cushion losses in affected locations, while changes in labour supply and housing demand in receiving regions affect wages, rents, and production costs. In our counterfactual simulations, we isolate the combined role of trade and

**Table 2:** Global GDP per capita losses and counterfactual comparisons in 2100

| | GDP per capita loss (%) | | Difference (pp) | |
|---|---|---|---|---|
| | SSP2-4.5 | SSP5-8.5 | SSP2-4.5 | SSP5-8.5 |
| Full model | 6.4 | 18.5 | — | — |
| *Linkages removed* | | | | |
| Spatial linkages | 7.8 | 21.3 | +1.3 | +2.8 |
| Input–output linkages | 3.7 | 10.8 | −2.7 | −7.8 |
| *Adjustment restricted* | | | | |
| Labour | 6.7 | 19.4 | +0.3 | +0.9 |
| Trade | 7.2 | 19.8 | +0.7 | +1.3 |
| Labour and trade | 7.2 | 20.1 | +0.8 | +1.5 |

*Source:* Authors' calculations.
*Notes:* Losses are expressed as positive percentages relative to the relevant no-climate-change reference path. Differences equal counterfactual losses minus full-model losses, in percentage points. Positive differences indicate that removing linkages or restricting adjustment increases losses. Spatial linkages comprise trade and migration within and across countries. Labour adjustment comprises sectoral reallocation and migration. Each recalibrated model uses its own reference path. Restricted-adjustment simulations retain the full model's calibration and reference path. Values are rounded to one decimal place.

migration linkages by preventing the movement of goods and people between locations, both within and across countries. This allows us to measure the importance of spatial linkages in determining local economic impacts around the world.

Input–output linkages connect production across sectors and locations through purchases of material inputs. When a shock raises costs or reduces output in one sector, it affects the firms that purchase its products and the suppliers from which it buys inputs, propagating the shock through the production network. These linkages can amplify the initial damage, particularly in economies with strong upstream and downstream dependencies. Our separate counterfactual without input–output linkages isolates the contribution of these production relationships to aggregate and regional losses.

Figure 9 shows how spatial and input–output linkages affect the geographical distribution of GDP per capita losses in 2100 under the intermediate-emissions benchmark. Each panel reports the loss in the full model minus the loss in the corresponding recalibrated counterfactual. Positive values, shown in red, indicate amplification by the linkages, while negative values, shown in green, indicate attenuation. Country-level comparisons are reported in Figure A.14 in Appendix A.

Panel A shows that spatial linkages reduce losses across many locations in Africa and Latin America, as well as parts of the United States and Australia. Their effects are not uniformly beneficial: Canada and several Northern European countries experience larger losses when goods and workers can move between locations. These outcomes reflect the combined effects of access to alternative suppliers and markets, the transmission of shocks through trading partners, and labour reallocation across locations. The regional comparisons illustrate the size of this redistribution. In Northern Africa, losses are approximately 8.3% in the full model, compared with 13.7% with-

out spatial linkages. Globally, spatial linkages reduce losses from approximately 7.8% to 6.4%, a difference of 1.3 percentage points, or around 17% relative to the counterfactual without these linkages.

Panel B shows that input–output linkages amplify climate losses across most locations. Changes in the costs and availability of intermediate inputs transmit shocks through suppliers and customers, raising aggregate losses relative to the recalibrated economy without these production relationships. This amplification is not universal, as general equilibrium changes in relative costs and demand can offset damages or reinforce gains in particular locations. Under the intermediate-emissions benchmark, global losses rise from approximately 3.7% without input–output linkages to 6.4% in the full model, an increase of 2.7 percentage points, or roughly 72% relative to the counterfactual loss.

The main transmission results also hold under the very high-emissions scenario (Table 2 and Figure A.13). Input–output linkages increase global losses from approximately 10.8% to 18.5%, implying proportional amplification of around 72%, close to the intermediate-emissions result. Spatial linkages reduce losses from approximately 21.3% to 18.5%, an attenuation of around 13%. The absolute effects of both sets of linkages are larger under this scenario, although spatial linkages produce a smaller proportional reduction in global losses. Across both scenarios, their aggregate effect coexists with substantial variation in local outcomes.

### 5.3. The role of adjustment: how trade and labour mobility shape the distribution of global losses

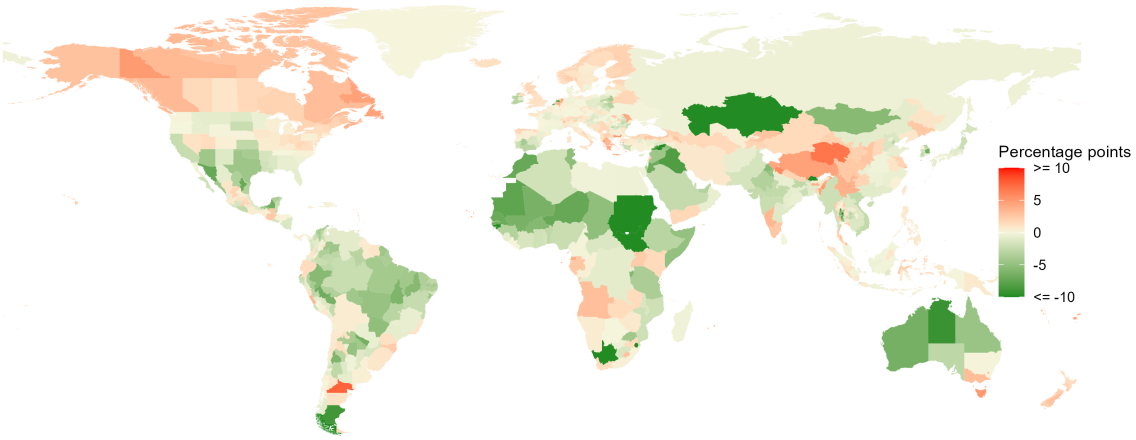
We now quantify how adjustment through trade and labour reallocation changes climate-induced GDP per capita losses. These responses arise from agents' optimising decisions, but their effects need not reduce GDP per capita losses in every location. When households and firms adjust simultaneously, their decisions interact through goods and factor markets, generating spillovers that can either mitigate or amplify local losses. For example, migration allows workers to leave highly climate-exposed locations, but also changes labour supply and demand for housing in both origin and destination regions. The resulting changes in wages, rents, and production costs can redistribute climate losses across locations. The results that follow should therefore be interpreted as the net effect of each adjustment mechanism, combining local responses with the spillover effects generated by adjustment elsewhere.

To quantify these mechanisms, we retain the baseline calibration and re-simulate the climate shocks while holding selected allocation shares fixed along their no-climate-change paths. We distinguish labour adjustment from trade adjustment.

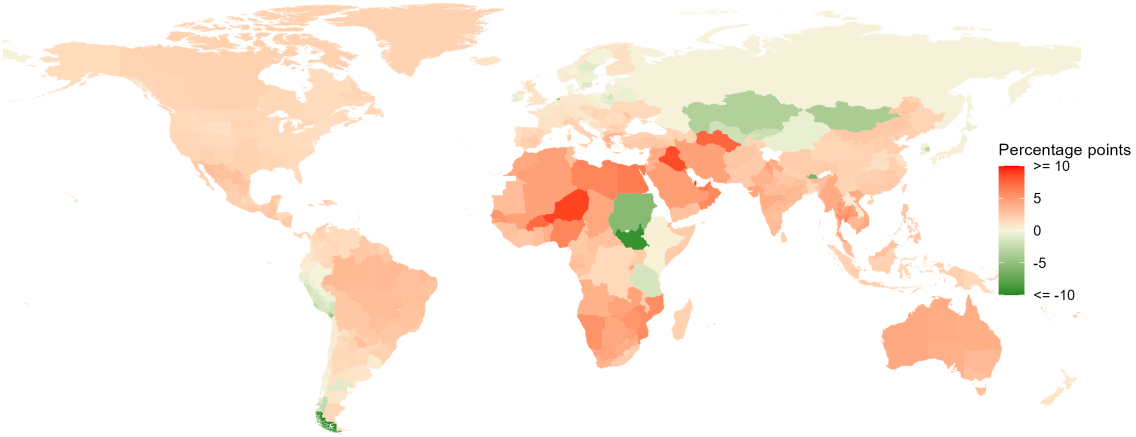
Labour adjustment operates through both sectoral reallocation and migration. As climate hazards affect sectors unevenly, workers can move across industries within a location in response to changing labour demand. Households can also relocate between regions within countries or migrate internationally in response to differences in economic conditions. We restrict these margins by fixing within-location sectoral employment shares and migration shares at their corresponding

**Figure 9:** How economic linkages change climate-induced GDP per capita losses in 2100

**(a)** Additional percentage point loss in GDP per capita in 2100 due to spatial linkages




**(b)** Additional percentage point loss in GDP per capita in 2100 due to input–output linkages




*Source:* Authors' calculations.
*Notes:* The panels report differences in climate-induced GDP per capita losses between the full model and a recalibrated counterfactual without the indicated linkages, in percentage points. Each model measures climate losses relative to its own no-climate-change reference path. Positive values indicate that the linkages increase losses, while negative values indicate that they reduce losses. Both panels use the same colour scale. For display, values below $-10$ and above 10 percentage points are assigned the endpoint colours. Climate projections follow SSP2-4.5.

values along the no-climate-change path.

Trade adjustment allows firms and households to change where they source intermediate and final goods as relative production costs evolve. We restrict this margin by fixing bilateral expenditure shares at their corresponding values along the no-climate-change path. The joint restriction holds trade shares, migration shares, and sectoral employment shares fixed simultaneously.

Figure 10 shows how labour and trade adjustment change GDP per capita losses in 2100 under the intermediate-emissions benchmark. Each panel reports the loss in the full model minus the loss when the indicated adjustment margins are restricted. Positive values, shown in red, indicate that allowing adjustment increases losses, while negative values, shown in green, indicate that it reduces them. Figure A.17 in Appendix A reports country-level comparisons for OECD+ countries.

Panel A shows the effect of labour adjustment through sectoral reallocation and migration. It reduces losses across many locations in Africa and Latin America and in parts of the United States and Australia, while increasing losses in Canada, New Zealand, and several Northern European countries. Labour reallocation changes production, expenditure, and demand for local factors in both sending and receiving locations. These general equilibrium effects explain why adjustment need not reduce GDP per capita losses everywhere, even when it follows households' and firms' optimising decisions. Globally, labour adjustment reduces losses from approximately 6.7% to 6.4%, or around 4–5% relative to the restricted-adjustment counterfactual.

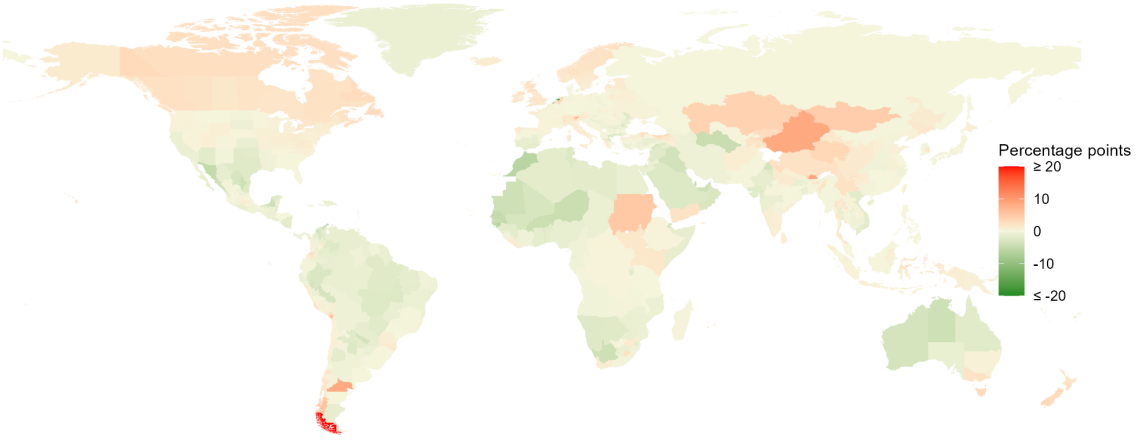
Panel B shows the effect of allowing bilateral sourcing shares to respond to climate change. Trade adjustment reduces GDP per capita losses across many locations in Africa, Latin America, and Australia, while increasing them in some locations in Europe, North America, and Asia. Flexibility in sourcing can cushion increases in consumption prices and intermediate-input costs by allowing substitution towards relatively less affected suppliers. At the same time, changes in comparative advantage and expenditure redirect demand across producers and locations. A location's net outcome therefore depends on both its own exposure and the response of its trading partners. At the global level, trade adjustment reduces losses from approximately 7.2% to 6.4%, or around 10% relative to the counterfactual with trade shares fixed.

Panel C reports the joint effect of labour and trade adjustment. Their combined effect is not obtained by adding Panels A and B, because changes in sourcing and labour allocation interact through goods and factor markets. Joint adjustment reduces global losses from approximately 7.2% to 6.4%, also around 11% relative to the jointly restricted counterfactual. The similar global loss levels under the trade-only and joint restrictions are rounded values and coexist with differences in the geographical distribution of impacts. In Northern Africa, joint adjustment reduces losses from approximately 12.3% to 8.3%, and in Western Asia from 12.1% to 9.9%. In Northern Europe, by contrast, the impact changes from an approximately 0.6% gain with both margins restricted to a 1.0% loss in the full model. Within countries such as the United States and Australia, adjustment also reduces losses in some regions while increasing them in others.

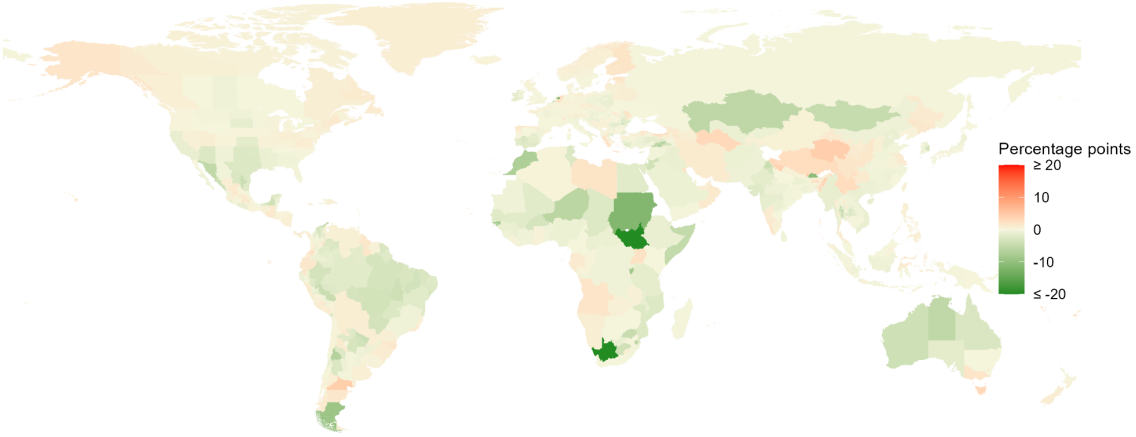
The aggregate benefits of adjustment remain positive under the very high-emissions scenario (Table 2 and Figure A.16). Labour adjustment reduces losses by around 4–5%, trade adjustment

**Figure 10:** How adjustment changes climate-induced GDP per capita losses in 2100

**(a)** Additional percentage point loss in GDP per capita in 2100 due to adjustments via labour mobility

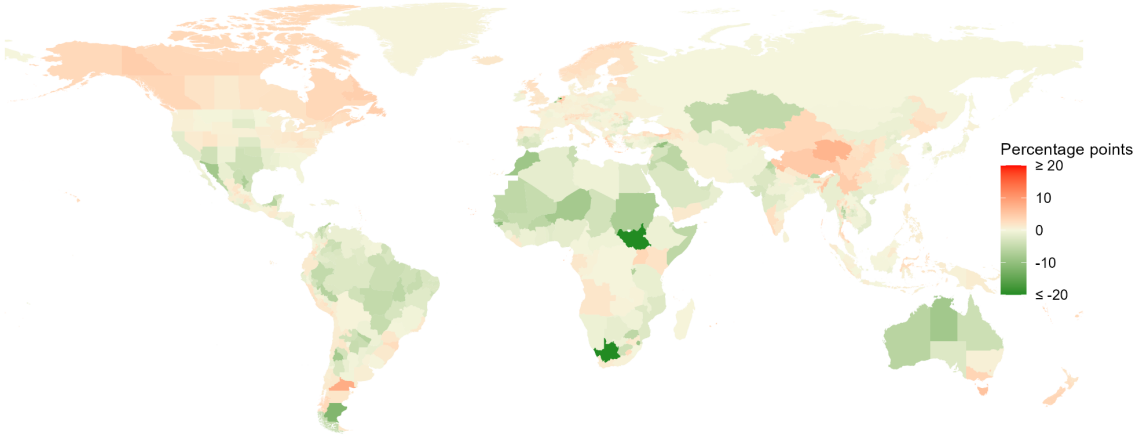



**(b)** Additional percentage point loss in GDP per capita in 2100 due to trade adjustment




*Source:* Authors' calculations.
*Notes:* The panels report differences in climate-induced GDP per capita losses between the full model and simulations with the indicated adjustment margins restricted, in percentage points. The baseline calibration is retained. Restricted allocation shares follow their no-climate-change paths. Positive values indicate that allowing adjustment increases losses, while negative values indicate that it reduces losses. Climate projections follow SSP2-4.5. Values outside $[-20, 20]$ are shown at the endpoints of the colour scale.

**(c)** Additional percentage point loss in GDP per capita in 2100 due to joint labour and trade adjustment




*Source:* Authors' calculations.
*Notes:* The panels report differences in climate-induced GDP per capita losses between the full model and simulations with the indicated adjustment margins restricted, in percentage points. The baseline calibration is retained. Restricted allocation shares follow their no-climate-change paths. Positive values indicate that allowing adjustment increases losses, while negative values indicate that it reduces losses. Climate projections follow SSP2-4.5. Values outside $[-20, 20]$ are shown at the endpoints of the colour scale.

by around 6%, and joint adjustment by around 8%, each relative to its corresponding restricted-adjustment counterfactual. The joint reduction is larger in percentage points under this scenario, at approximately 1.5 rather than 0.8 points, but smaller relative to counterfactual losses. The geographical incidence is not identical across scenarios. For example, joint adjustment increases losses in Southern Europe from approximately 3.2% to 3.6% under the intermediate-emissions benchmark, while having an approximately neutral effect there under the very high-emissions scenario. The common finding is that adjustment moderates global losses while redistributing their incidence across locations.

Joint labour and trade adjustment also reduces cross-regional dispersion in GDP per capita losses. Under the intermediate-emissions benchmark, the population-weighted standard deviation falls from roughly 7 percentage points in the jointly restricted counterfactual to 5.75 percentage points in the full model, a reduction of around 18%. The coefficient of variation falls from 0.97 to 0.89, indicating an approximately 8% reduction in dispersion relative to the mean loss. Under the very high-emissions scenario, the corresponding reductions are around 23% for the standard deviation and 16% for the coefficient of variation. Both measures also decline under both scenarios when regions receive equal weight.

## 6. Conclusion

This paper develops a bottom-up approach to quantify how local climate damages translate into aggregate economic losses in an interconnected global economy. We combine granular empirical evidence and physical climate projections for heat stress, changes in agro-climatic conditions, flooding,

and sea-level rise with a quantitative spatial general equilibrium model featuring trade, migration, production networks, and capital accumulation. This allows us to distinguish three components of the economic effects of climate change: the direct exposure of individual locations, the propagation of these shocks through economic linkages, and the endogenous adjustment of production, trade and labour across sectors and space.

We find substantial and highly heterogeneous economic losses from climate change. Relative to a counterfactual in which climate conditions remain at historical levels, global GDP per capita is 3% lower in 2050 and 6.4% lower in 2100 under our intermediate-emissions benchmark (SSP2-4.5), compared with losses of 5.9% and 18.5%, respectively, under the very high-emissions scenario (SSP5-8.5). Losses are generally larger at lower latitudes and vary considerably both across and within countries. Among the hazards considered, heat stress accounts for most global damages, followed by changes in agro-climatic conditions, while flooding and sea-level rise generate more geographically concentrated losses.

Economic linkages substantially change how these local damages aggregate. Production networks are an important amplification mechanism: global GDP per capita losses in 2100 are around 72% larger with input–output linkages under both scenarios, relative to the corresponding counterfactuals without these linkages. Spatial linkages through trade and migration reduce global losses under both scenarios, although their local effects vary. Allowing trade patterns and labour allocations to respond to climate change reduces global losses by around 11% under the intermediate-emissions benchmark and 8% under the very high-emissions scenario, relative to counterfactuals in which both remain on their no-climate-change paths. These adjustments also substantially redistribute losses across locations. The economic incidence of climate change therefore cannot be inferred from local exposure alone: it reflects the interaction between where damages occur, how they propagate through production and spatial linkages, and how households and firms respond to the resulting changes in relative economic conditions.

These results also clarify the role of spatial adjustment in assessments of climate damages. The same interconnectedness that transmits shocks across regions and sectors creates opportunities to adjust sourcing, sectoral employment, and location in response. These responses reduce aggregate losses in our simulations, but their effects are not uniformly beneficial across space: adjustment that cushions losses in some locations can shift part of their incidence elsewhere through changes in prices, wages, demand, and factor allocation.

Our quantitative estimates abstract from additional climate hazards, non-market damages, non-linear responses outside the historical range of observed climate variation, and explicit investments in protective adaptation. Incorporating these margins and richer forms of endogenous adaptation is an important direction for future research.

## References


Abel, G. and Cohen, J. (2019). Bilateral international migration flow estimates for 200 countries. *Scientific Data*, 6(1).

Acemoglu, D., Carvalho, V. M., Ozdaglar, A., and Tahbaz-Salehi, A. (2012). The network origins of aggregate fluctuations. *Econometrica*, 80(5):1977–2016.

Anderson, J. and van Wincoop, E. (2003). Gravity with gravitas: A solution to the border puzzle. *American Economic Review*, 93(1):170–192.

Balboni, C. (2025). In harm's way? infrastructure investments and the persistence of coastal cities. *American Economic Review*, 115(1).

Balboni, C., Boehm, J., and Waseem, M. (2025). Firm adaptation in production networks: Evidence from extreme weather events in pakistan. November 12 manuscript. Forthcoming in the American Economic Review.

Bank of England (2025). The heat is on: why monetary policy makers are increasingly focusing on the impact of climate risks. Speech by James Talbot.

Baptista, D. et al. (n.d.). When the levee breaks: Capital losses, spillovers, and firm recovery. Forthcoming, OECD Economics Department.

Barrage, L. and Nordhaus, W. (2024). Policies, projections, and the social cost of carbon: Results from the DICE-2023 model. *Proceedings of the National Academy of Sciences*, 121(13):e2312030121.

Barrot, J.-N. and Sauvagnat, J. (2016). Input specificity and the propagation of idiosyncratic shocks in production networks. *The Quarterly Journal of Economics*, 131(3):1543–1592.

Bearpark, T., Bhandari, A., and Rosenthal-Kay, J. (2025). The economic geography of climate risk. Working paper, November 3 version.

Bilal, A. and Känzig, D. R. (2026). The macroeconomic impact of climate change: Global versus local temperature. *The Quarterly Journal of Economics*, 141(2):889–944.

Bilal, A. and Rossi-Hansberg, E. (2023). Anticipating climate change across the United States. NBER Working Paper 31323, National Bureau of Economic Research. Revised working paper; conditionally accepted at Econometrica.

Bosello, F., Roson, R., and Tol, R. S. J. (2007). Economy-wide estimates of the implications of climate change: Sea level rise. *Environmental and Resource Economics*, 37(3):549–571.

Burke, M., Hsiang, S. M., and Miguel, E. (2015). Global non-linear effect of temperature on economic production. *Nature*, 527:235–239.

Burzyński, M., Deuster, C., Docquier, F., and de Melo, J. (2022). Climate change, inequality, and human migration. *Journal of the European Economic Association*, 20(3):1145–1197.

Caliendo, L., Parro, F., Rossi-Hansberg, E., and Sarte, P.-D. (2018). The impact of regional and sectoral productivity changes on the U.S. economy. *The Review of Economic Studies*, 85(4):2042–2096.

Carleton, T., Greenstone, M., Hsiang, S., Hultgren, A., Kopp, R. E., McCusker, K. E., Nath, I., Rising, J., and Rode, A. (2026). The local damages from global climate change. Working Paper 2026-86, Becker Friedman Institute for Economics, University of Chicago.

Carvalho, V. M., Nirei, M., Saito, Y. U., and Tahbaz-Salehi, A. (2021). Supply chain disruptions: Evidence from the Great East Japan Earthquake. *The Quarterly Journal of Economics*, 136(2):1255–1321.

Castro-Vincenzi, J., Khanna, G., Morales, N., and Pandalai-Nayar, N. (2025). Weathering the storm: Supply chains and climate risk. Working paper, September version.

Conte, B. (2026). Climate change and migration: The case of Africa. *Journal of the European Economic Association*. Advance online publication, article jvag035.

Conte, B., Desmet, K., Nagy, D. K., and Rossi-Hansberg, E. (2021). Local sectoral specialization in a warming world. *Journal of Economic Geography*, 21(4):493–530.

Conte, B., Desmet, K., and Rossi-Hansberg, E. (2026). On the geographic implications of carbon taxes. *The Economic Journal*, 136(677):1547–1581.

Costa, H., Franco, G., Unsal, F., Mudigonda, S., and Caldas, M. P. (2024). The heat is on: Heat stress, productivity and adaptation among firms. OECD Economics Department Working Papers 1828, OECD Publishing.

Costa, H. and Hooley, J. (2025). The macroeconomic implications of extreme weather events. OECD Economics Department Working Papers 1837, OECD Publishing.

Costinot, A., Donaldson, D., and Smith, C. (2016). Evolving comparative advantage and the impact of climate change in agricultural markets: Evidence from 1.7 million fields around the world. *Journal of Political Economy*, 124(1):205–248.

Cruz, J.-L. (2024). Global warming and labor market reallocation. Working paper, September 4 version.

Cruz, J.-L., Desmet, K., and Rossi-Hansberg, E. (2026). Evaluating the spatial consequences of a climate tipping point. NBER Working Paper 35811, National Bureau of Economic Research.

Cruz, J.-L. and Rossi-Hansberg, E. (2024). The economic geography of global warming. *The Review of Economic Studies*, 91(2):899–939.

Cruz, J.-L. and Rossi-Hansberg, E. (2026). Local carbon policy. In Chernozhukov, V., Hörner, J., La Ferrara, E., and Werning, I., editors, *Advances in Economics and Econometrics: Twelfth World Congress*, volume 2, pages 292–332. Cambridge University Press.

Dell, M., Jones, B. F., and Olken, B. A. (2012). Temperature shocks and economic growth: Evidence from the last half century. *American Economic Journal: Macroeconomics*, 4(3):66–95.

Dellink, R., Lanzi, E., and Chateau, J. (2019). The sectoral and regional economic consequences of climate change to 2060. *Environmental and Resource Economics*, 72(2):309–363.

Desmet, K., Kopp, R. E., Kulp, S. A., Nagy, D. K., Oppenheimer, M., Rossi-Hansberg, E., and Strauss, B. H. (2021). Evaluating the economic cost of coastal flooding. *American Economic Journal: Macroeconomics*, 13(2):444–486.

Desmet, K. and Rossi-Hansberg, E. (2015). On the spatial economic impact of global warming. *Journal of Urban Economics*, 88:16–37.

Desmet, K. and Rossi-Hansberg, E. (2024). Climate change economics over time and space. *Annual Review of Economics*, 16:271–304.

Desmet, K. and Rossi-Hansberg, E. (2026). The economic geography of climate change: Recent progress and open questions. *Journal of Economic Geography*, 26(1):5–12.

Dingel, J. I. and Meng, K. C. (2025). Spatial correlation, trade, and inequality: Evidence from the global climate. May 20 manuscript. Forthcoming in the Review of Economics and Statistics.

Eaton, J. and Kortum, S. (2002). Technology, geography, and trade. *Econometrica*, 70(5):1741–1779.

European Central Bank (2021). Climate change and central banking. Technical report. Keynote speech by Christine Lagarde.

Fried, S. (2022). Seawalls and stilts: A quantitative macro study of climate adaptation. *The Review of Economic Studies*, 89(6):3303–3344.

Gouel, C. and Laborde, D. (2021). The crucial role of domestic and international market-mediated adaptation to climate change. *Journal of Environmental Economics and Management*, 106:102408.

Greenwood, J., Hercowitz, Z., and Krusell, P. (1997). Long-run implications of investment-specific technological change. *American Economic Review*, 87(3):342–362.

Hausfather, Z. (2025). An assessment of current policy scenarios over the 21st century and the reduced plausibility of high-emissions pathways. *Dialogues on Climate Change*, 2(1):26–32.

Head, K. and Ries, J. (2001). Increasing returns versus national product differentiation as an explanation for the pattern of u.s.-canada trade. *American Economic Review*, 91(4):858–876.

Hsiang, S., Kopp, R., Jina, A., Rising, J., Delgado, M., Mohan, S., Rasmussen, D. J., Muir-Wood, R., Wilson, P., Oppenheimer, M., Larsen, K., and Houser, T. (2017). Estimating economic damage from climate change in the United States. *Science*, 356(6345):1362–1369.

Huizinga, J., De Moel, H., and Szewczyk, W. (2017). Global flood depth-damage functions: Methodology and the database with guidelines. Technical report.

IPCC (2021). *Climate Change 2021: The Physical Science Basis. Contribution of Working Group I to the Sixth Assessment Report of the Intergovernmental Panel on Climate Change*. Cambridge University Press.

IPCC, editor (2022). *Climate Change 2022: Impacts, Adaptation, and Vulnerability. Contribution of Working Group II to the Sixth Assessment Report of the Intergovernmental Panel on Climate Change, Cambridge University Press*. Cambridge University Press.

Kahn, M. E., Mohaddes, K., Ng, R. N. C., Pesaran, M. H., Raissi, M., and Yang, J.-C. (2021). Long-term macroeconomic effects of climate change: A cross-country analysis. *Energy Economics*, 104:105624.

Kalkuhl, M. and Wenz, L. (2020). The impact of climate conditions on economic production. evidence from a global panel of regions. *Journal of Environmental Economics and Management*, 103:102360.

Kleinman, B., Liu, E., and Redding, S. J. (2023). Dynamic spatial general equilibrium. *Econometrica*, 91(2):385–424.

Kompas, T., Pham, V. H., and Che, T. N. (2018). The effects of climate change on GDP by country and the global economic gains from complying with the Paris Climate Accord. *Earth's Future*, 6(8):1153–1173.

Krugman, P. (1991). Increasing returns and economic geography. *Journal of Political Economy*, 99:483–499.

Lemoine, D., Hausman, C., and Shrader, J. G. (2025). A guide to climate damages. NBER Working Paper 34348, National Bureau of Economic Research.

Morten, M. and Oliveira, J. (2024). The effects of roads on trade and migration. *American Economic Journal: Applied Economics*, 16(2):389–421.

Nath, I. (2025). Climate change, the food problem, and the challenge of adaptation through sectoral reallocation. *Journal of Political Economy*, 133(6):1705–1756.

Nicholls, R. and Cazenave, A. (2010). Sea-level rise and its impact on coastal zones. *Science*, 328(5985):1517–1520.

Pankratz, N. M. C. and Schiller, C. M. (2024). Climate change and adaptation in global supply-chain networks. *The Review of Financial Studies*, 37(6):1729–1777.

Redding, S. and Rossi-Hansberg, E. (2017). Quantitative spatial economics. *Annual Review of Economics*, 9:21–58.

Rudik, I., Lyn, G., Tan, W., and Ortiz-Bobea, A. (2022). The economic effects of climate change in dynamic spatial equilibrium. Working paper, July 12 version.

Saiz, A. (2010). The geographic determinants of housing supply. *Quarterly Journal of Economics*, 125(3):1253–1296.

Sarofim, M. C., Smith, C. J., Malek, P., McDuffie, E. E., Hartin, C. A., Lay, C. R., and McGrath, S. (2024). High radiative forcing climate scenario relevance analyzed with a ten-million-member ensemble. *Nature Communications*, 15:8185.

Scussolini, P. et al. (2016). Flopros: an evolving global database of flood protection standards. *Natural Hazards and Earth System Sciences*, 16(5):1049–1061.

Sun, Y., Zhu, S., Wang, D., Duan, J., Lu, H., Yin, H., Tan, C., Zhang, L., Zhao, M., Cai, W., Wang, Y., Hu, Y., Tao, S., and Guan, D. (2024). Global supply chains amplify economic costs of future extreme heat risk. *Nature*, 627(8005):797–804.

Tellman, B. et al. (2021). Satellite imaging reveals increased proportion of population exposed to floods. *Nature*, 596:80–86.

Tiggeloven, T. et al. (2020). Global-scale benefit–cost analysis of coastal flood adaptation. *Natural Hazards and Earth System Sciences*, 20(4):1025–1044.

van Vuuren, D. P., O'Neill, B. C., Tebaldi, C., et al. (2026). The scenario model intercomparison project for CMIP7 (ScenarioMIP-CMIP7). *Geoscientific Model Development*, 19:2627–2656.

Wooldridge, J. (2009). On estimating firm-level production functions using proxy variables. *Economics Letters*, 104(3):112–114.

Zappalà, G. (2024). Propagation of extreme heat in agriculture across sectors and space. Working paper, December 14 version.

## A. Additional figures

This appendix provides additional figures on climate inputs, model calibration, climate impacts, and the transmission and adjustment counterfactuals. The counterfactual comparisons refer to 2100, with global results summarised in Table 2.

### A.1. Climate inputs and model calibration

Figures A.1 and A.2 provide additional detail on the coastal-flood and agricultural projections. Figure A.3 documents the model's geographical coverage, and Figure A.4 compares calibrated country GDP per capita with the data.

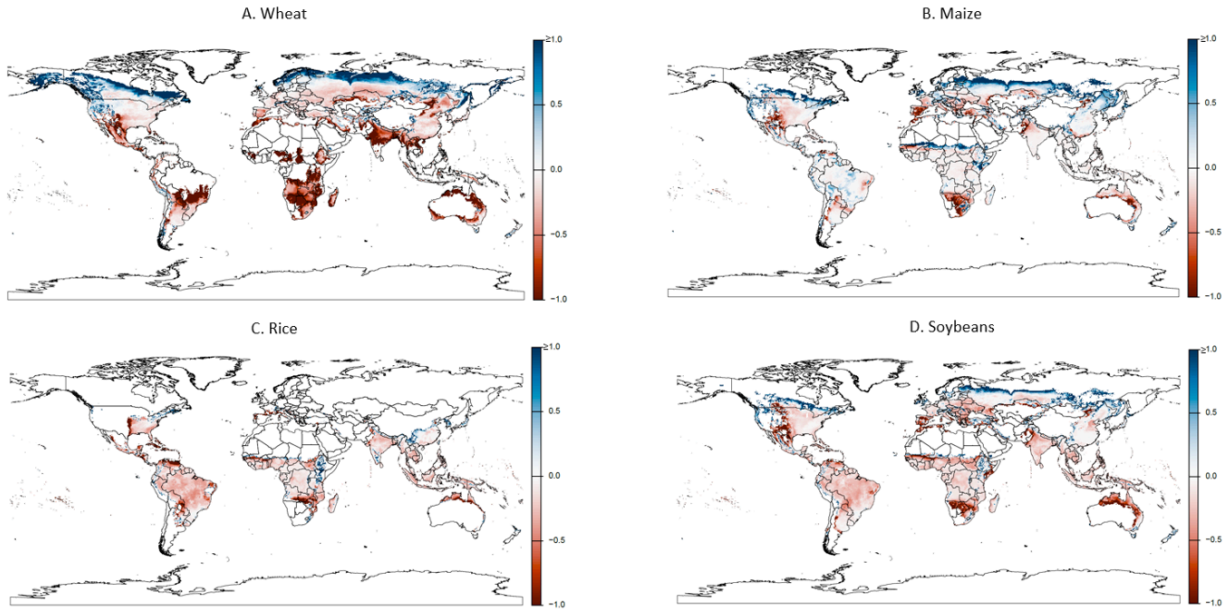
**Figure A.1:** Effect of climate change on coastal flood frequency in 2080 relative to 1980

Percent change in the annual frequency of coastal flooding under RCP8.5 (ensemble mean)



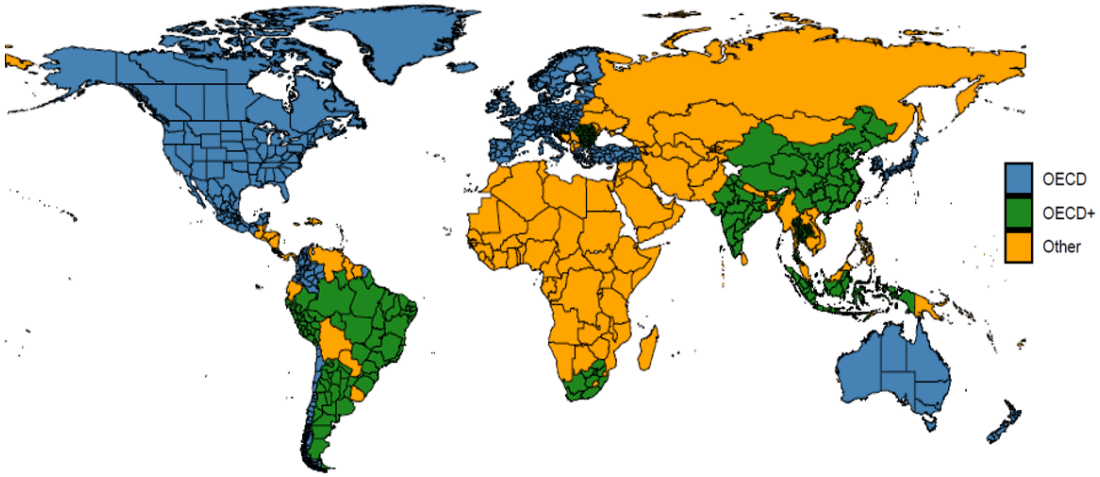

*Source:* Scussolini et al. (2016), World Resources Institute (Aqueduct), and authors' calculations.
*Notes:* The map reports values at the resolution of a 0.25° × 0.25° grid cell (approximately 25 km at the equator). Values greater than 50% and less than -50% are winsorised at 50% and -50%, respectively. The projections assume flood protection standards remain the same as in the baseline period (i.e. 1980).

**Figure A.2:** Change in agro-climatic potential yields of major crops in 2071–2100 relative to 2011–2040 under RCP8.5



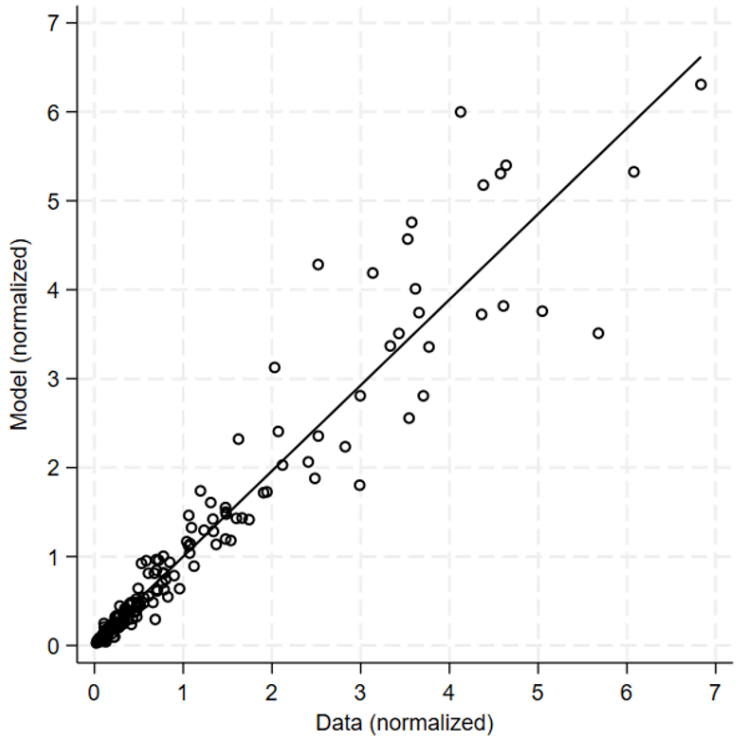

*Source:* FAO-GAEZ and authors' calculations.
*Notes:* Potential yields estimated under rain-fed conditions and high input usage. Figures show the median relative change across climate-crop growth models. Values greater than 1 are winsorised at 1.

**Figure A.3:** Regions in calibrated model by OECD status




*Source:* Authors' calculations.
*Notes:* The map shows the regions included in the calibration, classified by each country's status as OECD member country, accession candidate or key partner (OECD+), or other countries. OECD member countries are subdivided into TL2 regions, the OECD's second-level territorial classification corresponding to major subnational administrative areas. OECD accession candidate countries and OECD key partners are subdivided into Admin-1 units from GADM (Global Administrative Areas). For all other countries, the model is calibrated for the entire national territory as a single entity.

**Figure A.4:** Country GDP per capita in 2011–2020: model vs data



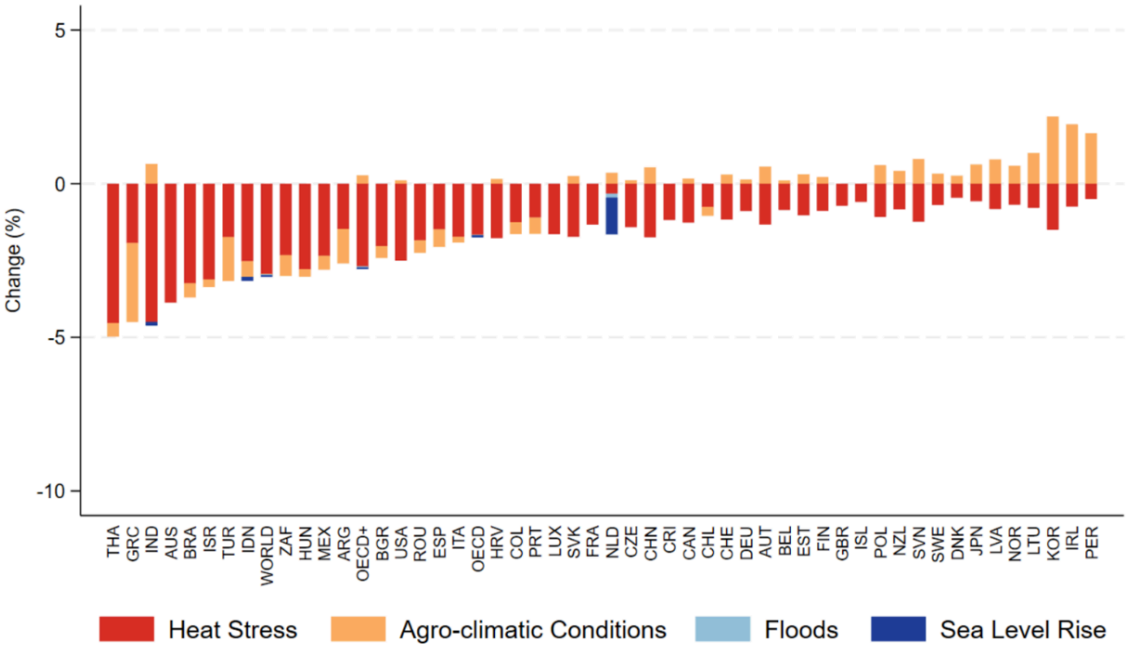

*Source:* Authors' own calculations and World Bank data.
*Notes:* The figure plots GDP per capita levels implied by the baseline model calibration (using data for 2011–2020) against their empirical counterparts from World Bank data (GDP per capita, constant 2015 US$); for comparability, country-level values in both series are normalized by dividing by the cross-country average.

### A.2. Additional estimates of climate impacts

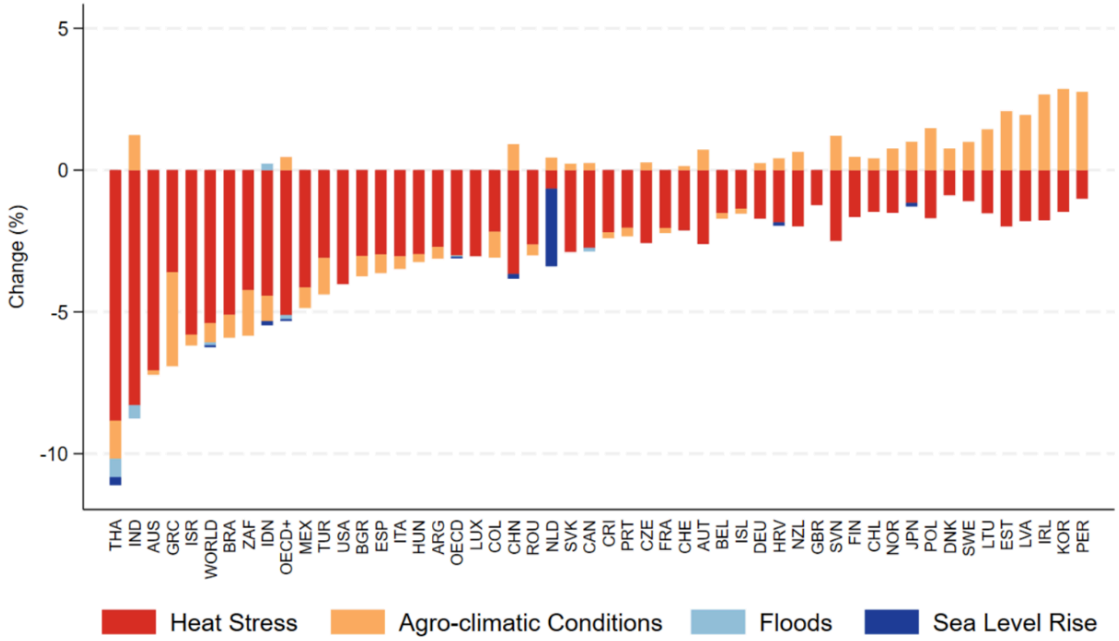
The following figures report GDP per capita impacts and their decomposition by climate-impact channel for OECD+ countries, OECD countries, and broad geographical regions under both scenarios. Additional country-level estimates for OECD members show the range associated with alternative climate projections.

**Figure A.5:** Impact by channel in OECD+ countries under the intermediate-emissions scenario (SSP2-4.5)

**(a)** Percentage change in GDP per capita in 2050



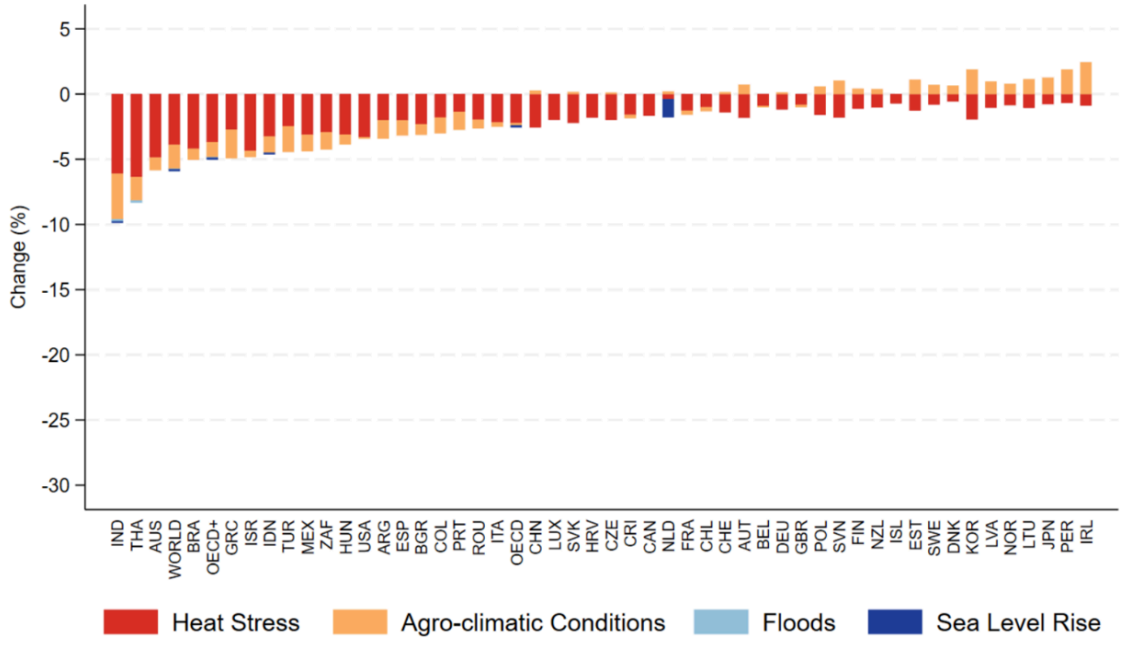

**(b)** Percentage change in GDP per capita in 2100



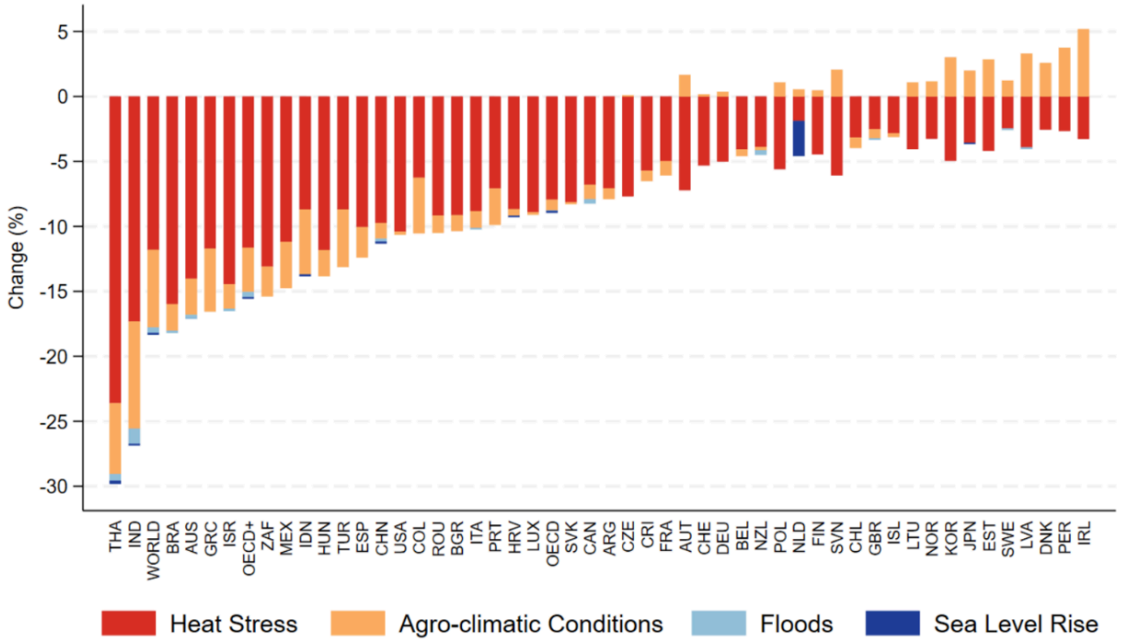

*Source:* Authors' calculations.
*Notes:* The figures show the model-implied loss in annual GDP per capita relative to a no-climate change scenario.

**Figure A.6:** Impact by channel in OECD+ countries under the very high-emissions scenario (SSP5-8.5)

**(a)** Percentage change in GDP per capita in 2050



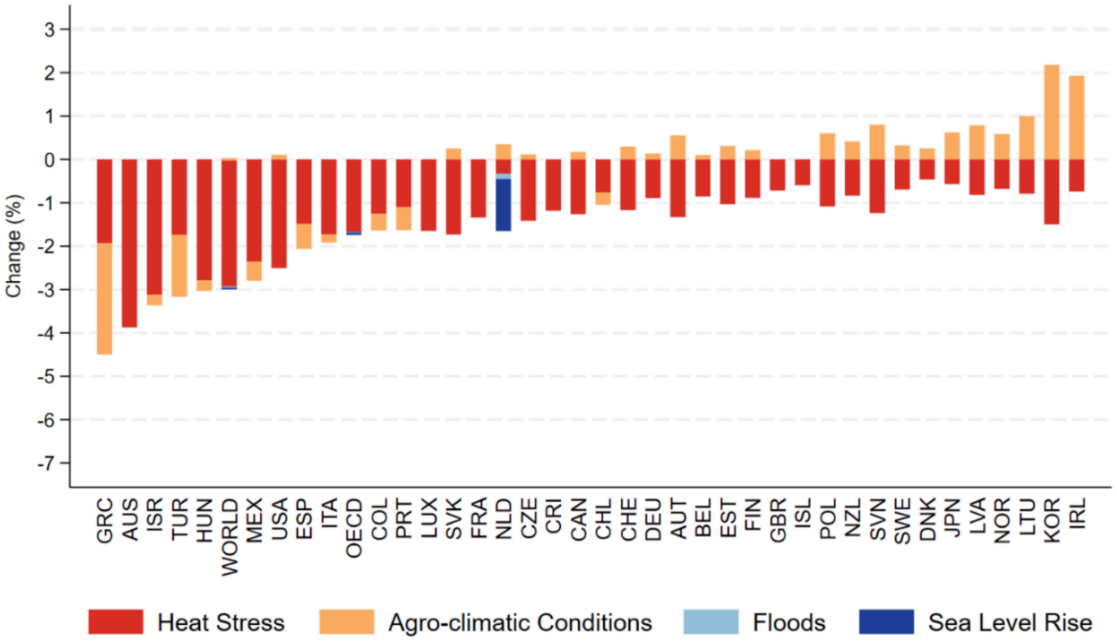

**(b)** Percentage change in GDP per capita in 2100



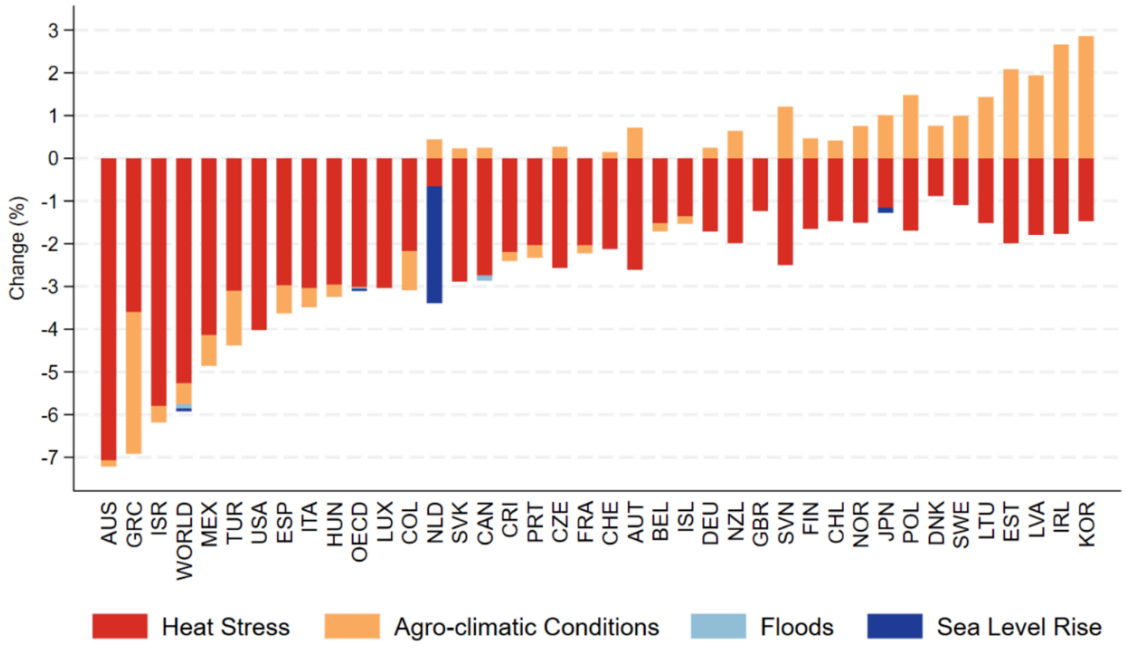

*Source:* Authors' calculations.
*Notes:* The figures show the model-implied loss in annual GDP per capita relative to a no-climate change scenario.

**Figure A.7:** Impact by channel in OECD countries under the intermediate-emissions scenario (SSP2-4.5)

**(a)** Percentage change in GDP per capita in 2050



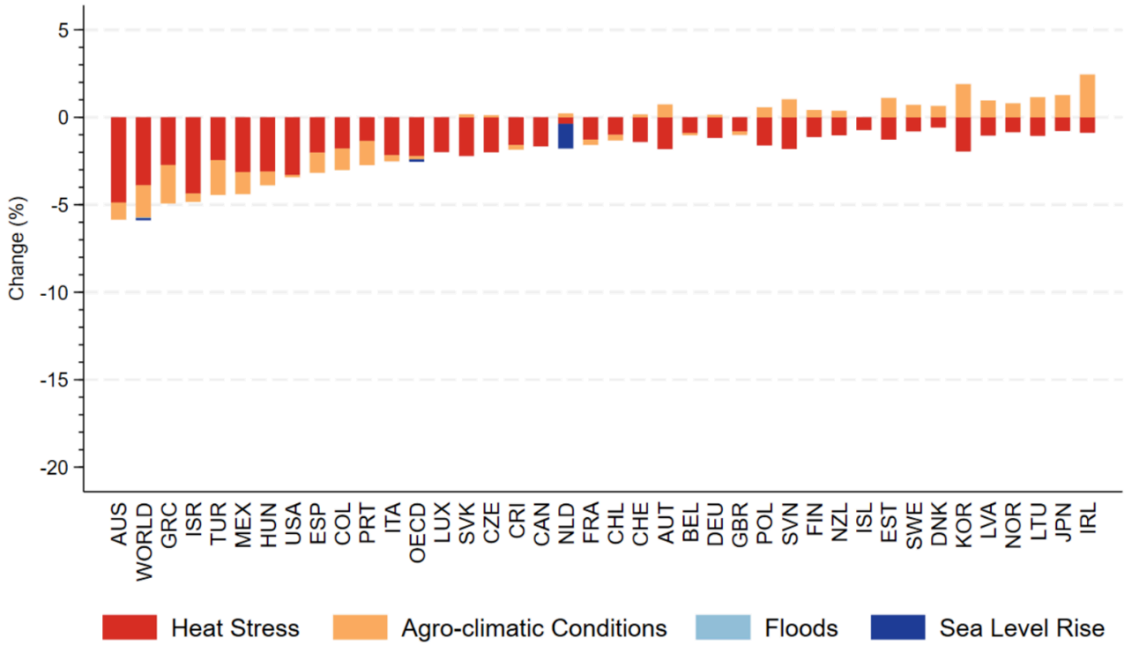

**(b)** Percentage change in GDP per capita in 2100



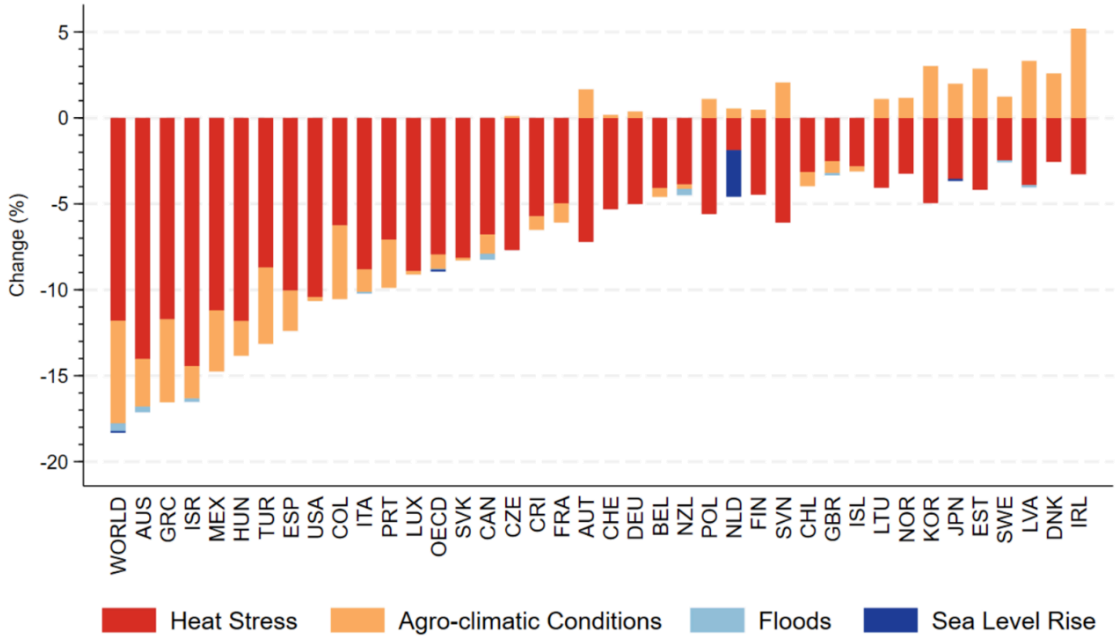

*Source:* Authors' own calculations.
*Notes:* The figure shows the model-implied loss in annual GDP per capita relative to a no-climate change scenario.

**Figure A.8:** Impact by channel in OECD countries under the very high-emissions scenario (SSP5-8.5)

**(a)** Percentage change in GDP per capita in 2050



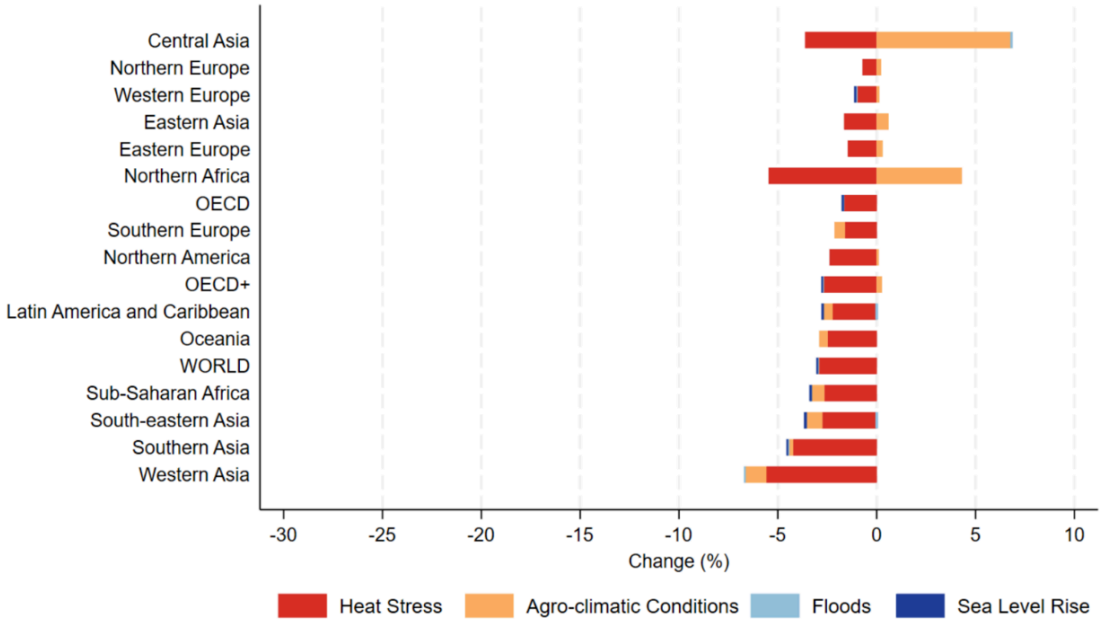

**(b)** Percentage change in GDP per capita in 2100



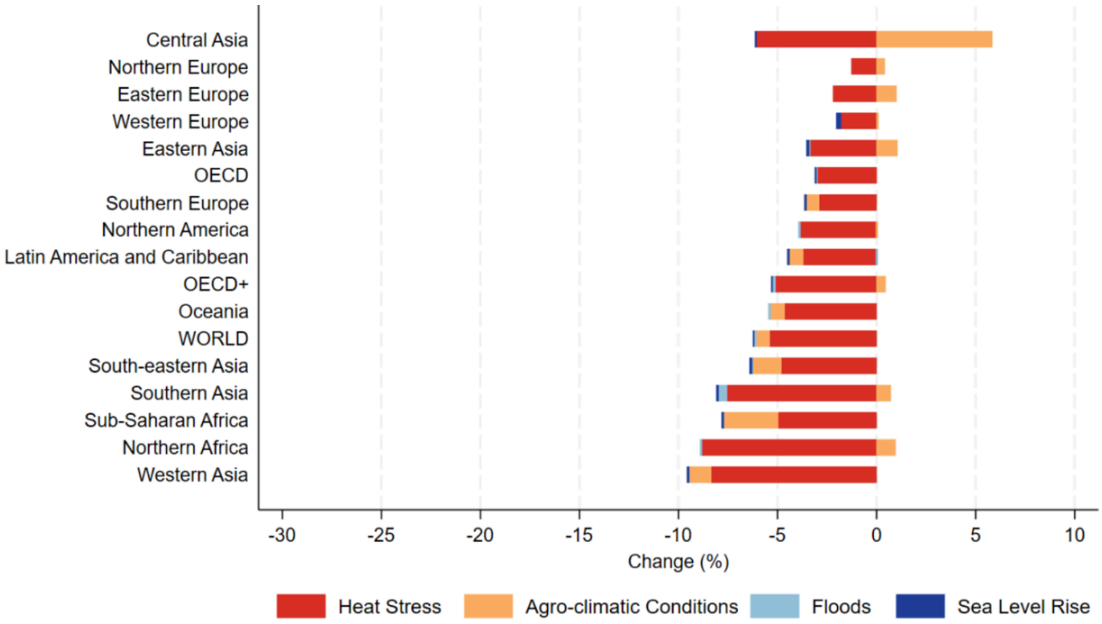

*Source:* Authors' own calculations.
*Notes:* The figure shows the model-implied loss in annual GDP per capita relative to a no-climate change scenario.

**Figure A.9:** Regional impact by channel under the intermediate-emissions scenario (SSP2-4.5)

**(a)** Percentage change in GDP per capita in 2050



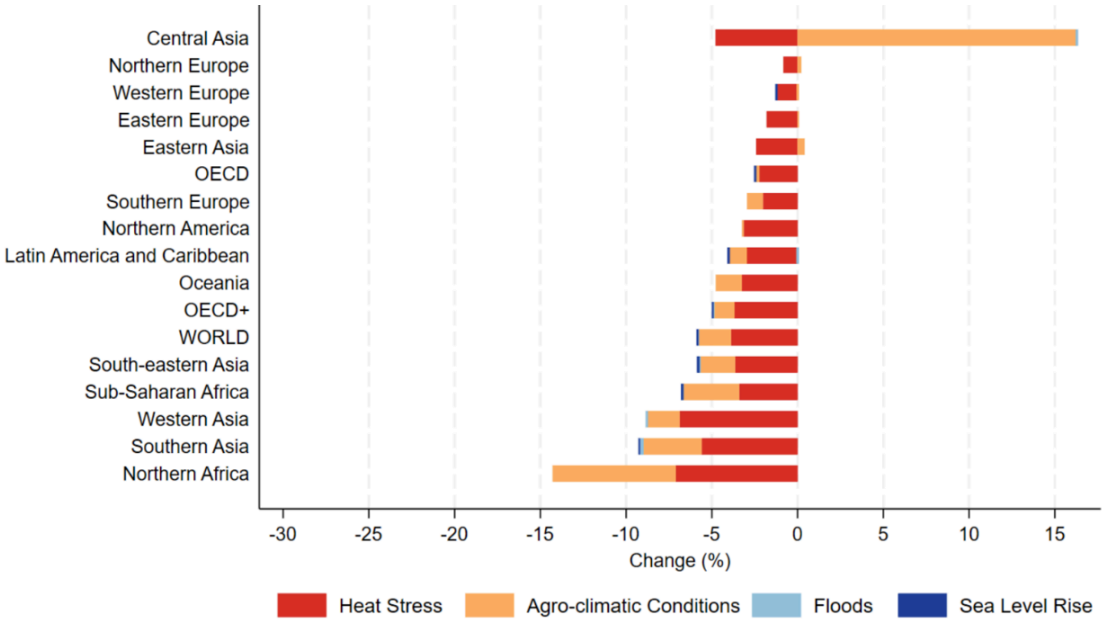

**(b)** Percentage change in GDP per capita in 2100



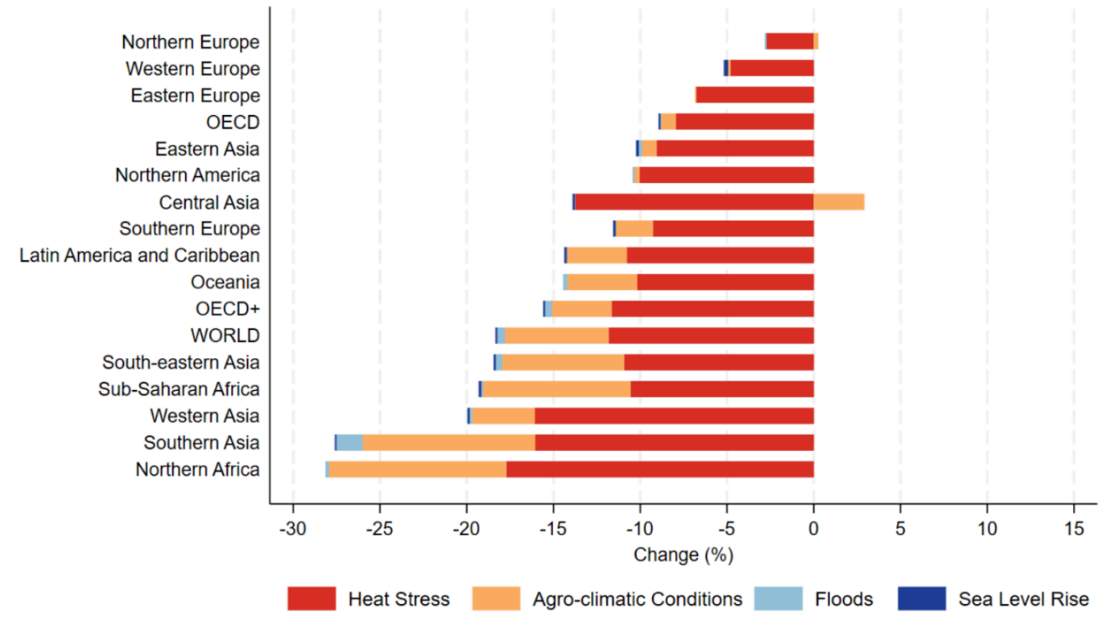

*Source:* Authors' own calculations.
*Notes:* The figures show the model-implied loss in annual GDP per capita relative to a no-climate change scenario. Regional GDP per capita losses are computed as a country population-weighted average.

**Figure A.10:** Regional impact by channel under the very high-emissions scenario (SSP5-8.5)

**(a)** Percentage change in GDP per capita in 2050



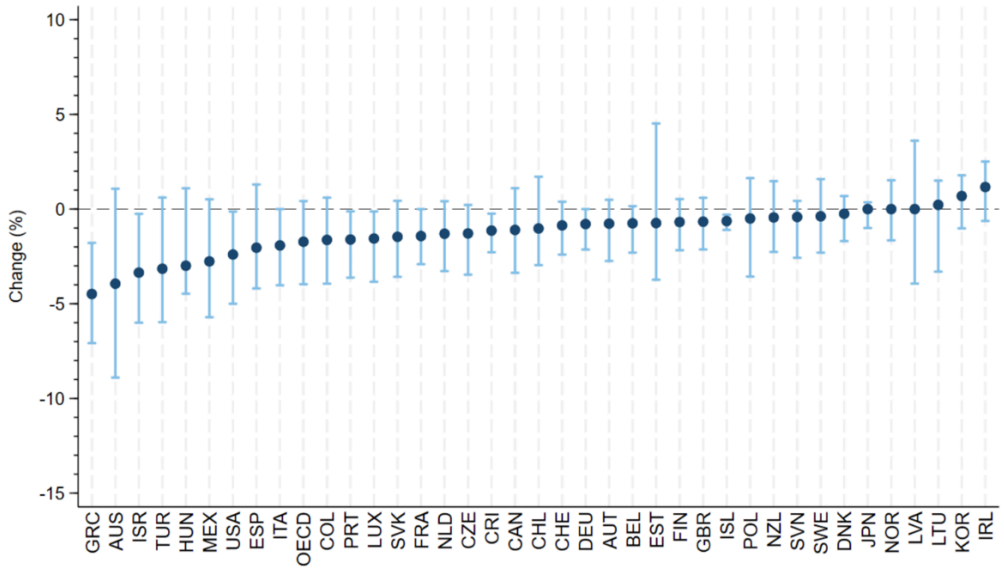

**(b)** Percentage change in GDP per capita in 2100



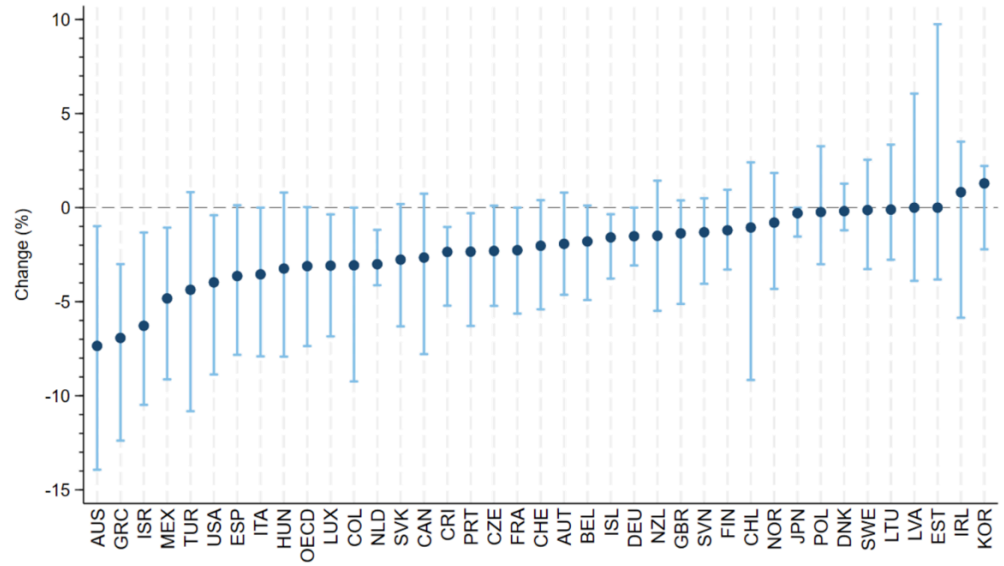

*Source:* Authors' own calculations.
*Notes:* The figures show the model-implied loss in annual GDP per capita relative to a no-climate change scenario. Regional GDP per capita losses are computed as a country population-weighted average.

**Figure A.11:** Impact in OECD countries under the intermediate-emissions scenario (SSP2-4.5)

**(a)** Percentage change in GDP per capita in 2050




**(b)** Percentage change in GDP per capita in 2100

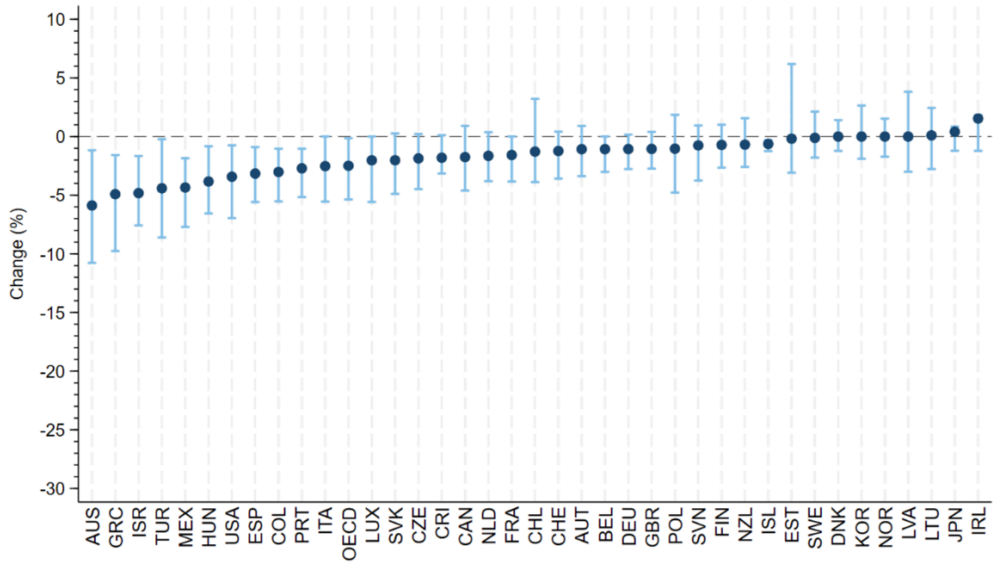



*Source:* Authors' own calculations.

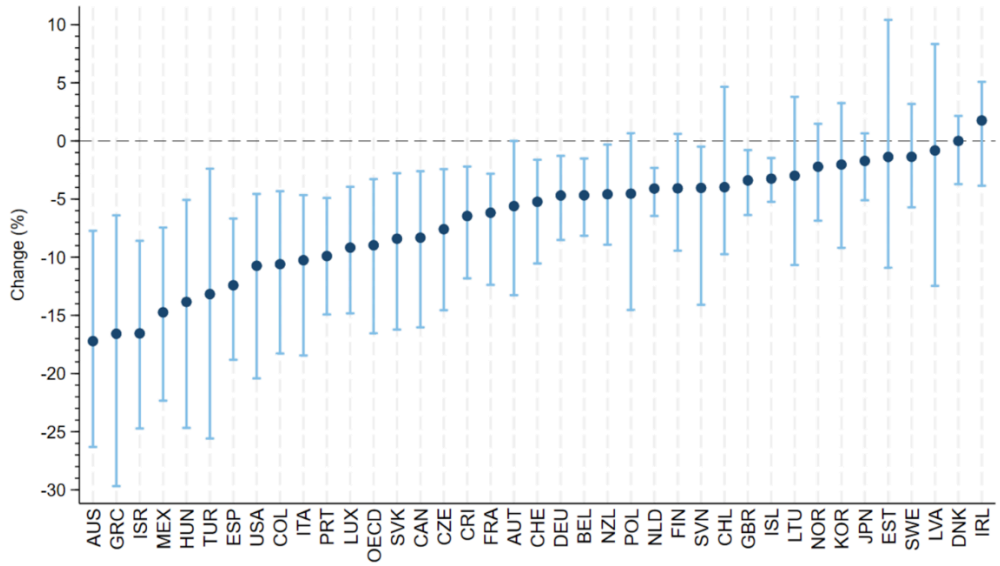
*Notes:* The figure shows model-implied percentage changes in annual GDP per capita relative to the corresponding no-climate-change scenario. The dots represent estimates under the central climate projections, while the intervals show the range obtained from alternative climate projections. The lower- and higher-damage cases use, respectively, 10th- and 90th-percentile projections for hot days and the agricultural climate models generating the lowest and highest global damages. Each selected agricultural model is applied across all countries, so this selection does not identify country-specific minimum and maximum losses. Coastal flooding and sea-level rise use the corresponding lower and higher coastal projections, while riverine flood projections remain at their central values.

**Figure A.12:** Impact in OECD countries under the very high-emissions scenario (SSP5-8.5)

**(a)** Percentage change in GDP per capita in 2050




**(b)** Percentage change in GDP per capita in 2100




*Source:* Authors' own calculations.

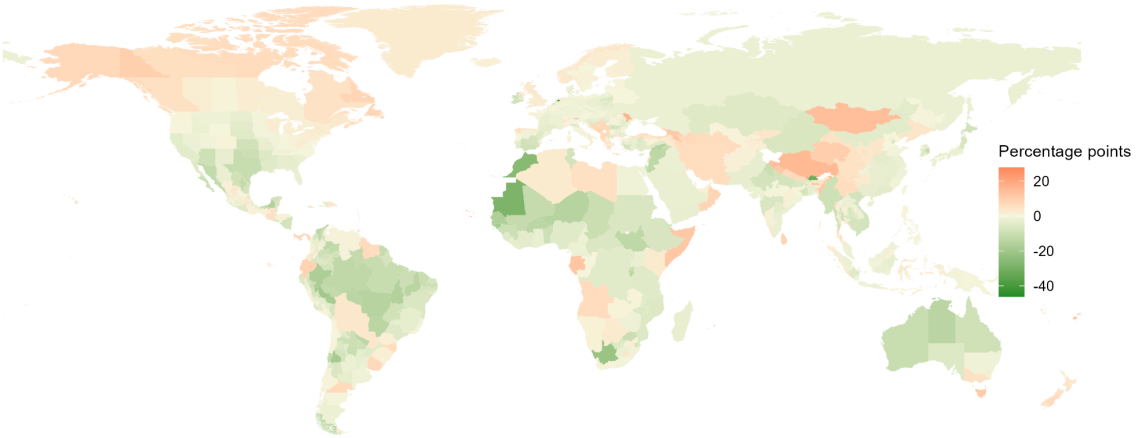
*Notes:* The figure shows model-implied percentage changes in annual GDP per capita relative to the corresponding no-climate-change scenario. The dots represent estimates under the central climate projections, while the intervals show the range obtained from alternative climate projections. The lower- and higher-damage cases use, respectively, 10th- and 90th-percentile projections for hot days and the agricultural climate models generating the lowest and highest global damages. Each selected agricultural model is applied across all countries, so this selection does not identify country-specific minimum and maximum losses. Coastal flooding and sea-level rise use the corresponding lower and higher coastal projections, while riverine flood projections remain at their central values.

## A.3. Transmission through economic linkages

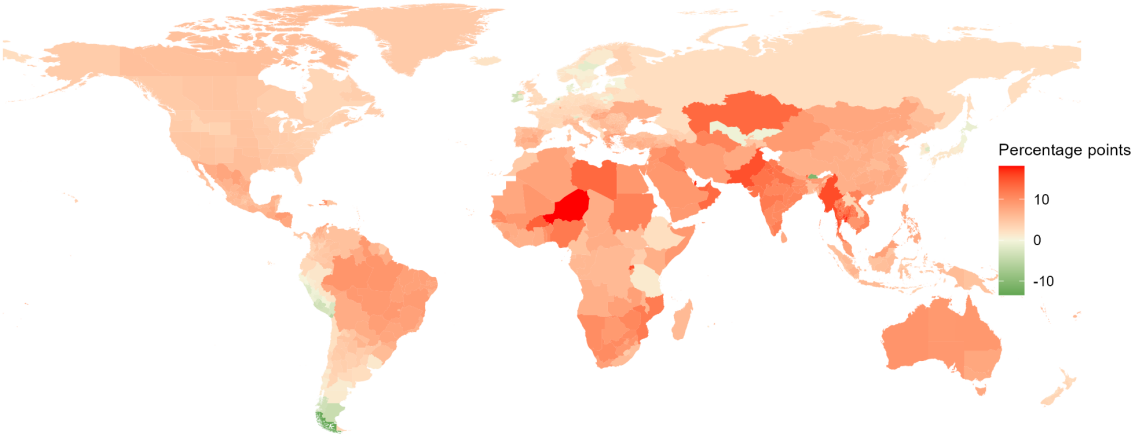
This subsection complements Section 5.2. It presents the transmission maps for the very high-emissions scenario, followed by OECD+ country comparisons under both scenarios. The intermediate-emissions maps appear in the main text. Each recalibrated model measures losses relative to its own no-climate-change reference path.

**Figure A.13:** How economic linkages change climate-induced GDP per capita losses in 2100: very high-emissions scenario

**(a)** Additional percentage point loss in GDP per capita in 2100 due to spatial linkages under SSP5-8.5



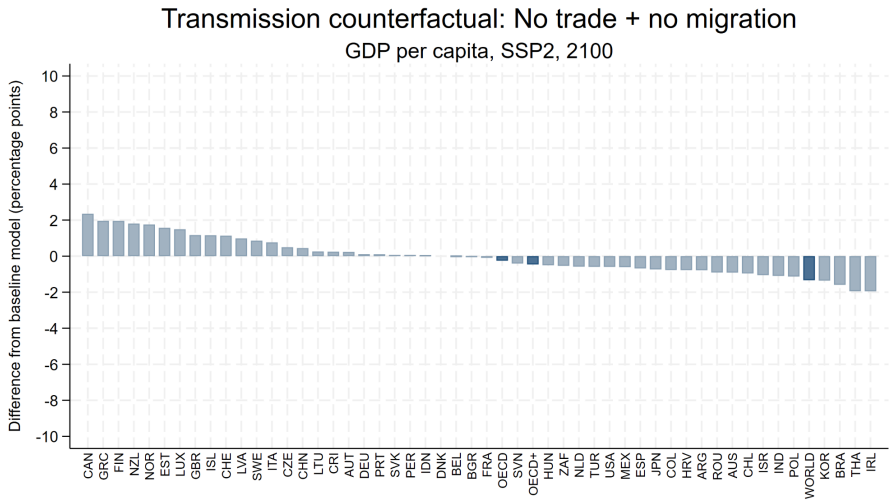

**(b)** Additional percentage point loss in GDP per capita in 2100 due to input–output linkages under SSP5-8.5



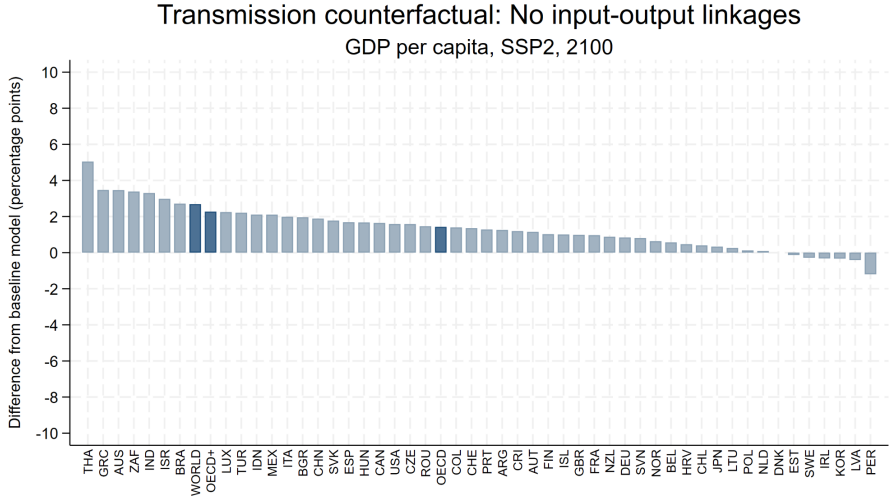

*Source:* Authors' calculations.
*Notes:* The panels report differences in climate-induced GDP per capita losses between the full model and a recalibrated counterfactual without the indicated linkages, in percentage points. Each model measures climate losses relative to its own no-climate-change reference path. Positive values indicate that the linkages increase losses, while negative values indicate that they reduce losses. Climate projections follow SSP5-8.5.

**Figure A.14:** Effects of economic linkages on GDP per capita losses across OECD+ countries in 2100: intermediate-emissions benchmark

**(a)** Additional percentage point loss in GDP per capita in 2100 due to spatial linkages under SSP2-4.5



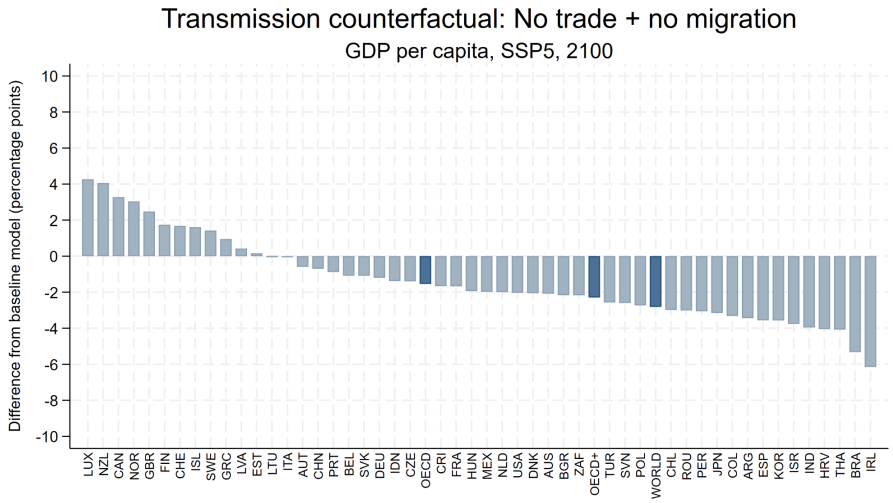

**(b)** Additional percentage point loss in GDP per capita in 2100 due to input–output linkages under SSP2-4.5



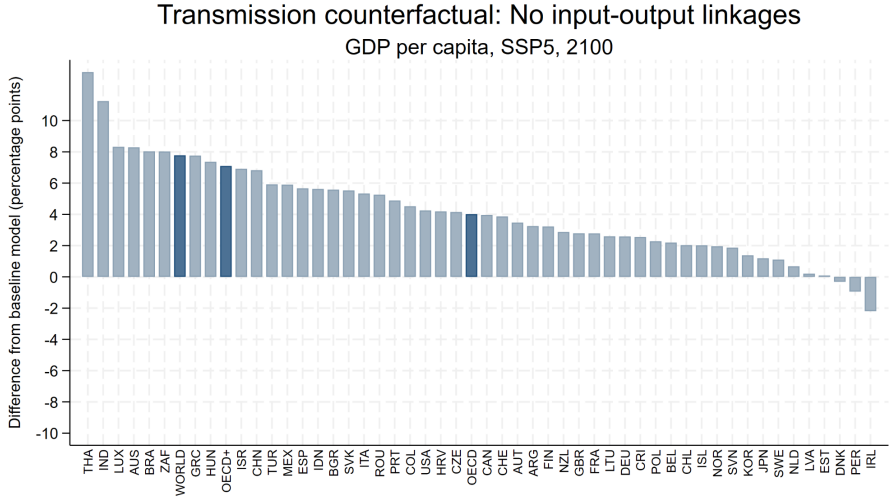

*Source:* Authors' calculations.
*Notes:* The panels report differences in climate-induced GDP per capita losses between the full model and a recalibrated counterfactual without the indicated linkages, in percentage points. Each model measures climate losses relative to its own no-climate-change reference path. Positive values indicate that the linkages increase losses, while negative values indicate that they reduce losses. Climate projections follow SSP2-4.5.

**Figure A.15:** Effects of economic linkages on GDP per capita losses across OECD+ countries in 2100: very high-emissions scenario

**(a)** Additional percentage point loss in GDP per capita in 2100 due to spatial linkages under SSP5-8.5




**(b)** Additional percentage point loss in GDP per capita in 2100 due to input–output linkages under SSP5-8.5



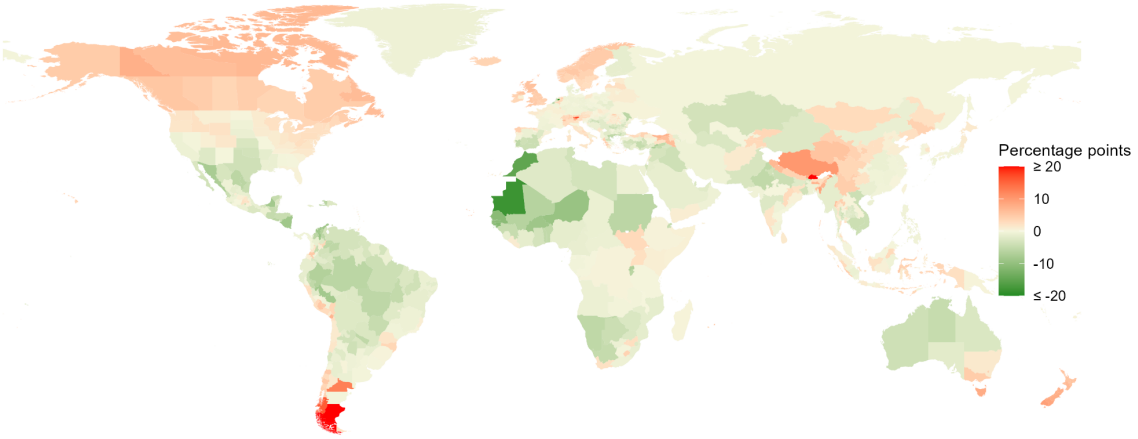

*Source:* Authors' calculations.
*Notes:* The panels report differences in climate-induced GDP per capita losses between the full model and a recalibrated counterfactual without the indicated linkages, in percentage points. Each model measures climate losses relative to its own no-climate-change reference path. Positive values indicate that the linkages increase losses, while negative values indicate that they reduce losses. Climate projections follow SSP5-8.5.

## A.4. Adjustment through trade and labour reallocation

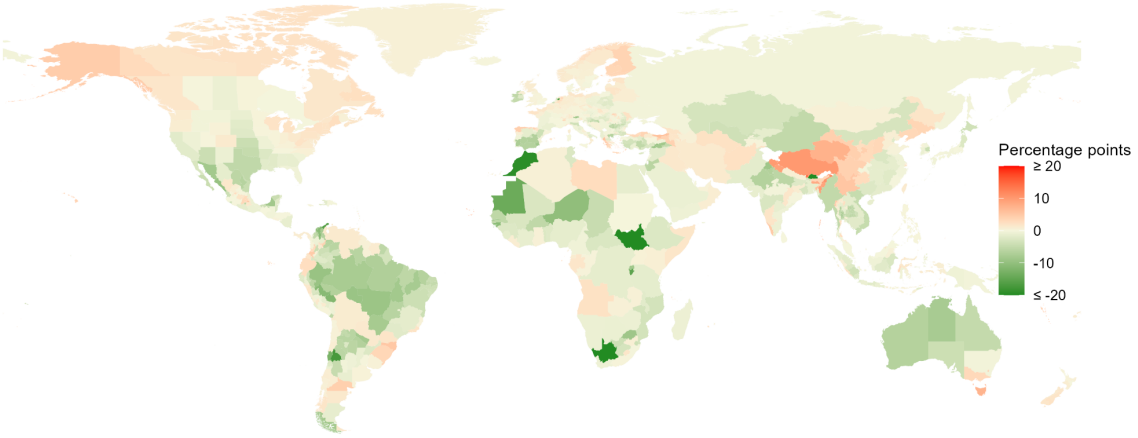
This subsection complements Section 5.3. It presents the adjustment maps for the very high-emissions scenario, followed by OECD+ country comparisons under both scenarios. The intermediate-emissions maps appear in the main text. The exercises retain the baseline calibration and restrict the indicated allocation shares to their no-climate-change paths.

**Figure A.16:** How adjustment changes climate-induced GDP per capita losses in 2100: very high-emissions scenario

**(a)** Additional percentage point loss in GDP per capita in 2100 due to adjustments via labour mobility under SSP5-8.5



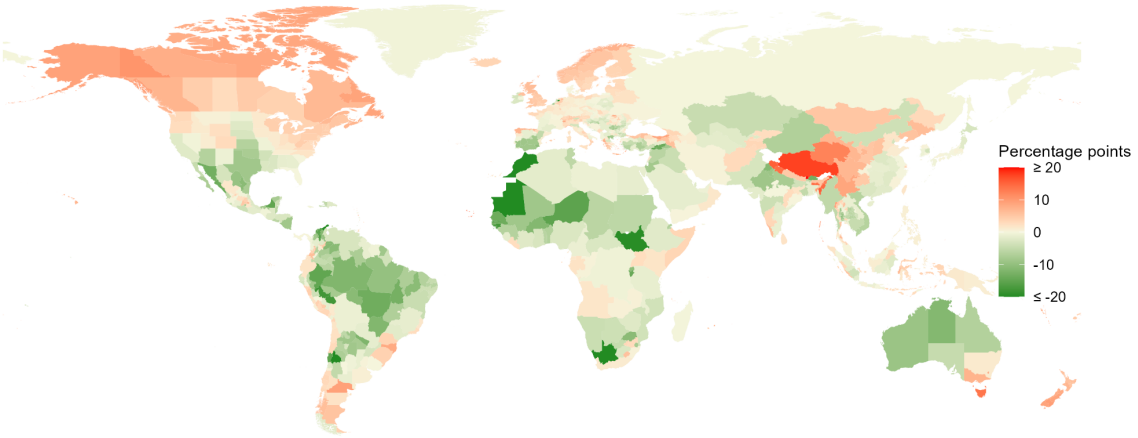

**(b)** Additional percentage point loss in GDP per capita in 2100 due to trade adjustment under SSP5-8.5




*Source:* Authors' calculations.
*Notes:* The panels report differences in climate-induced GDP per capita losses between the full model and simulations with the indicated adjustment margins restricted, in percentage points. The baseline calibration is retained. Restricted allocation shares follow their no-climate-change paths. Positive values indicate that allowing adjustment increases losses, while negative values indicate that it reduces losses. Climate projections follow SSP5-8.5. Values outside $[-20, 20]$ are shown at the endpoints of the colour scale.

**Figure A.16:** How adjustment changes climate-induced GDP per capita losses in 2100: very high-emissions scenario (continued)

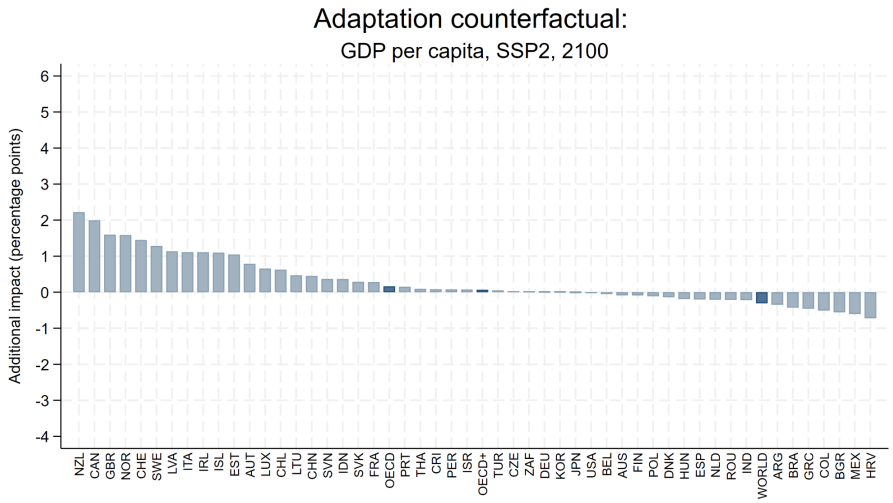
**(c)** Additional percentage point loss in GDP per capita in 2100 due to labour and trade adjustment under SSP5-8.5



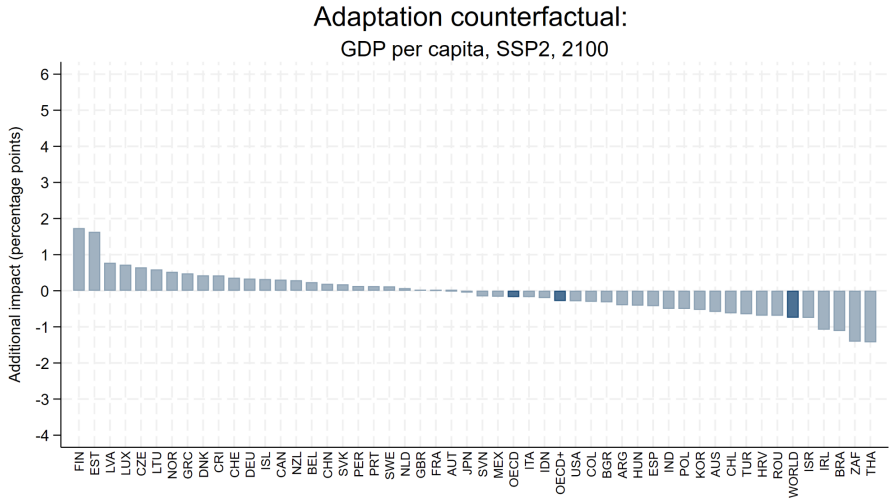

*Source:* Authors' calculations.
*Notes:* The panels report differences in climate-induced GDP per capita losses between the full model and simulations with the indicated adjustment margins restricted, in percentage points. The baseline calibration is retained. Restricted allocation shares follow their no-climate-change paths. Positive values indicate that allowing adjustment increases losses, while negative values indicate that it reduces losses. Climate projections follow SSP5-8.5. Values outside $[-20, 20]$ are shown at the endpoints of the colour scale.

**Figure A.17:** Effects of adjustment on GDP per capita losses across OECD+ countries in 2100: intermediate-emissions scenario

**(a)** Additional percentage point loss in GDP per capita due to adjustment in labour mobility



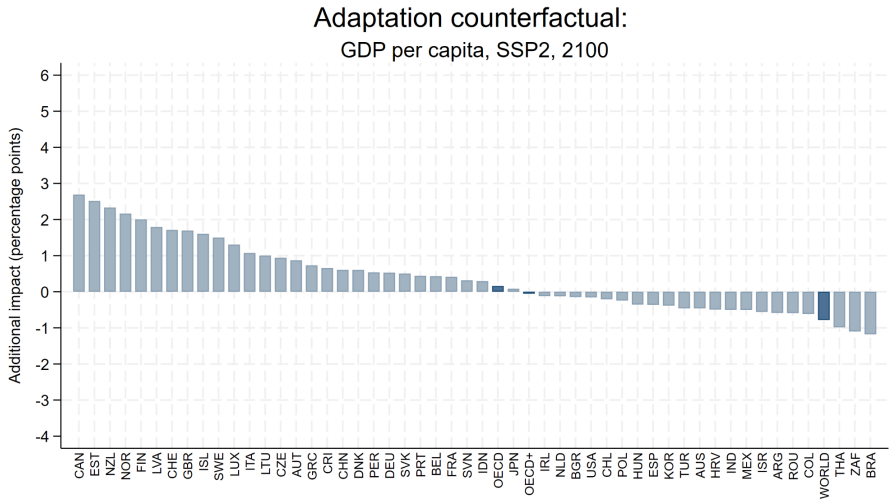

**(b)** Additional percentage point loss in GDP per capita due to adjustment in trade shares




*Source:* Authors' calculations.
*Notes:* The panels report differences in climate-induced GDP per capita losses between the full model and simulations with the indicated adjustment margins restricted, in percentage points. Positive values indicate that allowing adjustment increases losses, while negative values indicate that it reduces losses. OECD+ follows the country grouping used in the model outputs. Climate projections follow SSP2-4.5.

**Figure A.17:** Effects of adjustment on GDP per capita losses across OECD+ countries in 2100: intermediate-emissions scenario (continued)

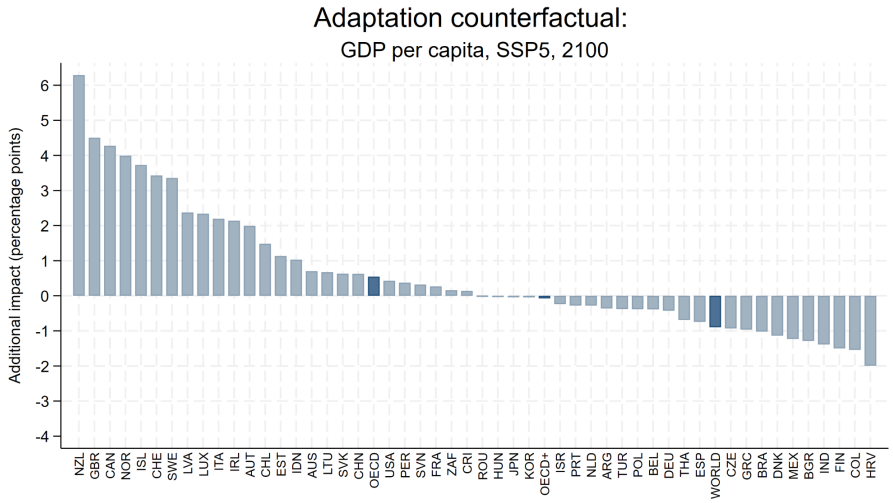
**(c)** Additional percentage point loss in GDP per capita due to joint adjustment in labour mobility and trade shares



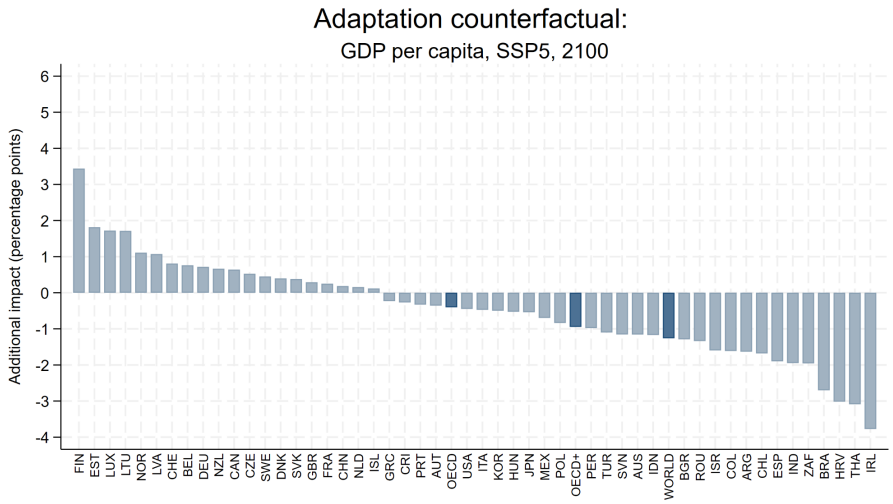

*Source:* Authors' calculations.
*Notes:* The panels report differences in climate-induced GDP per capita losses between the full model and simulations with the indicated adjustment margins restricted, in percentage points. Positive values indicate that allowing adjustment increases losses, while negative values indicate that it reduces losses. OECD+ follows the country grouping used in the model outputs. Climate projections follow SSP2-4.5.

**Figure A.18:** Effects of adjustment on GDP per capita losses across OECD+ countries in 2100: very high-emissions scenario

**(a)** Additional percentage point loss in GDP per capita in 2100 due to adjustments via labour mobility under SSP5-8.5



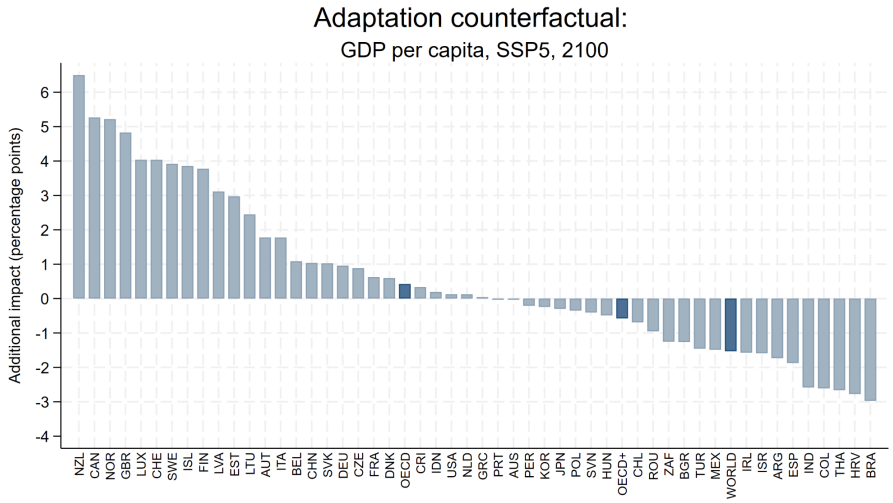

**(b)** Additional percentage point loss in GDP per capita in 2100 due to trade adjustment under SSP5-8.5




*Source:* Authors' calculations.
*Notes:* The panels report differences in climate-induced GDP per capita losses between the full model and simulations with the indicated adjustment margins restricted, in percentage points. Positive values indicate that allowing adjustment increases losses, while negative values indicate that it reduces losses. OECD+ follows the country grouping used in the model outputs. Climate projections follow SSP5-8.5.

**Figure A.18:** Effects of adjustment on GDP per capita losses across OECD+ countries in 2100: very high-emissions scenario (continued)

**(c)** Additional percentage point loss in GDP per capita in 2100 due to labour and trade adjustment under SSP5-8.5




*Source:* Authors' calculations.
*Notes:* The panels report differences in climate-induced GDP per capita losses between the full model and simulations with the indicated adjustment margins restricted, in percentage points. Positive values indicate that allowing adjustment increases losses, while negative values indicate that it reduces losses. OECD+ follows the country grouping used in the model outputs. Climate projections follow SSP5-8.5.

## B. Further detail: flood firm-level analysis

Floods are among the most economically damaging natural hazards and are expected to become more frequent and severe in many regions as climate change progresses (IPCC, 2021). Unlike heat stress, which primarily affects productivity, flooding can disrupt economic activity through multiple channels, including damage to physical capital, disruptions to transport and infrastructure networks, supply-chain interruptions, and financial constraints that hinder recovery. Understanding the relative importance of these channels is therefore essential for translating future flood risk into economic damages.

To quantify these effects, we draw on estimates from Baptista et al. (forthcoming), who combine high-resolution information on flood events with firm-level balance sheet data to estimate the impact of flooding on firms. This annex provides a brief overview of the data, methodology and key findings used to calibrate flood damages in OECD-CASGEM.

### B.1. Regression specification

The analysis combines firm-level balance-sheet information from Moody's Orbis with high-resolution flood maps from the Global Flood Database (Tellman et al., 2021) and meteorological data from the ERA-5 global reanalysis dataset produced by the European Centre for Medium-Range Weather Forecasts and available through the Copernicus Climate Change Service. The resulting dataset covers more than 2.5 million firms across 17 European and Asian advanced economies over the period 2000–2018. Precise geographical information at the headquarters level allows firms to be matched to flood events and enables the identification of both directly affected firms and firms indirectly exposed through local spillovers.[19]

To estimate the effect of flooding on firm outcomes, the analysis compares firms inside flooded areas with a control group of firms located more than 100 km from flooded areas, using the following specification:

$$\begin{aligned} Y_{i(cs),t} = {} & \beta_1 \,\text{Flooded}_{i(cs),t} + \beta_2 \,\text{Spillover}_{i(cs),t} \\ & + \boldsymbol{\beta}_3' \mathbf{X}_{i(cs),t-1} + \boldsymbol{\beta}_4' \mathbf{W}_{i(cs),t} \\ & + \delta_{st} + \delta_{ct} + \delta_{i(cs)} + \varepsilon_{i(cs),t}. \end{aligned} \tag{15}$$

Here, $Y_{i(cs),t}$ is the outcome of interest for firm $i$ in sector $s$ and country $c$ in year $t$. The outcomes include value added, capital stock measured by the deflated value of fixed assets, multi-factor productivity, and employment, all in logarithms.[20] The variable $\text{Flooded}_{i(cs),t}$ is an indicator equal to one if a firm is flooded in year $t$ and remains equal to one in subsequent years within the estimation window.[21] The post-flood period is treated as an absorbing treatment state because the

[19] The estimated spillover effects are not used separately in the model calibration, since the model generates spillovers endogenously through economic linkages. Including the spillover term in the regression helps avoid bias in the estimated direct effect that would arise from including indirectly affected firms in the control group.

[20] Firm-level multifactor productivity is estimated using the value-added-based GMM procedure of Wooldridge (2009).

[21] The analysis is restricted to the four years following each flood event. This window helps ensure that estimated

economic consequences of a flood can extend beyond the physical inundation.

The variable $\text{Spillover}_{i(cs),t}$ is an indicator equal to one if firm $i$ was not directly affected by a flood but was located within 100 km of a flooded area. The vector $\mathbf{X}_{i(cs),t-1}$ contains lagged firm-level controls, including firm size, age, profitability, and a measure of capital intensity and liquidity.[22] The vector $\mathbf{W}_{i(cs),t}$ contains annual weather controls, including wind speed, precipitation, humidity, and the number of warm days, as described in Costa et al. (2024). The specification includes firm fixed effects $\delta_{i(cs)}$, sector-year fixed effects $\delta_{st}$, and country-year fixed effects $\delta_{ct}$.

### B.2. Results

The results indicate that flooding primarily affects firms through capital destruction and slower capital accumulation rather than persistent productivity or employment losses. Direct flood exposure leads to a statistically significant decline in firms' capital stocks of 2.7% on average in the four years after the flood, while estimated effects on multifactor productivity and employment are small and generally not statistically significant. The decline in capital stock is reflected in a decrease in firm value added. Figure B.1 shows the estimated impacts on these four outcomes.

Flooding generates economically meaningful spillovers to firms that are not directly inundated. For capital stock, productivity, and value added, negative spillover effects are sizeable and statistically significant, with magnitudes between 38% and 68% of the direct effect. These findings suggest that disruptions to infrastructure, local supply chains, demand conditions, or financial markets can transmit flood damages beyond directly affected locations. The impacts of flooding are heterogeneous, depending on both the severity of the event and firm characteristics that shape resilience. Longer flooding episodes generate substantially larger capital losses than shorter events. Firm size is also an important margin of vulnerability: smaller firms, particularly micro firms, experience considerably larger capital losses, whereas estimated effects for large firms are not statistically significant.

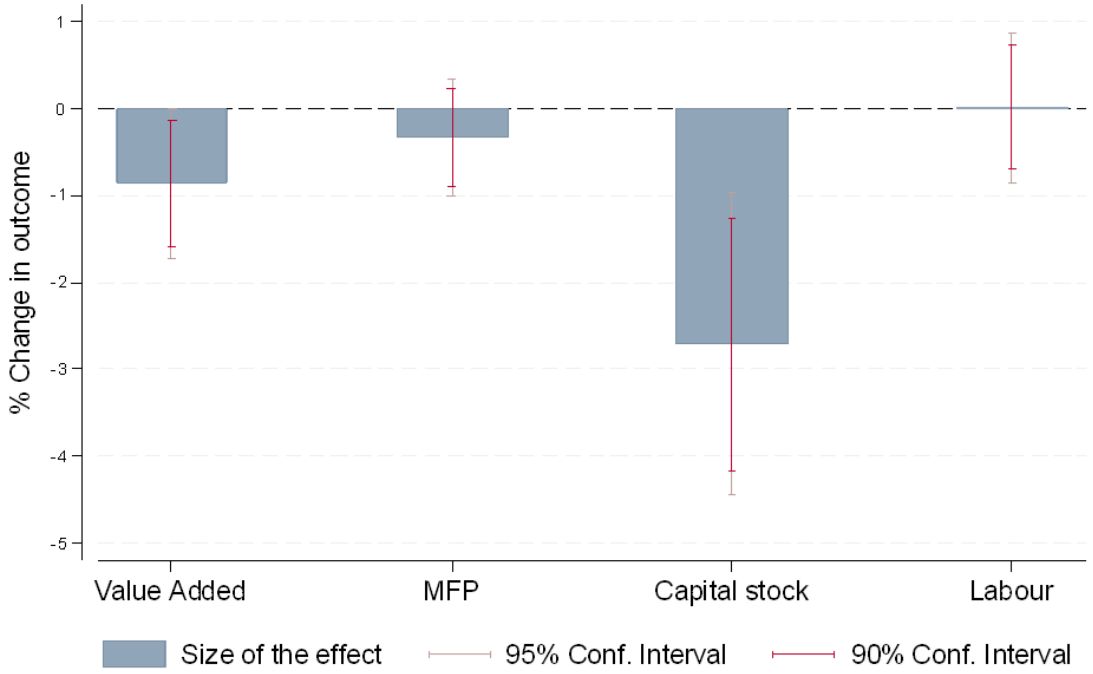
Taken together, the results highlight three key features of flood-related economic damage at the firm level. First, floods primarily affect firms through capital losses rather than immediate declines in productivity. Second, indirect spillovers to nearby firms are substantial, underscoring the importance of accounting for spatial linkages. Third, impacts vary with flood duration and firm size. These empirical findings motivate incorporating capital dynamics and spatial transmission into the macroeconomic framework presented in Section 4.

effects remain attributable to the original shock, maintains a consistent comparison across events, and avoids the sample loss associated with longer horizons given firms' uneven observation patterns. The results are similar when varying the number of years and when returning the flooding indicator to zero after four years. Firms affected by more than one flood in a year, which account for 0.45% of flooded firms, are excluded.

[22] The controls vary with the dependent variable. Regressions with labour productivity and value added include all controls, those with multifactor productivity exclude capital intensity, and those with employment exclude the size categories.

**Figure B.1:** Floods affect firms mainly through their impact on capital stocks

Percentage change in outcome variables due to being affected by a flood




*Notes:* Bars represent estimated coefficients and vertical lines the respective 95% and 90% confidence intervals. The estimates are obtained from equation (15), with log value added, multifactor productivity, fixed assets, and employment as the respective dependent variables. Coefficients are multiplied by 100 to express approximate percentage changes.
*Source:* Authors' calculations based on Baptista et al. (forthcoming), using data from Orbis, the Global Flood Database, and Copernicus.

## C. Further detail: impact of heat stress on firm productivity

We use and build on estimates of the impact of heat stress on labour productivity from Costa et al. (2024) to calibrate the size of climate damages. Costa et al. (2024) use firm-level data from Orbis (Moody's), providing detailed information on output, input usage, firm characteristics, and the geographic location of over 2.7 million firms across 23 advanced economies from 2000 to 2021. To capture climatic conditions, it uses ERA-5 reanalysis data containing high-resolution daily temperature and other weather variables at approximately 28 x 28 km resolution near the equator. With these two datasets, one can examine the relationship between firm-level outcomes and localized climatic variations with high spatial and temporal precision. To measure the impact of heat stress, we follow their paper in defining hot days as the number of annual days in which the maximum daily temperature falls within a given temperature bin, allowing us to assess the effects of varying temperature exposures on firm performance.

### C.1. Regression specification

To account for the heterogeneous impact of heat stress, we employ a regression specification that accommodates varying levels of heat stress and local average temperature as a mediating factor. This approach enables us to capture differential vulnerabilities across sectors while also considering the broader climatic context in which firms operate, whereby the same level of heat may have a smaller or larger impact. The impact of heat stress has been found to vary depending on whether a location has a predominantly cold or warm climate, as different adaptation systems and infrastructures are in place to manage temperature extremes (Costa et al., 2024). Hotter countries are likely to be better prepared for high temperatures, whereas firms in colder regions may face greater disruptions due to a lack of pre-existing heat adaptation measures. We estimate the following regression using the full sample in the paper:

$$Z^j_{int} = \sum_{b=1}^{B} \left( \beta^b + \sum_{h=1}^{H} \delta_h \, \text{AvgTemp}^h_n \right) \text{HotDays}^b_{nt} + \gamma_1 \, \mathbf{X}_{it} + \gamma_2 \, \mathbf{W}_{nt} + \theta_i + \lambda_{c(n)t} + \varepsilon^j_{int} \tag{16}$$

where $i$ denotes firm, $j$ denotes sector, $n$ denotes location, $c(n)$ denotes the country to which location $n$ belongs and $t$ denotes year. The variables above are defined as follows:

- $Z^j_{int}$: firm-level productivity measured as multi-factor productivity. This is estimated using the generalized method of moments value added-based procedure from Wooldridge (2009). This procedure relies on a system of moment conditions where firm-level inputs serve as proxies for productivity shocks. The estimated residual from the production function represents TFP, which captures variations in output not explained by firm inputs. The deflated value

of fixed assets is used as a proxy for the capital input, the number of employees as a proxy for the labour input, and intermediate inputs as an instrument for unobserved firm-specific productivity shocks.

- $\text{AvgTemp}_n^h$: dummy for whether average annual maximum daily temperature in 2000–2021 in location $n$ falls within band $h \in \{1, \ldots, H\}$
- $\text{HotDays}_{nt}^b$: number of hot days where daily maximum temperature falls within band $b \in \{1, \ldots, B\}$
- $\mathbf{X}_{it}$: time-varying firm characteristics including firm size, age, and average profitability
- $\mathbf{W}_{nt}$: yearly averages of weather variables, namely wind speed, moisture, and precipitation
- $\theta_i$: firm fixed effect controlling for all time-invariant firm characteristics
- $\lambda_{c(n)t}$: country-year fixed effects controlling for common time-trends in each country

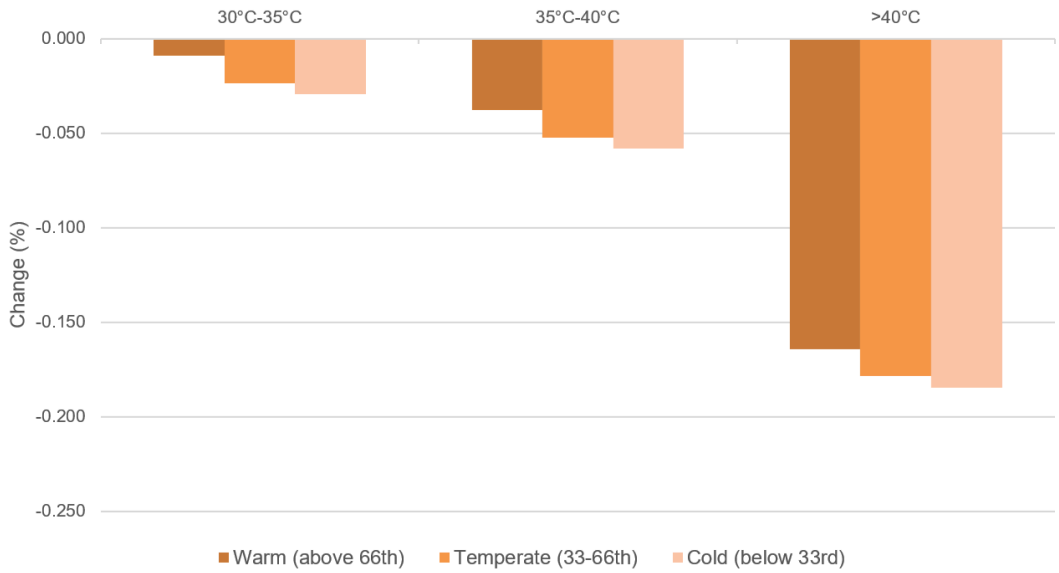
We parameterize average temperature bins $h \in \{1, \ldots, H\}$ by categorizing locations based on their average maximum daily temperature percentiles: below the 33rd (cold), between and including the 33rd and 66th (temperate), and above the 66th (warm). In turn, hot day bins $b \in \{1, \ldots, B\}$ are parameterized by separating each day into those whose maximum temperature was between 30°C and 35°C, between 35°C and 40°C, and above 40°C. Standard errors are clustered at the firm-year level.

### C.2. Results

Figure C.1 shows the productivity effects of an additional hot day by temperature band and baseline climatic conditions, based on the estimated coefficients from equation (16). All estimates should be interpreted as the level of firm productivity relative to a day when the temperature is lower than 30°C, which is the temperature bin we set as the baseline.

**Figure C.1:** Impact of an additional hot day on firm productivity

Percent change in annual TFP by temperature bin and climate type




*Source:* Authors' own calculations based on Costa et al. (2024) and Climate Change Knowledge Portal (World Bank).
*Notes:* The figure shows the impact of an additional day for locations on log multi-factor productivity. The values are derived from the estimated coefficients in Equation (16). The legend denotes the percentile interval of average annual maximum daily temperature.

## D. Further detail: projections of future flood damages

### D.1. Flood Protection Standards

A necessary first step in projecting future flood risk is to characterise the baseline probability of flooding. Historical flood exposure reflects not only natural hydrological conditions, but also the level of protection provided by existing flood defences, such as levees, dikes and coastal barriers. Understanding the relationship between natural flood hazard and protection standards is therefore essential for assessing how the frequency of flooding may evolve under future climate scenarios.

Baseline protection levels for riverine flooding are obtained from the FLOPROS (Flood Protection Standards) database, developed by Scussolini et al. (2016) as part of a joint effort by researchers at IVM (Vrije Universiteit Amsterdam), the World Bank, and other partners. FLOPROS provides spatially explicit estimates of existing flood protection standards across the globe, expressed in terms of return periods (e.g. a 1-in-50-year or 1-in-100-year level of protection). These values represent the capacity of local flood defences and are compiled using a combination of national reports, engineering assessments, model-derived simulations and proxy indicators such as income levels and urbanisation. Protection values for coastal flooding are obtained from Tiggeloven et al. (2020) . Both FLOPROS and the dataset from Tiggeloven et al. (2020) are available at a sub-national resolution, allowing one to account for variation in protection standards within countries.

### D.2. Climate-Driven Hazard Projections

To translate these protection standards into measures of flood risk under future climatic conditions, we combine them with riverine and coastal flood hazard maps produced under the Aqueduct Floods framework by the World Resources Institute (WRI). These maps provide spatial estimates of flood depth for a range of return periods (from 1-in-2 to 1-in-1000-year events), at a very high spatial resolution of 30 arc-seconds - roughly 1 x 1 km at the equator in the years 2030, 2050, and 2080 under RCP4.5 and RCP8.5. The projections are based on downscaled climate model outputs combined with hydrological and hydraulic modelling, allowing them to capture changes in precipitation patterns, river discharge and storm-surge dynamics. Separate sets of maps are available for riverine flooding and coastal flooding.

Using these data, we assess how the frequency of flooding is expected to change under the assumption that current flood protection standards remain constant over time. Specifically, for each location, we compare projected flood depths to the historical protection threshold implied by the local FLOPROS return period. If the projected flood depth exceeds the historical protection level more frequently in the future, this implies an increase in the probability of overtopping or failure, and therefore a higher frequency of damaging flood events. This approach allows us to isolate the effect of changing climatic conditions on flood risk, holding the existing level of protection infrastructure constant.

To assess economic relevance, we combine the geographic extent of flood-prone areas with spatial population data provided by the Gridded Population of the World, Version 4 (GPWv4) dataset.

This allows us to compute, for each location, the share of the population residing in areas subject to flooding under baseline protection standards. We do this by first identifying the pixels in which the projected flood depth exceeds zero in a 1-in-100-year flood and then computing the share of total population in each GPW grid cell residing in flood-exposed land.

**Figure D.1:** Effect of climate change on coastal flood frequency in 2080 relative to 1980

Percent change in the annual frequency of coastal flooding under RCP8.5 (ensemble mean)




*Source:* Scussolini et al. (2016), World Resources Institute (Aqueduct), and authors' own calculations.
*Note:* The map reports values at the resolution of a 0.25° × 0.25° grid cell (approximately 25 km at the equator). Values greater than 50% and less than -50% are winsorised at 50% and -50%, respectively. The projections assume flood protection standards remain the same as in the baseline period (i.e. 1980).

For coastal flooding, the WRI projections incorporate both changes in storm surge behaviour and the effects of rising mean sea levels, which increase the baseline water level on which storm surges are superimposed. In areas where the annual probability of coastal flooding reaches 50 percent - effectively implying a permanent or near-permanent inundation - the hazard is no longer characterised as intermittent flooding. In such cases, we treat the impact as a separate and distinct risk, captured under sea level rise rather than episodic coastal flooding. The treatment of sea-level rise as a standalone hazard is done separately. For all other cases, we treat coastal flooding similarly to riverine flooding. Figure D.1 shows projected changes in the frequency of coastal flooding in such cases.

### D.3. Baseline Exposure and Population Overlay

Flood risk does not affect all locations equally. Large parts of the world's population and economic activity lie outside flood-prone areas, while others are highly exposed to recurrent riverine or coastal flooding. Before assessing the potential economic consequences of future flood events, it is therefore important to establish the underlying extent and spatial distribution of exposure. In

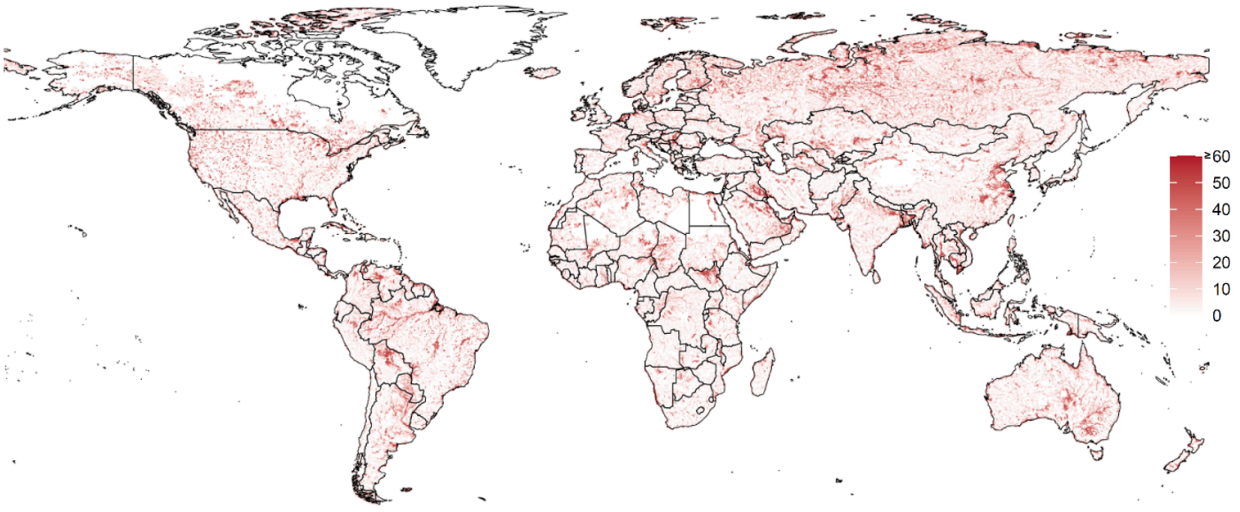
this context, exposure is defined as the presence of people, assets and economic activity in areas that are subject to inundation, conditional on a given hazard threshold.

To measure the extent of exposure, we first take historical 1-in-100-year flood hazard maps for both riverine and coastal flooding. For each grid cell, we identify whether the projected flood depth exceeds zero. All locations for which the estimated flood depth is strictly positive are classified as flood-exposed under the historical baseline, irrespective of the precise depth or recurrence probability beyond this threshold. This binary classification allows us to establish the geographic extent of areas that are potentially subject to flooding under current climatic and protection conditions, and to treat all such locations as equally exposed in the baseline.

To translate this geographic extent into a measure of economic exposure, we overlay the flood hazard maps with high-resolution population data from the Gridded Population of the World, Version 4 (GPWv4) dataset, produced by the Center for International Earth Science Information Network (CIESIN) in collaboration with the National Aeronautics and Space Administration (NASA). GPWv4 provides gridded estimates of population counts and densities at the same spatial resolution of 30 arc-seconds as the flood hazard maps, offering a globally consistent depiction of the geographic distribution of population. We use population as a proxy for overall economic exposure, recognising that this abstracts from potential differences in asset intensity and infrastructure density across locations. By combining the flood exposure mask with the GPWv4 population grid, we compute, for each sub-national region, the share of the population residing in flood-exposed areas.

**Figure D.2:** Population exposed to riverine flooding

Percentage of population exposed to a 1-in-100-year riverine flood




*Source:* World Resources Institute (Aqueduct), Gridded Population of the World (GPW v4.11), and authors' own calculations.
*Note:* The map reports values at the resolution of a 0.25° × 0.25° grid cell (approximately 25 km at the equator). Values greater than 60% are winsorised at 60%.

Figure D.2 maps the share of the population exposed to a 1-in-100-year riverine flood across the globe, revealing substantial spatial variation. High exposure is concentrated in densely populated river basins, including parts of Central and Eastern Europe, northern Italy, the Rhine and Danube basins, regions along major river systems in the United States and, most notably, the Netherlands. In several of these locations, a sizeable share of the population resides within the historical 100-year floodplain, reflecting the long-standing co-location of economic activity and settlement patterns with river networks. In contrast, large parts of OECD countries characterised by limited river networks or lower population density, display lower exposure. The map highlights where baseline hydrological risk intersects with population density, offering a clearer sense of the human footprint in flood-prone areas. The figure captures potential exposure, not expected damage: many regions with high exposure may face low damages if they have significant protective infrastructure, while those with low exposure may still face substantial impacts if protective capacity is limited and/or flooding is frequent.

## E. Model description, equilibrium, calibration, and counterfactuals

This appendix provides the supporting derivations and complete equilibrium system for the model in Section 4, followed by the calibration and counterfactual procedures. Bilateral indices are ordered as destination followed by origin, and all prices and allocations refer to period $t$ unless stated otherwise.

### E.1. Supporting derivations

#### E.1.1 Workers' expenditure and location choices

Workers supply one unit of labour and spend their wage income on goods and housing. Let $C_{nt}^W$ and $h_{nt}^W$ denote goods consumption and housing services per worker in destination $n$. With Cobb–Douglas preferences, their expenditure demands satisfy

$$P_{nt}C_{nt}^W = \alpha w_{nt}, \qquad Q_{nt}h_{nt}^W = (1-\alpha)w_{nt}. \tag{17}$$

The goods aggregate uses sectoral expenditure shares $\alpha^j$, with $\sum_j \alpha^j = 1$. We normalise the Cobb–Douglas aggregators so that their dual price indices are $P_{nt} = \prod_j (P_{nt}^j)^{\alpha^j}$ and $P_{nt}^{\alpha}Q_{nt}^{1-\alpha}$ for goods and for the combined goods–housing basket, respectively.

Conditional on initially residing in $i$, a worker chooses the destination that maximises $b_{ni,t}B_n w_{nt}/(\kappa_{ni}P_{nt}^{\alpha}Q_{nt}^{1-\alpha})$. Independent Fréchet preference draws with dispersion $\varepsilon$ yield the migration probabilities in equation (34). These are choices over current utility. The specification does not include a continuation value for workers, although successive location choices change the distribution of population over time.

#### E.1.2 Production costs, sourcing, and sectoral prices

Perfect competition implies that the factory-gate price of a variety equals its unit production cost:

$$p_{nt}^j(\iota^j) = \frac{x_{nt}^j}{A_{nt}^j z_n^j(\iota^j)}. \tag{18}$$

For the production function in the main text, the constant in the input-bundle cost is

$$\mu_n^j = (\lambda\beta_n^j)^{-\lambda\beta_n^j}(\eta\beta_n^j)^{-\eta\beta_n^j}\left[(1-\lambda-\eta)\beta_n^j\right]^{-(1-\lambda-\eta)\beta_n^j}\prod_{k=1}^{J}(\gamma_n^{jk})^{-\gamma_n^{jk}}, \tag{19}$$

where a factor with zero expenditure share is interpreted by continuity as one. The expenditure shares satisfy $\beta_n^j + \sum_k \gamma_n^{jk} = 1$.

Competitive final goods producers combine intermediate varieties according to

$$\widetilde{Q}_{nt}^j = \left[\int_0^1 \left(\widetilde{q}_{nt}^j(\iota^j)\right)^{(\nu-1)/\nu} d\iota^j\right]^{\nu/(\nu-1)}, \qquad \nu > 1, \tag{20}$$

and source each variety at the lowest delivered price,

$$\widetilde{p}^{j}_{nt}(\iota^j) = \min_{i\in\{1,\dots,N\}} \left\{ \tau^{j}_{ni} p^{j}_{it}(\iota^j) \right\}. \tag{21}$$

With independent productivity draws $F_j(z) = \exp(-z^{-\theta^j})$, define $\Phi^{j}_{nt} = \sum_i (A^{j}_{it})^{\theta^j} (x^{j}_{it}\tau^{j}_{ni})^{-\theta^j}$. The distribution of the minimum delivered price is $\Pr(\widetilde{p}^{j}_{nt} \le p) = 1 - \exp[-\Phi^{j}_{nt} p^{\theta^j}]$. Integrating this distribution in the CES price index gives

$$P^{j}_{nt} = g^j (\Phi^{j}_{nt})^{-1/\theta^j}, \qquad g^j = \left[ \Gamma\left(1 + \frac{1-\nu}{\theta^j}\right) \right]^{1/(1-\nu)}, \tag{22}$$

where $\Gamma(\cdot)$ is the gamma function and $\theta^j > \nu - 1$. Origin $i$'s contribution to $\Phi^{j}_{nt}$ determines its expenditure share, yielding equation (6).

### E.1.3 Structures, factor demands, and land income

Aggregating intermediate producers' Cobb–Douglas factor demands within each location and sector gives

$$w_{nt} L^{j}_{nt} = \lambda \beta^{j}_{n} R^{j}_{nt}, \quad r_{nt} K^{j}_{nt} = \eta \beta^{j}_{n} R^{j}_{nt}, \quad Q_{nt} H^{j}_{nt} = (1-\lambda-\eta)\beta^{j}_{n} R^{j}_{nt}. \tag{23}$$

The real estate technology is $H_{nt} = (K^{H}_{nt})^{\mu} T^{1-\mu}_{nt}$. Cost minimisation gives $r_{nt} K^{H}_{nt} = \mu Q_{nt} H_{nt}$, while the residual $(1-\mu) Q_{nt} H_{nt}$ is paid to local landowners. Combining the capital demand with the technology yields

$$H_{nt} = T_{nt} \left( \frac{\mu Q_{nt}}{r_{nt}} \right)^{\mu/(1-\mu)}. \tag{24}$$

Demand for structures comes from workers' housing and firms' floor space. Substituting the structures supply into market clearing gives

$$Q_{nt} = \left( \frac{r_{nt}}{\mu} \right)^{\mu} \left[ \frac{(1-\alpha) w_{nt} L_{nt} + \sum_j (1-\lambda-\eta)\beta^{j}_{n} R^{j}_{nt}}{T_{nt}} \right]^{1-\mu}. \tag{25}$$

The allocation conditions are $\sum_j L^{j}_{nt} = L_{nt}$ and $\sum_j K^{j}_{nt} + K^{H}_{nt} = \widetilde{K}_{nt}$. Together with factor demands, they imply the labour and capital market-clearing equations below.

### E.1.4 Capital owners' intertemporal problem

Capital owners take prices and destruction rates as given and choose consumption and next period's capital to solve

$$\max_{\{C^{K}_{n,t+s}, K_{n,t+s+1}\}_{s=0}^{\infty}} E_t \sum_{s=0}^{\infty} \beta^s \log C^{K}_{n,t+s}, \tag{26}$$

subject in each period to

$$C_{nt}^K + K_{n,t+1} = \left(\frac{r_{nt}}{P_{nt}} + 1 - \bar{\delta}\right)\widetilde{K}_{nt}, \qquad \widetilde{K}_{nt} = (1 - d_{nt})K_{nt}. \tag{27}$$

Consumption is positive and next period's capital is non-negative. Investment is reversible, so investment $I_{nt} = K_{n,t+1} - (1 - \bar{\delta})\widetilde{K}_{nt}$ is not constrained to be non-negative. Rental income is the sole income source, and capital cannot be transferred across locations. Under these assumptions, logarithmic utility implies the constant saving fraction in Kleinman et al. (2023, Lemma 1). The consumption rule is

$$C_{nt}^K = (1 - \beta)\left(\frac{r_{nt}}{P_{nt}} + 1 - \bar{\delta}\right)\widetilde{K}_{nt}, \tag{28}$$

and the remaining resources become next period's capital according to equation (36). Ordinary depreciation applies to capital that survives the flood, so the fraction of inherited capital surviving both forms of loss is $(1 - \bar{\delta})(1 - d_{nt})$.

#### E.1.5 Expenditure accounting and trade balance

Workers spend $\alpha w_{nt} L_{nt}$ on goods, capital owners spend $P_{nt}(C_{nt}^K + I_{nt})$, and landowners spend $\mathcal{R}_{nt}^T$. The capital owners' budget implies $P_{nt}(C_{nt}^K + I_{nt}) = r_{nt}\widetilde{K}_{nt}$, giving the final-expenditure expression below. To see why trade balances at the location level, sum goods-market clearing across sectors:

$$\sum_j X_{nt}^j = \sum_j (1 - \beta_n^j) R_{nt}^j + E_{nt}. \tag{29}$$

Labour, capital, and structures market clearing, together with local land-rent expenditure, imply $E_{nt} = \sum_j \beta_n^j R_{nt}^j$. Hence $\sum_j X_{nt}^j = \sum_j R_{nt}^j$. This is a location-level accounting restriction and does not impose balance for each bilateral flow or sector.

### E.2. Equilibrium conditions

Given economic parameters, bilateral frictions, amenities, initial capital and population, and the exogenous paths of productivity, usable land, flood destruction, and demographic change, the following system determines prices and allocations. The origin population immediately before migration is $L_{it}^- = \mathcal{D}_{it}(L_{i,t-1})$, where $\mathcal{D}_{it}$ denotes an exogenous demographic update. Without demographic change, $\mathcal{D}_{it}(L) = L$. Nominal prices require a common numeraire in each period.

**Cost of input bundle**

$$x_{nt}^j = \mu_n^j \left(w_{nt}^\lambda r_{nt}^\eta Q_{nt}^{1-\lambda-\eta}\right)^{\beta_n^j} \prod_{k=1}^J (P_{nt}^k)^{\gamma_n^{jk}}. \tag{30}$$

**Sectoral goods price index**

$$P_{nt}^j = g^j \left[\sum_{i=1}^N (A_{it}^j)^{\theta^j} (x_{it}^j \tau_{ni}^j)^{-\theta^j}\right]^{-1/\theta^j}. \tag{31}$$

**Final goods price index**

$$P_{nt} = \prod_{j=1}^{J} (P_{nt}^{j})^{\alpha^{j}}, \qquad \sum_{j=1}^{J} \alpha^{j} = 1. \tag{32}$$

**Optimal trade shares**

$$\pi_{nit}^{j} = \frac{(A_{it}^{j})^{\theta^{j}} (x_{it}^{j} \tau_{ni}^{j})^{-\theta^{j}}}{\sum_{m=1}^{N} (A_{mt}^{j})^{\theta^{j}} (x_{mt}^{j} \tau_{nm}^{j})^{-\theta^{j}}}. \tag{33}$$

**Optimal migration shares**

$$\lambda_{nit} = \frac{\left[ B_n w_{nt} / (\kappa_{ni} P_{nt}^{\alpha} Q_{nt}^{1-\alpha}) \right]^{\varepsilon}}{\sum_{m=1}^{N} \left[ B_m w_{mt} / (\kappa_{mi} P_{mt}^{\alpha} Q_{mt}^{1-\alpha}) \right]^{\varepsilon}}. \tag{34}$$

**Capital available for production**

$$\widetilde{K}_{nt} = (1 - d_{nt}) K_{nt}. \tag{35}$$

**Law of motion of capital**

$$K_{n,t+1} = \beta \left( \frac{r_{nt}}{P_{nt}} + 1 - \bar{\delta} \right) \widetilde{K}_{nt}. \tag{36}$$

**Population distribution**

$$L_{nt} = \sum_{i=1}^{N} \lambda_{nit} L_{it}^{-}. \tag{37}$$

**Producer revenue**

$$R_{nt}^{j} = \sum_{i=1}^{N} \pi_{int}^{j} X_{it}^{j}. \tag{38}$$

**Land rental income**

$$\mathcal{R}_{nt}^{T} = (1 - \mu) Q_{nt} H_{nt}. \tag{39}$$

**Final expenditure on goods**

$$E_{nt} = \alpha w_{nt} L_{nt} + r_{nt} \widetilde{K}_{nt} + \mathcal{R}_{nt}^{T}. \tag{40}$$

**Goods market clearing**

$$X_{nt}^{j} = \sum_{k=1}^{J} \gamma_{n}^{kj} R_{nt}^{k} + \alpha^{j} E_{nt}. \tag{41}$$

**Labour market clearing**

$$w_{nt} L_{nt} = \sum_{j=1}^{J} \lambda \beta_{n}^{j} R_{nt}^{j}. \tag{42}$$

**Capital market clearing**

$$r_{nt} \widetilde{K}_{nt} = \sum_{j=1}^{J} \eta \beta_{n}^{j} R_{nt}^{j} + \mu Q_{nt} H_{nt}. \tag{43}$$

**Supply of structures**

$$H_{nt} = T_{nt} \left( \frac{\mu Q_{nt}}{r_{nt}} \right)^{\mu/(1-\mu)}. \tag{44}$$

**Real estate market clearing**

$$Q_{nt} H_{nt} = (1-\alpha) w_{nt} L_{nt} + \sum_{j=1}^{J} (1-\lambda-\eta) \beta_n^j R_{nt}^j. \tag{45}$$

Sectoral factor allocations, real estate capital, capital owners' consumption, and investment are recovered from the conditions in the preceding derivations. The system applies to the unrestricted model. The counterfactual subsection below explains how selected trade and labour-allocation conditions are replaced when adjustment is restricted.

### E.3. Calibration of baseline model

This subsection provides the geographical and sectoral coverage, data sources, parameter choices, and calibration procedures underlying Section 4.2. We distinguish parameters assigned from the literature, shares constructed from observed accounts, and unobserved fundamentals recovered using the equilibrium conditions. Time subscripts are suppressed when describing the calibration economy, and bilateral indices denote destination followed by origin.

#### E.3.1 Regions and sectors

The model is calibrated for 927 regions across 186 countries, covering 11 sectors of production[23] in OECD member countries and 3 aggregate sectors (agriculture, manufacturing, and services) in all other countries. We divide countries into smaller administrative units depending on their relationship to the OECD. Figure A.3 shows a map of the calibrated administrative units. For OECD member states[24], we employ the Territorial Level 2 (TL2) classification, which is the OECD's system for defining large subnational regions such as provinces or states. For OECD accession candidate countries and OECD key partners[25], denoted OECD+ in Figure A.3, we use Admin-1 sub-national units from the GADM (Global Administrative Areas) database, which provide a consistent first-level administrative division for countries outside the OECD TL2 framework. For

[23]The sectors included are 1. Agriculture, forestry, and fishing; 2. Industry (except manufacturing and construction); 3. Manufacturing; 4. Construction; 5. Wholesale and retail trade; repair of motor vehicles and motorcycles; transportation and storage; accommodation and food service activities; 6. Information and communication; 7. Financial and insurance activities; 8. Real estate activities; 9. Professional, scientific and technical activities; administrative and support service activities; 10. Public administration, defence, education, human health and social work activities; 11. Arts, entertainment and recreation; other service activities; activities of household and extra-territorial organizations and bodies.

[24]The 38 OECD member countries are: Australia, Austria, Belgium, Canada, Chile, Colombia, Costa Rica, Czechia, Denmark, Estonia, Finland, France, Germany, Greece, Hungary, Iceland, Ireland, Israel, Italy, Japan, Korea, Latvia, Lithuania, Luxembourg, Mexico, Netherlands, New Zealand, Norway, Poland, Portugal, Slovakia, Slovenia, Spain, Sweden, Switzerland, Türkiye, the United Kingdom, and the United States.

[25]These reflect the current OECD categories as of 2025. Accession candidate countries include Argentina, Brazil, Bulgaria, Croatia, Indonesia, Peru, Romania, and Thailand. Key partners include Brazil, China, India, Indonesia, and South Africa.

all remaining countries, the model is calibrated at the national level, treating each country's entire territory as a single regional unit.

### E.3.2 Data sources and construction of calibration inputs

The calibration combines the following data sources, summarised in Table E.1. The date ranges describe the coverage of the source datasets; the input–output shares use the 2011–2020 reference period specified below.

**OECD Regional Data.** we obtain information on gross value added, population, and employment for all 38 OECD countries at the region- and sector-region-level for the period 2000-2023 from a series of OECD datasets.[26] Whenever sectoral data are absent at the regional level, we apply the region average and whenever that is not available, we apply the national average.

**Database of Sub-national Economic Output (DOSE v2).** for OECD accession countries and OECD key partners, we use GDP and employment figures from the MCC–PIK Database of Sub-national Economic Output (DOSE v2), produced by researchers at the Mercator Research Institute on Global Commons and Climate Change (MCC) and the Potsdam Institute for Climate Impact Research (PIK), and available at the Admin-1 level following the GADM regional boundaries. DOSE provides harmonised estimates of economic activity for approximately 1,660 first-level administrative regions across 83 countries from 1953 to 2020. Because DOSE reports GDP and employment only at an aggregated sectoral level - agriculture, manufacturing, and services - our calibration for these countries follows this three-sector breakdown.

**World Bank Development Indicators.** for all countries outside the sub-national datasets described above, we measure economic activity at the national level using sectoral indicators from the World Bank's World Development Indicators (WDI). Specifically, we collect GDP and employment data for the three broad sectors reported consistently across countries - agriculture, manufacturing, and services. These indicators provide internationally comparable measures constructed using national statistical offices and harmonised by the World Bank. Because WDI sectoral accounts are available for nearly all countries and extend over several decades, they provide information on country-level economic structure for regions where subnational information is unavailable. This allows us to maintain a consistent three-sector decomposition across the entire dataset.

**OECD Input–Output Tables.** These datasets provide country-level tables that record inter-industry transactions, capturing how goods and services flow between sectors within and across economies from 1995 until 2020. They include, for each sector, the value of purchases of goods and services from all sectors (including itself) to be used as inputs in production, and the value of

[26] These are: Gross value added by main economic activity – Regions (OECD Regions and Cities); Employment by main economic activity – Regions (OECD Regions and Cities); Gross domestic product - Regions (OECD Regions and Cities); Annual GDP and components (OECD National Accounts).

final consumption by households, gross output, and value-added. We use data from 2011-2020 to compute shares of value-added, material input expenditure shares, and consumption expenditure for each sector at the country-level.

**OECD International Migration Data.** we use data from the OECD International Migration Database to measure annual bilateral migration flows between OECD member countries for the period 2000–2023. The OECD dataset is based on harmonised national population registers, residence permit records, and labour-force surveys, providing comparable information on migration movements within the OECD. It reports inflows by country of origin and, for many destinations, outflows as well, enabling the construction of consistent bilateral flow matrices at an annual frequency. Because the OECD systematically standardises definitions of migrants, migration events, and residence changes, these data offer a reliable foundation for analysing international mobility patterns within the OECD bloc.

**OECD Internal Mobility Data.** to measure mobility within countries, we use OECD data on internal residential movements, which record the share of a region's population that relocates to another region within the same country.[27] These indicators are available annually for 2000–2021 and are constructed from national population registers and administrative records. The dataset captures moves across TL2 regions, which allows us to quantify the extent of within-country reallocation.

**United Nations Department of Economic and Social Affairs.** to extend migration coverage beyond OECD member countries, we complement the OECD International Migration Database with five-year bilateral migration flow estimates from Abel and Cohen (2019), which are constructed using the United Nations Department of Economic and Social Affairs (UN DESA) migrant stock data. UN DESA provides globally harmonised estimates of international migrant stocks for virtually all countries, reported at five-year intervals and available consistently from 1990 onward (with historical stock data extending back to 1960). Abel and Cohen (2019) apply demographic accounting and statistical smoothing methods to convert these stock figures into bilateral migration flows, producing a global dataset of inferred flows where direct statistics are unavailable.

**ITPD-E International Trade Data.** The International Trade and Production Database for Estimation (ITPD-E), provided by the United States International Trade Commission, contains information on international annual bilateral trade flows in 2000–2019 across 265 countries disaggregated by 170 industries. We aggregate all trade flows into the 11 sectors included in the model calibration for OECD countries, and also for the three broader sectors of agriculture, manufacturing, and services.

**SSP population projections.** The scenario inputs include country-level population projections from the International Institute for Applied Systems Analysis (IIASA), consistent with the SSP sce-

[27] Source: Population mobility within the country – Regions (OECD Regions and Cities).

**Table E.1:** Data sources used in the model calibration

| Category | Variables or calibration inputs | Sources |
|---|---|---|
| Regional economy | Population, output, wage measures, and sectoral employment | OECD regional and national accounts; DOSE v2; World Development Indicators |
| Production | Value-added shares and purchases of material inputs | OECD input–output tables |
| Consumption | Sectoral final expenditure shares | OECD input–output tables |
| Trade | Bilateral flows by sector and geographical information | ITPD-E; bilateral distance data |
| Migration | International flows and internal residential mobility | OECD International Migration Database; OECD Regions and Cities; Abel and Cohen (2019), using UN DESA stocks |
| SSP scenarios | Country-level population projections | IIASA |

*Notes:* The source descriptions above report coverage and the variables used. Production and sectoral expenditure shares are constructed from the 2011–2020 input–output data. SSP population projections are external scenario inputs.

narios. These external inputs are described with the reference-path construction below, separately from the estimation of trade and migration frictions.

### E.3.3 Parameter values and expenditure shares

Table E.2 reports the parameters and variables used in the calibration. The productivity-dispersion parameter is set to $\theta^j = 6$ for all sectors and the location-preference parameter to $\varepsilon = 4.5$. The production shares $\lambda = 0.67$ and $\eta = 0.19$ imply a floor-space share of $1 - \lambda - \eta = 0.14$ within the labour–capital–floor-space bundle. The goods expenditure share $\alpha$ and ordinary depreciation rate $\bar{\delta}$ are reported in the same table.

The structures-supply elasticity is $\zeta = 1.75$. To relate this parameter to the technology in the main text, cost minimisation implies $H_n = T_n(\mu Q_n / r_n)^{\mu/(1-\mu)}$. Holding land and the capital rental rate fixed, the elasticity with respect to $Q_n$ is therefore $\zeta = \mu/(1-\mu)$, so that $\mu = \zeta/(1+\zeta)$. This is the conditional supply elasticity; the capital rental rate also adjusts in general equilibrium.

OECD input–output tables provide the shares of producer revenue allocated to the primary-input bundle and to material inputs, $\beta_n^j$ and $\gamma_n^{jk}$, with $\beta_n^j + \sum_k \gamma_n^{jk} = 1$. Final consumption data discipline the sectoral expenditure shares $\alpha^j$, which sum to one. The empirical shares are constructed at the country level and mapped to the geographical and sectoral resolution of the calibration. These shares link observed production structures and expenditure patterns to the model's input demand and goods-market-clearing equations.

**Table E.2:** Calibrated model parameters and variables

| Parameter or variable | Description | Source or matched information |
|---|---|---|
| *Parameters assigned externally* | | |
| $\theta^j = 6$ | Productivity dispersion and trade elasticity | Eaton and Kortum (2002) |
| $\varepsilon = 4.5$ | Location-preference dispersion | Morten and Oliveira (2024) |
| $\zeta = 1.75$ | Conditional structures-supply elasticity | Saiz (2010) |
| $\lambda = 0.67$ | Labour share within the primary-input bundle | Baseline parameter choice |
| $\eta = 0.19$ | Capital share within the primary-input bundle | Greenwood et al. (1997) |
| $\alpha = 0.66$ | Goods share in workers' expenditure | Baseline parameter choice |
| $\beta = 0.95$ | Capital owners' discount factor | Baseline parameter choice |
| $\bar{\delta} = 0.05$ | Ordinary capital depreciation | Baseline parameter choice |
| *Objects constructed or estimated from data* | | |
| $L_{n0}$ | Initial population | Regional and national population inputs |
| $\beta_n^j$ | Primary-input expenditure shares | OECD input–output tables |
| $\gamma_n^{jk}$ | Material-input expenditure shares | OECD input–output tables |
| $\alpha^j$ | Sectoral final expenditure shares | OECD input–output tables |
| $\rho^j$ | Trade distance elasticity | Trade gravity relationship; ITPD-E and distance data |
| $\phi$ | Migration distance elasticity | Migration gravity relationship; bilateral migration and distance data |
| *Objects recovered through model inversion and moment matching* | | |
| $\varphi_{\sigma(n),\sigma(i)}$ | Country-pair trade-cost component | Bilateral and domestic trade shares; Head and Ries (2001) |
| $\psi_{\sigma(n),\sigma(i)}$ | Country-pair migration-cost component | International migration flows; OECD and UN-based estimates |
| $\eta_n$ | Local mobility factor | Regional out-migration and within-country mobility |
| $P_n^j$ | Sectoral prices | Spatial expenditure and revenue patterns; gravity price system |
| $A_n^j$ | Sectoral productivities | Wages, employment, and equilibrium sourcing and expenditure conditions |
| $B_n$ | Local amenities | Spatial population targets, conditional on mobility costs |
| $K_{n0}$ | Initial capital stock | Stationary-capital condition at the reference population distribution |

*Notes:* The calibration covers 927 regions across 186 countries, with 11 sectors in OECD members and three aggregate sectors elsewhere. The structures parameter satisfies $\mu = \zeta/(1+\zeta)$. The local mobility parameter $\eta_n$ is distinct from the capital input share $\eta$. Sectoral price levels and productivity levels are recovered under consistent normalisations.

### E.3.4 Trade costs

Trade costs depend on geographical distance and country-pair frictions. For distinct locations, we write

$$\tau_{ni}^{j} = (\text{dist}_{ni})^{\rho^j} \varphi_{\sigma(n),\sigma(i)}, \qquad n \neq i, \tag{46}$$

with domestic sourcing normalised to $\tau_{nn}^{j} = 1$. The country-pair component is normalised to one for pairs within the same country, $\varphi_{cc} = 1$; trade between distinct regions of that country still incurs the distance-related cost. We first describe the information on total bilateral trade costs and then the distance component.

**Bilateral trade-cost index.** Following Head and Ries (2001), bilateral trade shares identify trade costs relative to domestic costs without requiring the other equilibrium variables. For two model locations $i$ and $n$, combining expenditure shares in both directions with domestic expenditure shares yields

$$\frac{\pi_{ni}^{j}\pi_{in}^{j}}{\pi_{nn}^{j}\pi_{ii}^{j}} = \left(\frac{\tau_{ni}^{j}\tau_{in}^{j}}{\tau_{nn}^{j}\tau_{ii}^{j}}\right)^{-\theta^j}. \tag{47}$$

Productivity, input costs, and destination price indices cancel from this expression. The implied index is therefore

$$\left(\frac{\tau_{ni}^{j}\tau_{in}^{j}}{\tau_{nn}^{j}\tau_{ii}^{j}}\right)^{1/2} = \left(\frac{\pi_{ni}^{j}\pi_{in}^{j}}{\pi_{nn}^{j}\pi_{ii}^{j}}\right)^{-1/(2\theta^j)}. \tag{48}$$

With domestic costs normalised to one and symmetric bilateral costs, the index equals $\tau_{ni}^{j} = \tau_{in}^{j}$; without symmetry, it identifies their geometric mean. We use bilateral and domestic trade shares from ITPD-E to discipline country-pair trade frictions. The country-level index provides information on trade costs at that level of aggregation; the distance specification maps frictions to pairs of model regions.

**Distance component.** The trade-share equation implies a gravity relationship for bilateral expenditure $X_{ni}^{j}$, with destination $n$ and origin $i$:

$$\log X_{ni}^{j} = a_{n}^{j} + b_{i}^{j} - \theta^j \rho^j \log \text{dist}_{ni} - \theta^j \log \varphi_{\sigma(n),\sigma(i)} + u_{ni}^{j}. \tag{49}$$

Here, $a_{n}^{j}$ captures destination expenditure and inward price terms, while $b_{i}^{j}$ captures origin productivity and production costs. The coefficient on log distance is $-\theta^j\rho^j$. Denoting this coefficient by $b_{\text{dist}}^{j}$, the implied distance parameter is $\rho^j = -b_{\text{dist}}^{j}/\theta^j$.

The distance relationship is estimated by OLS using country-pair trade flows from ITPD-E and bilateral distance data, since trade flows between regions within countries are unavailable. The country-pair trade-cost index includes both distance and border-related frictions; extracting the latter therefore requires accounting for the distance component under a consistent geographical aggregation. The resulting distance and country-pair components jointly determine the regional

trade-cost matrix.

### E.3.5 Prices

We recover price terms from the spatial distribution of sectoral expenditure and producer revenue, conditional on trade costs. To connect the model to the gravity representation of Anderson and van Wincoop (2003), define the effective origin cost $c_i^j = x_i^j / A_i^j$. Bilateral expenditure is

$$X_{ni}^j = \frac{(c_i^j \tau_{ni}^j)^{-\theta^j}}{(P_n^j / g^j)^{-\theta^j}} X_n^j. \tag{50}$$

Summing sales across destinations gives

$$R_i^j = (c_i^j)^{-\theta^j} \sum_n \left( \frac{\tau_{ni}^j}{P_n^j / g^j} \right)^{-\theta^j} X_n^j. \tag{51}$$

Let $X^j = \sum_n X_n^j = \sum_i R_i^j$ denote world expenditure, which equals world producer revenue in sector $j$. Substituting origin revenues into bilateral expenditure yields the structural gravity representation

$$X_{ni}^j = \frac{R_i^j X_n^j}{X^j} \left( \frac{\tau_{ni}^j}{\Pi_i^j \mathcal{P}_n^j} \right)^{-\theta^j}, \tag{52}$$

where $\Pi_i^j$ and $\mathcal{P}_n^j$ are outward and inward multilateral resistance terms. The inward term is proportional to the model's sectoral price index; its scale depends on the sectoral normalisation. The resistance terms satisfy

$$\Pi_i^j = \left[ \sum_n \left( \frac{\tau_{ni}^j}{\mathcal{P}_n^j} \right)^{-\theta^j} \frac{X_n^j}{X^j} \right]^{-1/\theta^j}, \tag{53}$$

and, by adding expenditure across origins,

$$\mathcal{P}_n^j = \left[ \sum_i \left( \frac{\tau_{ni}^j}{\Pi_i^j} \right)^{-\theta^j} \frac{R_i^j}{X^j} \right]^{-1/\theta^j}. \tag{54}$$

These equations describe how a location's trading opportunities depend on its access to all potential partners. Bilateral trade increases with producer revenue at the origin and expenditure at the destination and decreases with bilateral trade costs relative to the multilateral resistance terms.

Equations (53) and (54) determine the resistance terms up to a normalisation within each sector. They discipline relative sectoral prices across locations. Linking them to the model's price indices requires consistent sectoral scales and the constant $g^j$; these choices also enter the recovery of productivity levels. Prices, input costs, and expenditures must jointly satisfy the remaining equilibrium conditions.

### E.3.6 Productivities

We recover local sectoral productivities by combining observed wages and employment with the model's expenditure and trade-share equations. Under Cobb–Douglas production, labour payments constitute the share $\lambda\beta_n^j$ of producer revenue, implying

$$R_n^j = \frac{w_n L_n^j}{\lambda \beta_n^j}. \tag{55}$$

Total expenditure on sector-$j$ goods in each location is obtained from goods market clearing:

$$X_n^j = \sum_{k=1}^{J} \gamma_n^{kj} R_n^k + \alpha^j E_n, \tag{56}$$

where $E_n = \alpha w_n L_n + r_n \widetilde{K}_n + \mathcal{R}_n^T$ includes workers' goods consumption, capital owners' consumption and investment, and landowners' consumption.

Producer revenue must equal sales across all destinations. Combining this condition with the trade-share equation and the sectoral price index gives

$$R_n^j = \left(\frac{A_n^j}{g^j x_n^j}\right)^{\theta^j} \sum_{i=1}^{N} \left(\frac{\tau_{in}^j}{P_i^j}\right)^{-\theta^j} X_i^j, \tag{57}$$

where $x_n^j$ is the input-bundle cost defined in equation (30) and $g^j$ is the constant in the sectoral price index. Conditional on expenditures, input costs, trade costs, and sectoral prices, productivity is therefore

$$A_n^j = g^j x_n^j \left[\frac{R_n^j}{\sum_{i=1}^{N} \left(\tau_{in}^j / P_i^j\right)^{-\theta^j} X_i^j}\right]^{1/\theta^j}. \tag{58}$$

This expression is a conditional inversion: input costs, expenditures, and prices must also satisfy the remaining equilibrium conditions under a consistent price normalisation. We therefore recover productivities jointly with the model-implied prices and allocations, using observed wages and sectoral employment to discipline producer revenues.

For initialisation with a stationary capital stock and reference flood exposure $d_n^0$, the capital accumulation equation additionally implies

$$\frac{r_n}{P_n} = \frac{1}{\beta(1 - d_n^0)} - (1 - \bar{\delta}). \tag{59}$$

In the absence of flood-related destruction, this reduces to $r_n/P_n = 1/\beta - (1 - \bar{\delta})$.

### E.3.7 Amenities and migration costs

We jointly calibrate amenities $B_n$ and migration costs using information on bilateral flows, internal mobility, and the spatial distribution of population. The migration-cost function includes a

distance component, a country-pair component, and an origin-specific mobility factor. An unnormalised representation of the specification is

$$\widehat{\kappa}_{ni} = e^{-\eta_i \mathbf{1}\{n=i\}} (\text{dist}_{ni})^{\phi} \psi_{\sigma(n),\sigma(i)}, \tag{60}$$

where own-location distance is normalised to one and $\psi_{cc} = 1$ for locations in the same country. The parameter $\eta_i$ shifts the attractiveness of remaining in origin $i$ relative to moving and is distinct from the capital share $\eta$ in production.

Multiplying all destination costs for a given origin by the same positive factor leaves migration shares unchanged. To maintain the convention $\kappa_{ii} = 1$ used in the main text, we divide by the own-location cost and write the equivalent normalised specification as

$$\kappa_{ni} = \frac{\widehat{\kappa}_{ni}}{\widehat{\kappa}_{ii}} = e^{\eta_i \mathbf{1}\{n\neq i\}} (\text{dist}_{ni})^{\phi} \psi_{\sigma(n),\sigma(i)}. \tag{61}$$

This normalisation preserves the migration allocations generated by the original specification. It does not change the mobility moments used for calibration.

**Distance component.** For moves between distinct locations, the migration-share equation implies

$$\log \lambda_{ni,t} = a_{nt} + b_{it} - \varepsilon\phi \log \text{dist}_{ni} - \varepsilon \log \psi_{\sigma(n),\sigma(i)} + u_{ni,t}, \qquad n \neq i. \tag{62}$$

The destination term $a_{nt}$ captures amenities and real wages, while $b_{it}$ captures the origin-specific choice denominator and mobility factor. The coefficient on log distance is $-\varepsilon\phi$, rather than $\phi$ itself. Bilateral migration flows and distance data discipline this component of migration costs.

**Cross-border migration costs.** Bilateral migration shares provide information on migration frictions relative to the option of remaining in the current location. Combining flows in both directions with the corresponding staying shares yields

$$\frac{\lambda_{ni}\lambda_{in}}{\lambda_{nn}\lambda_{ii}} = \left(\frac{\kappa_{ni}\kappa_{in}}{\kappa_{nn}\kappa_{ii}}\right)^{-\varepsilon}. \tag{63}$$

This relationship identifies a symmetric index of total bilateral migration frictions relative to staying costs. Separately recovering the cross-border component requires accounting for distance and the mobility shifters in the migration-cost function. We use OECD international migration data and the UN-based estimates of Abel and Cohen (2019) to discipline cross-border frictions, while internal mobility observations provide additional information on the costs of moving within countries.

**Within-country mobility factors and local amenities.** Conditional on the distance and country-pair components, we solve for local mobility factors $\eta_n$ and amenities $B_n$ through a nested moment-matching algorithm. In the inner loop, we update mobility factors for a candidate amenity vector. In the outer loop, we update amenities to match the population targets, taking account of

the associated inner-loop solution. This combines model inversion with simulated moment matching.

**Inner loop.** For a candidate vector of amenities, the share of workers initially in $i$ who choose destination $n$, including those who remain in $i$, is

$$\lambda_{ni} = \frac{\left[B_n w_n / (\kappa_{ni} P_n^{\alpha} Q_n^{1-\alpha})\right]^{\varepsilon}}{\sum_{m=1}^{N} \left[B_m w_m / (\kappa_{mi} P_m^{\alpha} Q_m^{1-\alpha})\right]^{\varepsilon}}. \tag{64}$$

We update the mobility parameters to match observed movement rates. Regional out-migration is the share of residents who leave their current location, $1 - \lambda_{ii}$. The model-implied rate of migration between distinct locations within country $c$ is

$$\widetilde{\lambda}_c = \sum_{i:\sigma(i)=c} \frac{L_i}{\sum_{\ell:\sigma(\ell)=c} L_\ell} \sum_{\substack{n:\sigma(n)=c \\ n \neq i}} \lambda_{ni}. \tag{65}$$

This expression weights each origin's internal out-migration rate by its share of the country's population and excludes residents who remain in the same location. Regional mobility observations discipline local movement frictions, while country-level internal migration rates discipline the aggregate intensity of mobility within countries. Where regional observations are unavailable, recovering location-specific parameters requires additional restrictions or imputed mobility moments.

**Outer loop.** Having obtained mobility factors conditional on amenities, we update amenities to match the spatial population targets. Combining the population law of motion and the migration probabilities gives the migration-implied distribution

$$L_{nt} = \sum_{i=1}^{N} \frac{\left[B_n w_{nt} / (\kappa_{ni}(B) P_{nt}^{\alpha} Q_{nt}^{1-\alpha})\right]^{\varepsilon}}{\sum_{m=1}^{N} \left[B_m w_{mt} / (\kappa_{mi}(B) P_{mt}^{\alpha} Q_{mt}^{1-\alpha})\right]^{\varepsilon}} L_{i,t-1}. \tag{66}$$

Here, $\kappa_{ni}(B)$ denotes the migration cost obtained from equation (61) using the mobility parameters determined by the inner loop for the candidate amenity vector $B$. Conditional on these costs and the associated wages, goods prices, and housing prices, we update amenities until the population distribution implied by equation (66) matches the calibration targets. Amenities are identified only up to a common multiplicative factor, which cancels from migration probabilities, so we normalise their unweighted mean across locations to one. We alternate between mobility-cost and amenity updates until both the targeted moments and parameter values converge.

### E.3.8 Initial capital and the reference path

We initialise capital at a stationary stock conditional on the reference population distribution, calibrated fundamentals, and historical climate conditions. Holding the population distribution and

these fundamentals fixed, we guess the local capital stocks, solve the within-period equilibrium, and update capital using equation (36) until $K_{n,t+1} = K_{nt}$ in every location. This condition incorporates flood-related destruction under historical climate conditions through $d_n^0$.

This initialisation concerns the capital stock conditional on the reference population distribution and does not require the full spatial economy to be in steady state. Once the simulations begin, population can redistribute through migration, while capital responds endogenously to the resulting paths of rental returns, goods prices, and flood-related destruction. The baseline model therefore need not remain at its initial allocation even when climate conditions are held constant.

The baseline path is the model's equilibrium sequence over 2025–2100 under historical climate conditions. The quantitative scenario specification also uses country-level population projections from IIASA consistent with each SSP. These are external scenario inputs rather than an additional behavioural demographic mechanism. Within each SSP, the same population assumptions are used in the climate-change and reference simulations, so the comparison isolates the effects of changing climate conditions and the associated equilibrium responses.

The climate-change paths use the same initial stocks and calibrated economic structure and introduce the projected changes in sectoral productivity, flood-related capital destruction, and usable land. The mapping from local flood estimates to capital destruction is described in the following subsection. The counterfactual subsections then explain which economic conditions or calibration objects are altered when linkages or adjustment margins are restricted.

### E.3.9 Mapping climate hazards into model inputs

The four climate hazards enter the model through three economic fundamentals: sectoral productivity, flood-related capital destruction, and usable land. We construct these inputs from geographically detailed empirical damage estimates and physical projections, rather than imposing losses directly on GDP. Their aggregate and regional consequences therefore depend on the model's production structure, economic linkages, and endogenous adjustment.

**Heat stress.** Annual hot-day projections are converted into three mutually exclusive temperature bins: 30–35°C, 35–40°C, and above 40°C. These exposures are combined with the estimated productivity responses, including their variation with local climatic conditions. The resulting annual heat inputs are normalised using the 1950–1979 reference period. Letting $a_{nt}^{\text{heat}}$ denote the resulting proportional productivity input, non-agricultural productivity is given by

$$A_{nt}^{j} = A_{n}^{j,0}\left(1 + a_{nt}^{\text{heat}}\right), \qquad j \neq \text{agr}. \tag{67}$$

Within each location, the same proportional heat shock is applied across non-agricultural sectors. Sectoral outcomes nevertheless differ because of differences in input requirements and the equilibrium responses of prices, factor allocation, and demand. Agricultural productivity instead follows the separate yield-based construction described below.

**Agro-climatic conditions.** Agricultural productivity inputs are constructed from projected potential yields for fifteen crops and grassland. For category $c$, climate model $m$, scenario $s$, and projection window $u$, let $y_{gcmsu}$ denote potential yield in grid cell $g$ and let $h^0_{gc}$ denote baseline harvested area. We first aggregate yield levels to administrative regions using fixed harvested-area weights,

$$Y_{rcmsu} = \frac{\sum_{g \in r} h^0_{gc} y_{gcmsu}}{\sum_{g \in r} h^0_{gc}}. \tag{68}$$

For each crop and climate model, projected yield changes are measured relative to the corresponding 2011–2040 yield level. The central crop-specific projection is the median of these relative changes across the five climate models,

$$g_{rcsu} = \text{median}_m \left\{ \frac{Y_{rcmsu}}{Y_{rcmsu_0}} - 1 \right\}, \qquad u_0 = \text{2011–2040}. \tag{69}$$

For countries represented by a single model location, these crop-specific changes are subsequently aggregated across administrative regions using baseline crop production weights. Crop changes and the grassland proxy for livestock productivity are then combined using fixed weights based on crop production values and the livestock share of agricultural production. Crops accounting for less than one per cent of a location's crop production value are excluded. Positive yield changes are capped at 100 per cent before the final aggregation, and the retained weights are normalised to sum to one. Writing $w^0_{nc}$ for these normalised weights, the agricultural productivity input is

$$g^{\text{agr}}_{nsu} = \sum_c w^0_{nc} \min \left\{ g_{ncsu}, 1 \right\}, \qquad \sum_c w^0_{nc} = 1. \tag{70}$$

This input enters agricultural productivity multiplicatively, $A^{\text{agr},s}_{nt} = A^{\text{agr},0}_n (1 + g^{\text{agr}}_{nsu})$, using the projection window assigned to year $t$. Crop and livestock weights remain fixed, abstracting from endogenous changes in crop mix within agriculture.

For the agricultural uncertainty exercises, we use the climate models generating the lowest and highest global damages as the lower- and higher-damage cases, respectively. The same selected model is applied across locations, preserving its geographical pattern of projected yield changes. These selections therefore reflect global damage rankings and need not produce the smallest and largest losses in every individual country.

**Flood-related capital destruction.** Riverine and coastal flood projections are combined with local exposure and the calibrated severity of capital destruction. Let $f^h_{nt}$ denote annual flood frequency for flood type $h \in \{\text{riverine}, \text{coastal}\}$, $e^h_n$ the corresponding population-exposure share, and $v_n$ the continental severity multiplier. The additional expected annual destruction input relative to reference flood conditions is

$$q^h_{nt} = \Delta v_n e^h_n \left( f^h_{nt} - f^h_{n0} \right). \tag{71}$$

The implementation uses an event-level destruction parameter $\Delta = 0.035$. Its calibration to the observed post-flood capital-stock response, together with the continental severity adjustments, is described in the following subsection. The annual capital-destruction input combines riverine and coastal contributions and is bounded between zero and 0.99. Where projected coastal flood frequency exceeds 50 per cent, the additional coastal capital-destruction contribution is set to zero and coastal exposure enters through the land-loss channel described below. Riverine destruction continues to apply separately.

**Sea-level rise and usable land.** Sea-level rise is represented through a reduction in effective usable land. For the future land-loss projections, locations with coastal flood frequency exceeding 50 per cent are assigned a land-loss input equal to their coastal population-exposure share. Otherwise, the land-loss input is zero. Letting $\ell_{nt}$ denote this input, usable land is

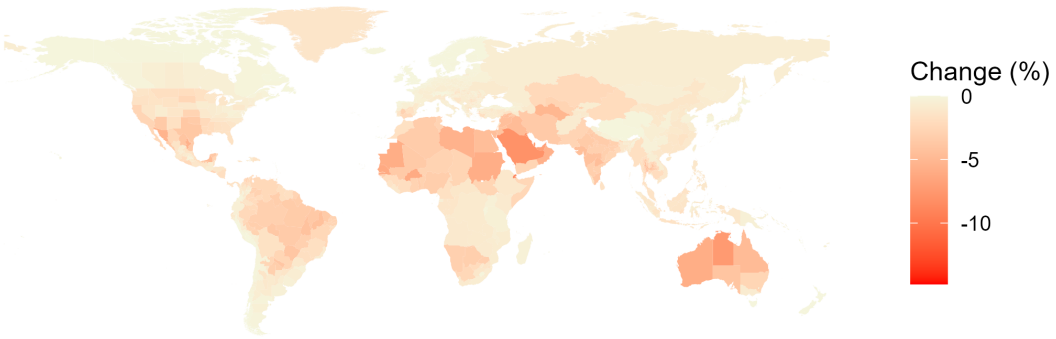
$$T_{nt} = T_n^0(1 - \ell_{nt}), \tag{72}$$

with the loss fraction bounded below one. The population-exposure share serves as a proxy for economically relevant land loss. It does not measure the geographical fraction of the region submerged. This channel reduces land available for housing and commercial floor space, allowing its consequences for production, rents, and spatial allocation to emerge within the model.

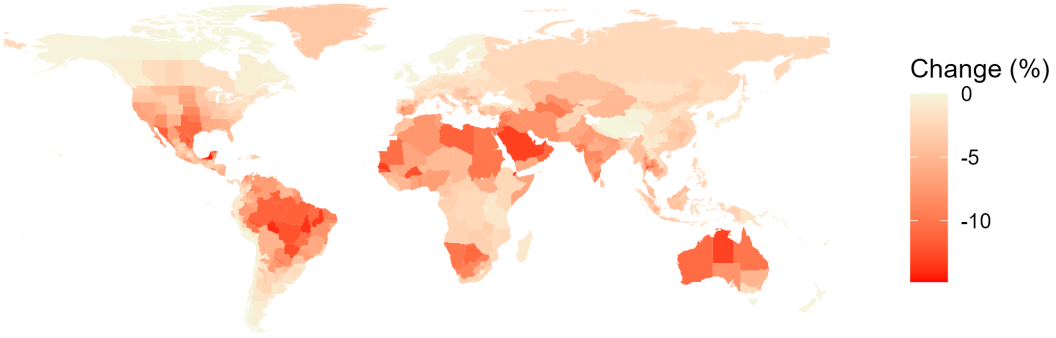
**Figure E.1:** Damages from climate change by impact channel in 2100

**(a)** Percentage change in productivity due to heat stress

Intermediate-emissions benchmark (SSP2-4.5)




Very high-emissions scenario (SSP5-8.5)

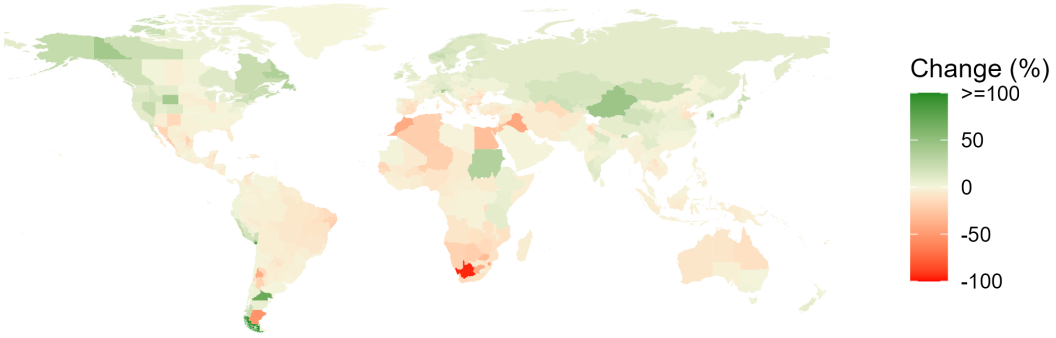



*Source:* Authors' calculations.
*Notes:* The maps show regional productivity changes attributable to heat stress. Non-agricultural productivity shocks are aggregated using baseline sectoral shares in total regional employment. Negative values indicate losses. The intermediate-emissions benchmark and very high-emissions scenario follow SSP2-4.5 and SSP5-8.5, respectively. Both maps use the same colour scale. White areas indicate unmatched or unavailable map data.

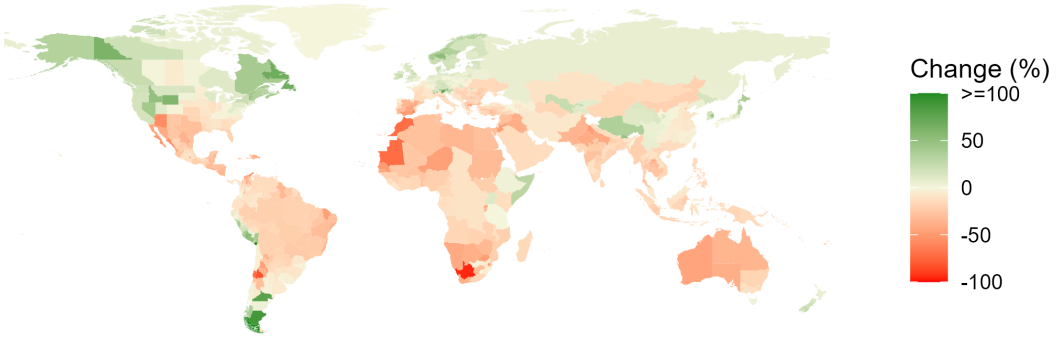
**Figure E.1:** Damages from climate change by impact channel in 2100 (continued)

**(b)** Percentage change in agricultural productivity due to changes in agro-climatic conditions

Intermediate-emissions benchmark (SSP2-4.5)




Very high-emissions scenario (SSP5-8.5)

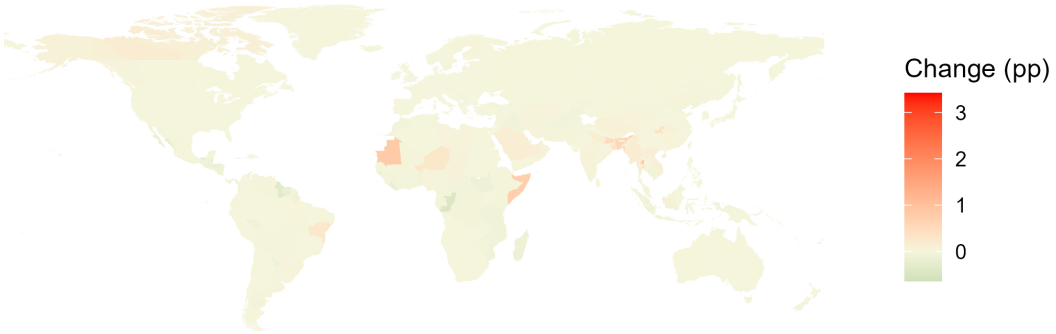



*Source:* Authors' calculations.
*Notes:* The maps show the agricultural productivity inputs used in the model. Negative values indicate losses and positive values indicate gains. The intermediate-emissions benchmark and very high-emissions scenario follow SSP2-4.5 and SSP5-8.5, respectively. Both maps use the same colour scale, ranging from −100% to 100%. White areas indicate unmatched or unavailable map data.

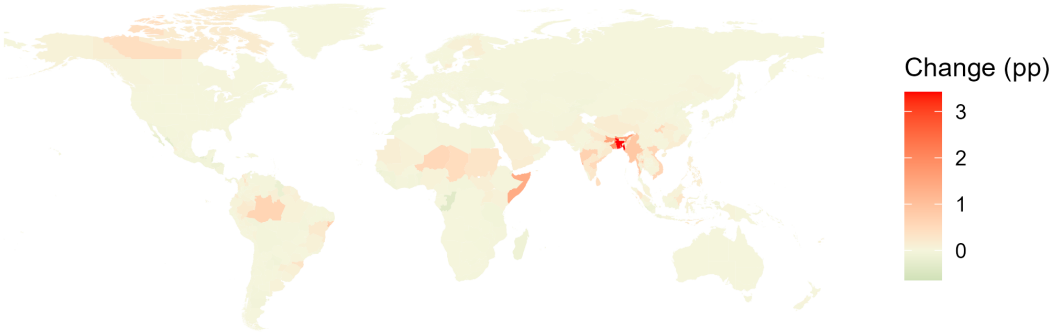
**Figure E.1:** Damages from climate change by impact channel in 2100 (continued)

**(c)** Percentage point change in annual capital destruction due to riverine flooding

Intermediate-emissions benchmark (SSP2-4.5)




Very high-emissions scenario (SSP5-8.5)

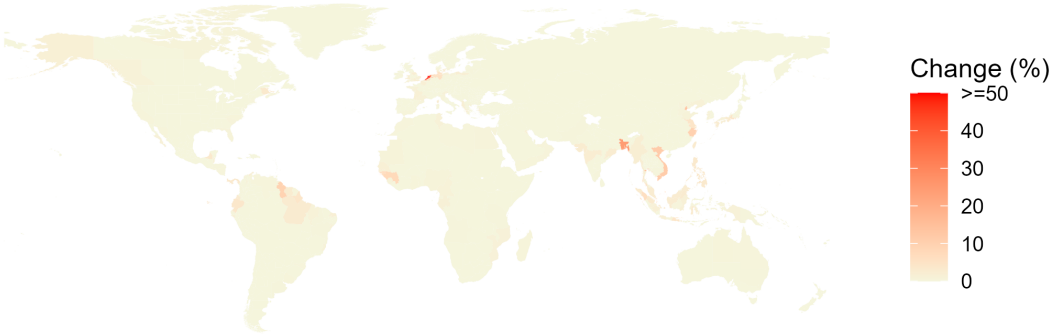



*Source:* Authors' calculations.
*Notes:* The maps show changes in annual capital destruction attributable to changes in riverine flood frequency relative to historical conditions, in percentage points. Positive values indicate increased destruction and negative values indicate reductions. The intermediate-emissions benchmark and very high-emissions scenario follow SSP2-4.5 and SSP5-8.5, respectively. Both maps use the same colour scale. White areas indicate unmatched or unavailable map data.

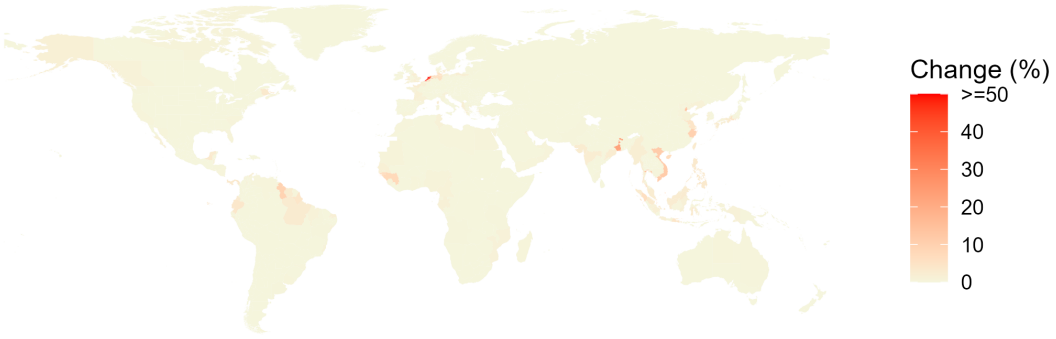
**Figure E.1:** Damages from climate change by impact channel in 2100 (continued)

**(d)** Percentage loss of usable land due to sea-level rise

Intermediate-emissions benchmark (SSP2-4.5)




Very high-emissions scenario (SSP5-8.5)




*Source:* Authors' calculations.
*Notes:* The maps show the model's usable-land loss, proxied by coastal population exposure in areas meeting the model's permanent-inundation criterion. This measure represents economically relevant land loss rather than the geographical share of land submerged. The intermediate-emissions benchmark and very high-emissions scenario follow SSP2-4.5 and SSP5-8.5, respectively. Both maps use the same colour scale. Losses of 50% or more receive the upper endpoint colour. White areas indicate unmatched or unavailable map data.

### E.4. Impact of flooding on capital

#### E.4.1 Calibration of capital destruction

Here we provide additional detail on how we calibrate flood-related damages using the firm-level estimates summarised in Section 2.1. We focus on the baseline specification in equation (15), reported in Figure B.1, which implies that a firm's capital stock is on average 2.7 percent lower in the four years following a flood. To translate this into a model-consistent parameter, we calibrate the fraction of capital destroyed by a flood so that the model's capital-stock response matches this observed decline relative to a reference path without the event.

Let $\Delta$ denote the fraction of inherited capital destroyed by a flooding event. Consistent with the timing of the model, the event reduces capital available for production to $(1-\Delta)K_{n0}$ in the period in which it occurs. We obtain $\Delta$ using an iterative search procedure. Starting from an initial guess, we simulate a one-off flooding event and allow capital to evolve according to equation (36), with no further flood shocks during the following four years. We compare the average capital-stock deviation over the four post-event years and across locations with the empirical target of a 2.7 percent decline, update $\Delta$, and iterate until convergence.

#### E.4.2 Continent resilience factors

Since our damage estimates rely primarily on data from European countries, we allow the impacts of flooding to differ across continents. To do so, we draw on the depth-damage functions provided by Huizinga et al. (2017), who develop a global, harmonised set of flood-damage curves for residential, commercial, and industrial assets. Their study combines several studies and data sources to estimate how damage varies with inundation depth across world regions while accounting for building types, construction costs, asset values, and flood vulnerability. These depth-damage functions give us a scalable way to adjust the magnitude of capital losses outside Europe, ensuring that our calibration reflects regional differences in exposure and structural vulnerability.

We combine these depth–damage functions with flood hazard maps from the World Resources Institute (WRI), which report expected inundation depths for different return periods. Using the damage function for commercial buildings, we compute in each location the share of assets damaged at flood depths of $\{0, 0.5, 1, 1.5, 2, 3, 4, 5, 6\}$ meters for Europe, North America, Central and South America, Asia, and Oceania, and use the global average curve for Africa. We then weight these damage shares by the probability of each flood intensity category and average the resulting values across locations within each continent.

Taking the ratio of each continent's average to that of Europe yields a continent-specific multiplier capturing differences in expected damage under this weighting procedure. We apply this multiplier to the calibrated value of $\Delta$ to scale flood-related capital destruction across regions. The values of the multiplier are 2.13 for North America, 3.51 for Central and South America, 2.12 for Asia, 1.43 for Africa, and 1.37 for Oceania.

### E.5. Counterfactual simulations

In this section, we describe how we implement the counterfactual simulations shown in Sections 5.2 and 5.3. The first set of counterfactual exercises - those examining the role of economic linkages in transmitting shocks - requires a full recalibration of the model, as the counterfactual economy differs structurally from the baseline climate-change scenario. By contrast, the second set of exercises - those assessing the role of adjustment mechanisms - relies on the same baseline calibration but alters the equilibrium conditions to reflect a world in which trade and migration shares are effectively "frozen". We discuss each set of exercises in turn below.

#### E.5.1 The role of economic linkages in transmitting climate shocks

We remove spatial linkages by imposing $\pi^j_{nit} = 0$ and $\lambda_{nit} = 0$ for all $i \neq n$, with $\pi^j_{nnt} = \lambda_{nnt} = 1$. Each location therefore sources goods locally and retains its population, apart from exogenous demographic changes. In the separate counterfactual without input–output linkages, we set $\beta^j_n = 1$ and $\gamma^{jk}_n = 0$ for all locations and sectors, eliminating intermediate-input purchases both within and across sectors.

For each restricted model, we recompute the calibration-implied prices and productivities under the altered economic structure and reinitialise capital using the stationary-capital condition. Where migration remains possible, we also recalibrate migration costs and amenities. When migration is shut down, amenities no longer affect population allocations and are normalised to one. The restrictions replace the corresponding trade or mobility conditions, so the recalibration does not require the restricted model to reproduce observed flows that it rules out by construction.

We then simulate both a path with climate change and a reference path with climate conditions held fixed at historical levels under the same restricted model. Climate losses are measured relative to that model's own reference path. Comparing these losses with those in the full model therefore assesses how economic linkages shape the consequences of climate change, rather than combining climate damages with the level effects of removing the linkages themselves.

#### E.5.2 The role of adjustment: how trade and labour mobility shape the distribution of global losses

In the no-trade-adjustment counterfactual, we retain the baseline calibration and hold bilateral expenditure shares at their corresponding values along the no-climate-change path:

$$\pi^j_{nit} = \bar{\pi}^j_{nit} \tag{73}$$

for every destination, origin, sector, and period. These shares may evolve over time along the reference path but cannot respond to climate change.

To close the counterfactual price system, we leave domestic sourcing costs unchanged and nor-

malise $\tau_{nn}^{j} = 1$. The domestic expenditure-share equation then implies

$$P_{nt}^{j} = g^{j} \frac{x_{nt}^{j}}{A_{nt}^{j}} \left(\bar{\pi}_{nnt}^{j}\right)^{1/\theta^{j}}, \tag{74}$$

where $g^{j}$ is the constant in the sectoral price index. This formulation is equivalent to introducing bilateral trade-cost adjustment factors that sustain the prescribed shares while leaving the domestic adjustment factor equal to one. Wages, prices, production, expenditure, and capital accumulation continue to respond endogenously to climate damages.

In the no-labour-adjustment counterfactual, we retain the baseline calibration but fix migration shares and within-location sectoral employment shares at their corresponding no-climate-change paths:

$$\lambda_{nit} = \bar{\lambda}_{nit}, \qquad L_{nt}^{j} = \bar{s}_{nt}^{j} L_{nt}, \tag{75}$$

where $\bar{s}_{nt}^{j} = \bar{L}_{nt}^{j} / \bar{L}_{nt}$. These restrictions prevent climate-induced changes in migration and sectoral labour allocation while preserving their evolution along the reference path.

Because labour can no longer move across sectors in response to climate shocks, sectoral wages need not equalise. We replace the common-wage labour-market condition with sector-specific market clearing:

$$w_{nt}^{j} = \frac{\lambda \beta_{n}^{j} R_{nt}^{j}}{\bar{s}_{nt}^{j} L_{nt}}, \tag{76}$$

where producer revenue remains $R_{nt}^{j} = \sum_{i} \pi_{int}^{j} X_{it}^{j}$. Sector-specific wages enter the corresponding production costs:

$$x_{nt}^{j} = \mu_{n}^{j} \left( (w_{nt}^{j})^{\lambda} r_{nt}^{\eta} Q_{nt}^{1-\lambda-\eta} \right)^{\beta_{n}^{j}} \prod_{k=1}^{J} (P_{nt}^{k})^{\gamma_{n}^{jk}}. \tag{77}$$

The employment-weighted local wage is

$$w_{nt} = \sum_{j=1}^{J} \bar{s}_{nt}^{j} w_{nt}^{j}. \tag{78}$$

Aggregate labour income is therefore $w_{nt} L_{nt} = \sum_{j} w_{nt}^{j} L_{nt}^{j}$, which determines workers' aggregate expenditure on goods and housing. Capital accumulation and capital allocation across uses remain endogenous.

In the counterfactual restricting both trade and labour adjustment, we impose the trade-share, migration-share, and sectoral employment-share restrictions jointly. Each restricted-adjustment simulation uses the full model's baseline calibration and is compared with the same no-climate-change reference path. These exercises isolate the consequences of restricting the specified adjustment margins while allowing the remaining equilibrium variables to respond.

## F. Further results on quantitative analysis: Impact on population

This appendix reports how population patterns respond endogenously to climate change under the intermediate-emissions scenario (SSP2-4.5) and the very high-emissions scenario (SSP5-8.5). Figures F.1 and F.2 show the model-implied change in population by 2050 and 2100 that results from households' optimal locational choices in response to the distribution of climate damages. These results should be interpreted as the population outcome given the modelled climate impacts, not a causal assessment of migration's contribution to GDP losses. The contribution of migration and other adjustment mechanisms to GDP per capita losses is quantified through the counterfactual simulations in Section 5.3.

By mid-century (2050), the very high-emissions scenario induces modest but noticeable shifts in population across regions. As shown in Figures F.2a and F.4a, Northern Africa, Western Asia, Southern Asia, and Sub-Saharan Africa record early losses, where climate damages reduce local productive capacity, prompting households to relocate to regions relatively less affected by climate. These departures from climate-vulnerable regions contribute directly to population gains observed elsewhere, such as Northern Europe, Central Asia, Southern Europe, and North America, which all register positive inflows by mid-century, typically in the range of 1–6 percent. These migration flows include not only cross-border migration but also significant shifts within countries. In many countries, such as Spain, internal movements from hotter southern provinces toward cooler northern regions constitute an important share of the overall migration response, highlighting that migratory responses occur not only internationally but also domestically.

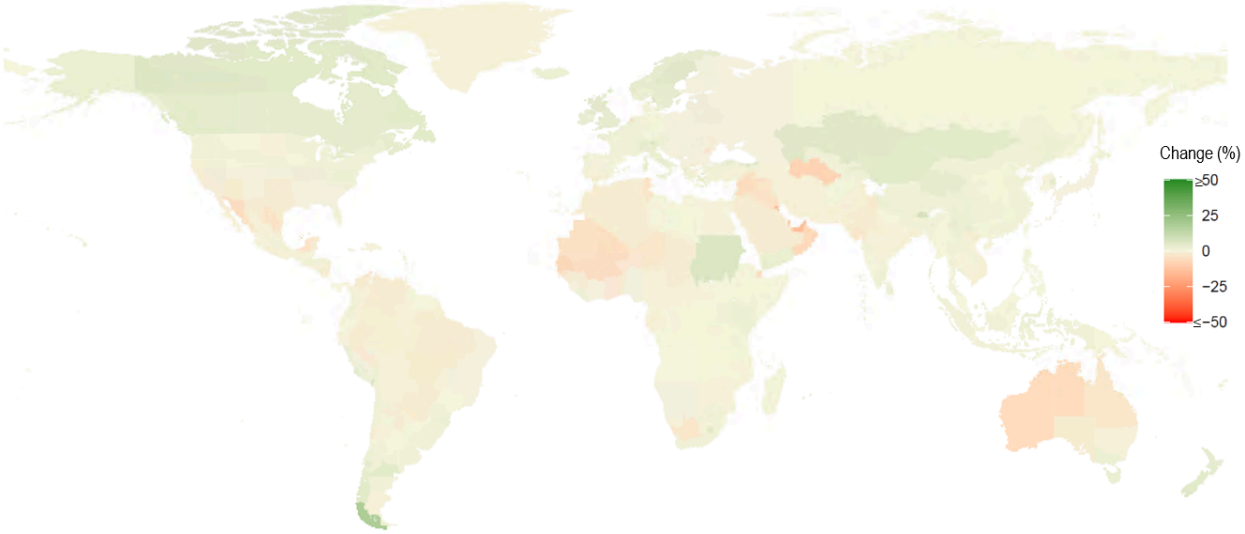
By 2100, these redistributive forces intensify substantially, with sharp contrasts emerging between population-losing and population-gaining regions. Figures F.2b and F.4b show large declines in Northern Africa (-11 percent), Western Asia (-8 percent), Southern Asia (-7 percent), and Sub-Saharan Africa (-7 percent), consistent with the severe GDP losses concentrated in these regions. The map in Figure F.2b highlights particularly pronounced outflows from the Sahel, the Horn of Africa, and parts of South Asia - areas facing some of the largest economic damages at the hands of climate hazards. These outflows, in turn, fuel sizable population gains in cooler, less climate-affected regions. Northern Europe (+20 percent), Central Asia (+10 percent), North America (+8 percent), and Oceania (+8 percent) become major net recipients of migrants by 2100. Among OECD countries, the map reveals strong inflows into Canada, Nordic countries, and northern parts of the United States, while internal migration continues to reshape national population distributions. This includes, for instance, movement toward cooler northern areas of Spain, Portugal, and Mexico. The OECD as a whole experiences population gains, but with substantial variation. Northern Europe and North America emerge as clear destinations for climate-driven migration, while Southern Europe sees only modest inflows owing to higher local damages. Oceania and parts of Eastern Asia also register increases, whereas some OECD+ economies in warmer climates face mild declines.

Overall, the figures show that climate change not only reduces economic output but also significantly reshapes global and domestic population patterns, as people move away from intensifying

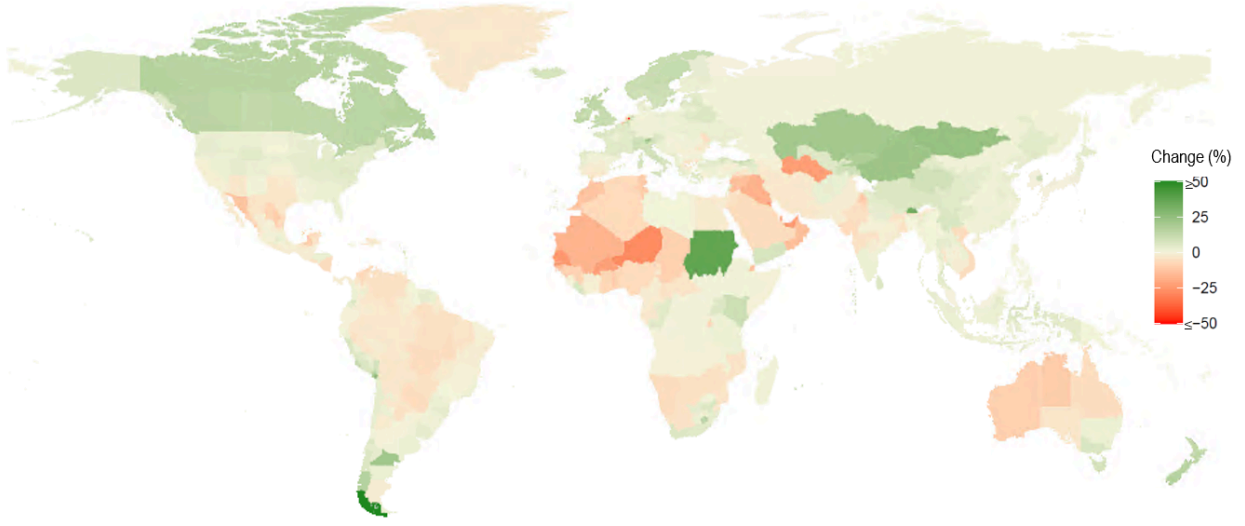
climate risks and towards less affected locations. These movements arise endogenously in the model and interact with economic outcomes in important ways. Section 5.3 quantifies the contribution of these adjustment mechanisms by holding selected allocation shares fixed along their no-climate-change paths.

**Figure F.1:** Change in population due to climate change under the intermediate-emissions scenario (SSP2-4.5)

**(a)** Percentage change in population in 2050



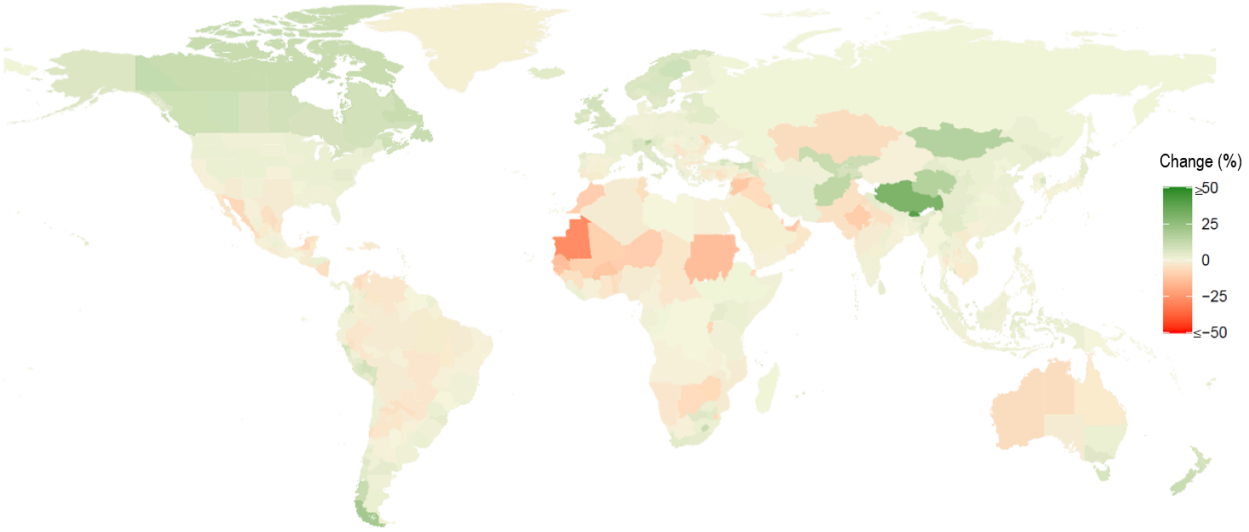

**(b)** Percentage change in population in 2100



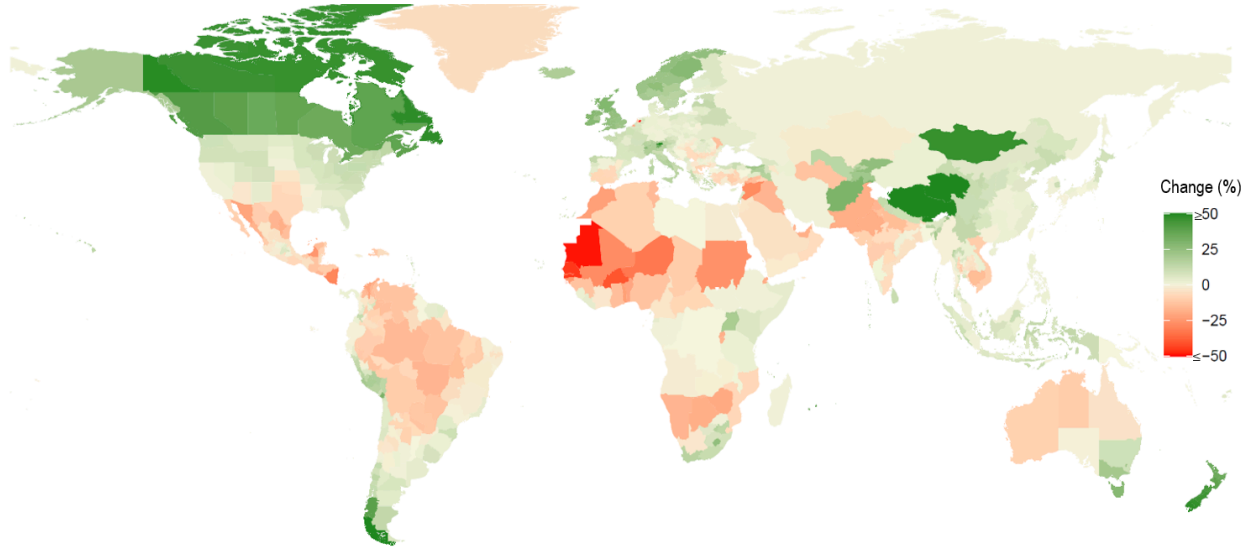

*Source:* Authors' own calculations.
*Note:* The figure shows the model-implied percent change in population relative to a no-climate-change scenario. All values below -50 and above 50 are winsorised at -50 and 50, respectively.

**Figure F.2:** Change in population due to climate change under the very high-emissions scenario (SSP5-8.5)

**(a)** Percentage change in population in 2050



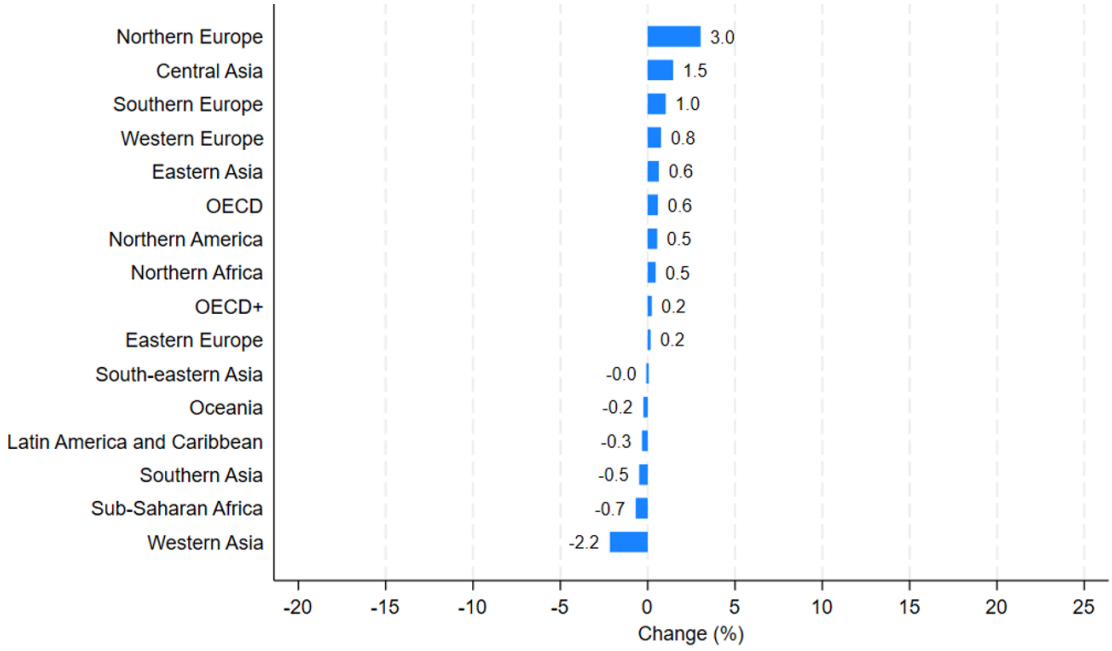

**(b)** Percentage change in population in 2100



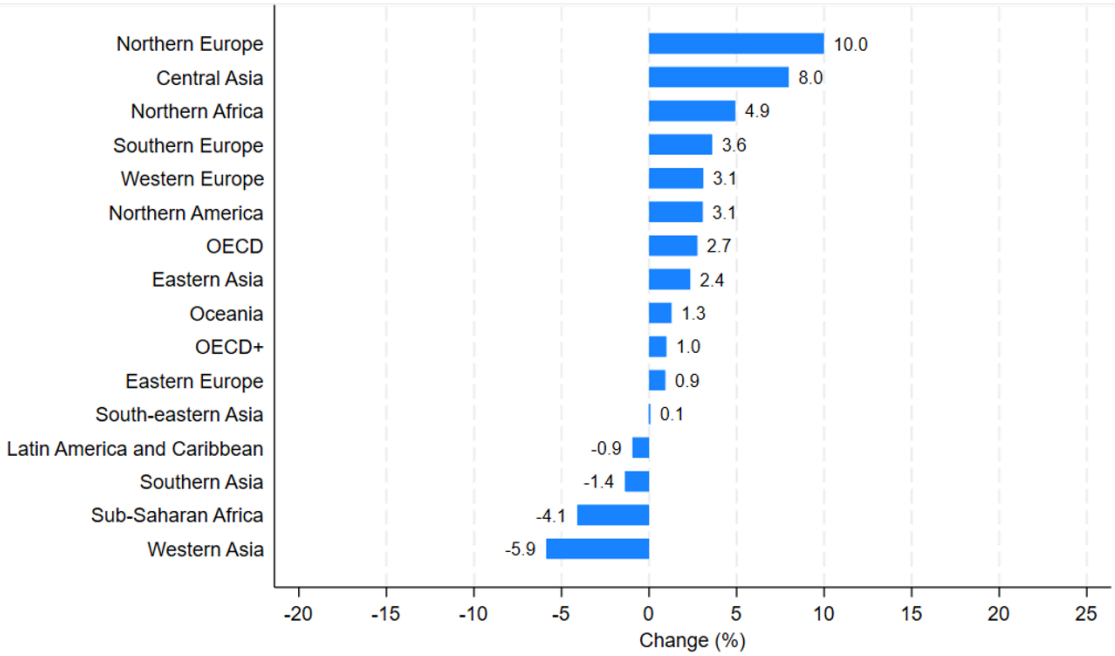

*Source:* Authors' own calculations.
*Note:* The figure shows the model-implied percent change in population relative to a no-climate-change scenario. All values below -50 and above 50 are winsorised at -50 and 50, respectively.

**Figure F.3:** Regional population changes under the intermediate-emissions scenario (SSP2-4.5)

**(a)** Percentage change in population in 2050



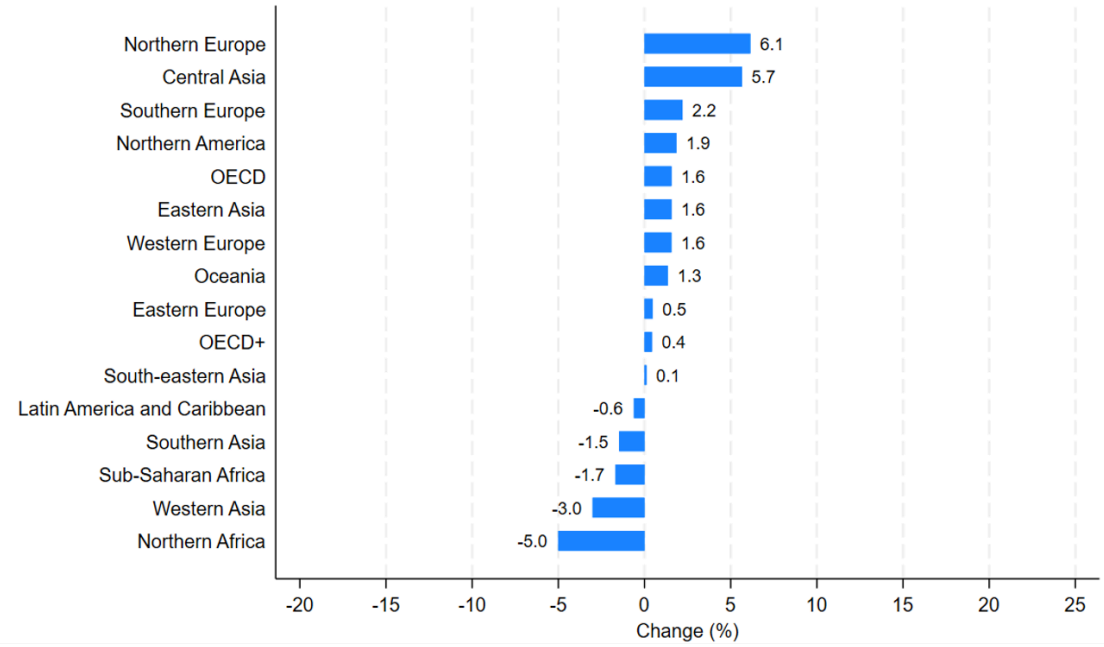

**(b)** Percentage change in population in 2100



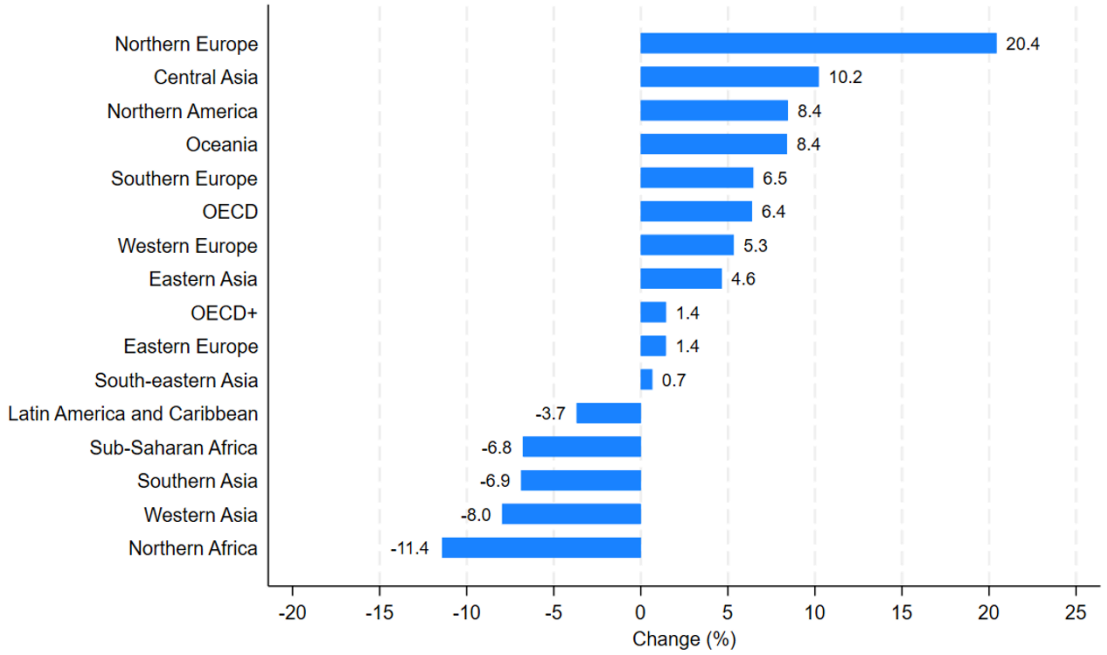

*Note:* The figure shows the model-implied change in population relative to a no-climate-change scenario. Regional population changes are computed as a country population-weighted average.
*Source:* Authors' calculations.

**Figure F.4:** Regional population changes under the very high-emissions scenario (SSP5-8.5)

**(a)** Percentage change in population in 2050




**(b)** Percentage change in population in 2100




*Note:* The figure shows the model-implied change in population relative to a no-climate-change scenario. Regional population changes are computed as a country population-weighted average.
*Source:* Authors' calculations.